



National Library  
of Canada

Bibliothèque nationale  
du Canada

Canadian Theses Service    Service des thèses canadiennes

Ottawa, Canada  
K1A 0N4

## NOTICE

The quality of this microform is heavily dependent upon the quality of the original thesis submitted for microfilming. Every effort has been made to ensure the highest quality of reproduction possible.

If pages are missing, contact the university which granted the degree.

Some pages may have indistinct print especially if the original pages were typed with a poor typewriter ribbon or if the university sent us an inferior photocopy.

Previously copyrighted materials (journal articles, published tests, etc.) are not filmed.

Reproduction in full or in part of this microform is governed by the Canadian Copyright Act, R.S.C. 1970, c. C-30.

## AVIS

La qualité de cette microforme dépend grandement de la qualité de la thèse soumise au microfilmage. Nous avons tout fait pour assurer une qualité supérieure de reproduction.

Si il manque des pages, veuillez communiquer avec l'université qui a conféré le grade.

La qualité d'impression de certaines pages peut laisser à désirer, surtout si les pages originales ont été dactylographiées à l'aide d'un ruban usé ou si l'université nous a fait parvenir une photocopie de qualité inférieure.

Les documents qui font déjà l'objet d'un droit d'auteur (articles de revue, tests publiés, etc.) ne sont pas microfilmés.

La reproduction, même partielle, de cette microforme est soumise à la Loi canadienne sur le droit d'auteur, SRC 1970, c. C-30.

THE UNIVERSITY OF ALBERTA

SCALES FOR THE DEVELOPMENT OF LONGITUDINAL VELOCITY IN A  
CURVED CHANNEL

by



DEBBIE LI-CHEN WENG

A THESIS

SUBMITTED TO THE FACULTY OF GRADUATE STUDIES AND RESEARCH  
IN PARTIAL FULFILMENT OF THE REQUIREMENTS FOR THE DEGREE  
OF MASTER OF SCIENCE IN WATER RESOURCES

DEPARTMENT OF CIVIL ENGINEERING

EDMONTON, ALBERTA

SPRING 1988

Permission has been granted to the National Library of Canada to microfilm this thesis and to lend or sell copies of the film.

The author (copyright owner) has reserved other publication rights, and neither the thesis nor extensive extracts from it may be printed or otherwise reproduced without his/her written permission.

L'autorisation a été accordée à la Bibliothèque nationale du Canada de microfilmer cette thèse et de prêter ou de vendre des exemplaires du film.

L'auteur (titulaire du droit d'auteur) se réserve les autres droits de publication; ni la thèse ni de longs extraits de celle-ci ne doivent être imprimés ou autrement reproduits sans son autorisation écrite.

ISBN 0-315-42882-1

THE UNIVERSITY OF ALBERTA

RELEASE FORM

NAME OF AUTHOR                 DEBBIE LI-CHEN WENG  
TITLE OF THESIS                 SCALES FOR THE DEVELOPMENT OF  
   LONGITUDINAL VELOCITY IN A CURVED  
   CHANNEL  
DEGREE FOR WHICH THESIS WAS PRESENTED   MASTER OF SCIENCE  
  
YEAR THIS DEGREE GRANTED    SPRING 1988

• Permission is hereby granted to THE UNIVERSITY OF ALBERTA LIBRARY to reproduce single copies of this thesis and to lend or sell such copies for private, scholarly or scientific research purposes only.

The author reserves other publication rights, and neither the thesis nor extensive extracts from it may be printed or otherwise reproduced without the author's written permission.

(SIGNED) *Debbie Li-Chen Weng*

PERMANENT ADDRESS:

*2609...105 A Street  
Edmonton, ALBERTA  
T6J 4A3.....*

DATED *February 15, 1988*

THE UNIVERSITY OF ALBERTA  
FACULTY OF GRADUATE STUDIES AND RESEARCH

The undersigned certify that they have read, and recommend to the Faculty of Graduate Studies and Research, for acceptance, a thesis entitled, SCALES FOR THE DEVELOPMENT OF LONGITUDINAL VELOCITY IN A CURVED CHANNEL submitted by DEBBIE LI-CHEN WENG in partial fulfilment of the requirements for the degree of MASTER OF SCIENCE IN WATER RESOURCES.

.....*R. S. Hoff*.....

Supervisor

.....*M. Peterson*.....

.....*B. C. Cheng*.....

Date. *February 15, 1988*.....

## ABSTRACT

The flow in a curved channel is a complicated three dimensional problem. It is important, but difficult, to fully understand the phenomenon with the existing knowledge. The increased concern about river bank erosion and river meandering in general has increased the demand for theoretical and empirical studies which can predict attack velocities on the outer bank of a meandering alluvial channel.

The purpose of this study is to examine mechanics of flow behavior in a bend; use the existing data to develop longitudinal velocity distribution curves; predict distributions of erosive attack on the banks of curved channels; and determine the starting and ending points for side bank protection. It is hoped that the scales which are derived in this study have some practical value in minimizing the cost of bank protection works.

## Acknowledgements

The writer wishes to acknowledge the financial support of the Research Management Division and the River Engineering Branch of Alberta Environment.

The writer would also like to express her gratitude to her supervisors, Professor A.W. Peterson and Dr. N. Rajaratnam for their support and advice; and is especially indebted to her supervisor, Dr. P. Steffler for his patient guidance, assistance and encouragement throughout the course of this study.

The writer would also like to thank Mrs. M. Zielsdorf, Mrs. D. Workun and Mrs. D. Harrison for their encouragement throughout the years of this study.

Finally, the writer thanks her husband, Han-I, who considerably provided his support, encouragement and assistance throughout this study.

## Table of Contents

Chapter	Page
1. Introduction .....	1
2. Review of the Significant Theoretical Studies .....	3
2.1 Introduction .....	3
2.1.1 Co-ordinate System .....	3
2.2 Odgaard (1986) .....	6
2.2.1 Governing Equations .....	7
2.2.2 Reduction of Equations' .....	8
2.3 Engelund (1974) .....	13
2.3.1 Governing Equations .....	13
2.3.2 Reduction of Equations .....	13
2.4 Conclusion .....	18
3. Theoretical Analysis .....	20
3.1 Introduction .....	20
3.2 Governing Equation .....	21
3.2.1 General Assumptions .....	21
3.2.2 Equations of Motion .....	21
3.2.3 Summary of the Motion Equations in Integral Forms .....	25
3.2.4 Similarity Hypothesis .....	26
3.2.4.1 Assumptions .....	26
3.2.4.2 Formulation .....	28
3.2.5 Length Scale for Developing Flow .....	33
3.3 Conclusion .....	37
4. Review of Significant Experimental Studies .....	41
4.1 Introduction .....	41
4.2 Ippen and Drinker (1962) .....	41
4.2.1 Analysis of the Experimental Results .....	42



4.2.2	The Experimental Conclusions .....	43
4.3	Yen (1965) .....	44
4.3.1	Analysis of the Experimental Results .....	45
4.3.2	The Experimental Conclusions .....	47
4.4	Varshney and Grade(1974) .....	48
4.4.1	Analysis of the Experimental Results .....	49
4.4.2	The Experimental Conclusions .....	50
4.5	Francis and Asfari (1970) .....	50
4.5.1	Analysis of the Experimental Results .....	51
4.5.2	The Experimental Conclusions .....	52
4.6	de Vriend and Koch (1977) .....	52
4.6.1	Analysis of the Experimental Results .....	53
4.6.2	The Experimental Conclusions .....	54
4.7	Steffler (1984) .....	55
4.7.1	Analysis of the Experimental Results .....	55
4.7.2	The Experimental conclusions .....	56
4.8	Conclusions .....	57
5.	Analysis of Existing Experiments .....	59
5.1	Introduction .....	59
5.2	Data Collecting Procedure .....	59
5.3	Definition of Zones for a Curved Channel .....	61
5.3.1	Zone I .....	66
5.3.2	Zone II .....	68
5.3.3	Zone III .....	69
5.3.4	Zone IV .....	70
5.4	Analysis of Results .....	70
5.4.1	Initial Velocity .....	73

5.4.2	Non-Dimensional Longitudinal Velocity Distribution Near the Outer Bank in Zone II .....	73
5.4.3	Non-Dimensional Development of Longitudinal Velocity near The Outer Bank	.94
5.4.4	Ultimate Velocity .....	98
5.4.5	Development Length Scale .....	98
6.	An Example of the Application for a Curved Channel	.104
6.1	DATA .....	104
6.2	Step 1 .....	105
6.3	Step 2 .....	105
6.4	Step 3 .....	105
6.5	Step 4 .....	105
6.6	Step 5 .....	105
7.	Conclusion .....	109
	Bibliography .....	111

## List of Tables

Table		Page
5.1	Data for the Rectangular Channels .....	71
5.2	Data for the Trapezoidal Channels .....	72
6.1	The Calculation Worksheet For the Example .....	106

## List of Figures

Figure	Page
2.1 Definition sketch - Plan .....	4
2.2 Definition sketch - Cross Section .....	5
3.1 Comparison of Ultimate Cross Sectional Velocity Distributions .....	34
3.2 Comparison of the Three Length Scale Methods .....	40
5.1 Non-Dimensional Shear Stress Distribution Near The Banks Ippen and Drinker(6) Run 1 .....	62
5.2 Non-Dimensional Shear Stress Distribution Near The Banks Yen(18), Run 2 .....	63
5.3 Non-Dimensional Shear Stress Distribution Near The Banks Varshney and Grade(14) Run 1 .....	64
5.4 Non-Dimensional Shear Stress Distribution Near The Banks Steffler(12) Run 1 .....	65
5.5 Definition of Zones for a Curved Channel. ....	67
5.6 Minimum Velocity Near the Outer Bank .....	74
5.7 Non-Dimensional Longitudinal Velocity Distributions Near the Outer Bank, Ippen and Drinker(6) Run 1 .....	75
5.8 Non-Dimensional Longitudinal Velocity Distributions Near the Outer Bank, Ippen and Drinker(6) Run 2 .....	76
5.9 Non-Dimensional Longitudinal Velocity Distributions Near the Outer Bank, Ippen and Drinker(6) Run 3 .....	77
5.10 Non-Dimensional Longitudinal Velocity Distributions Near the Outer Bank, Ippen and Drinker(6) Run 4 .....	78
5.11 Non-Dimensional Longitudinal Velocity Distributions Near the Outer Bank, Ippen and Drinker(6) Run 5 .....	79
5.12 Non-Dimensional Longitudinal Velocity Distributions Near the Outer Bank, Ippen and Drinker(6) Run 6 .....	80

Figure	Page
5.13 Non-Dimensional Longitudinal Velocity Distributions Near the Outer Bank, Ippen and Drinker(6) Run 7 .....	81
5.14 Non-Dimensional Longitudinal Velocity Distributions Near the Outer Bank, Yen(18) Run 1 .....	82
5.15 Non-Dimensional Longitudinal Velocity Distributions Near the Outer Bank, Yen(18) Run 2 .....	83
5.16 Non-Dimensional Longitudinal Velocity Distributions Near the Outer Bank, Yen(18) Run 3 .....	84
5.17 Non-Dimensional Longitudinal Velocity Distributions Near the Outer Bank, Varshney and Grade(14) Run 1 .....	85
5.18 Non-Dimensional Longitudinal Velocity Distributions Near the Outer Bank, Varshney and Grade(14) Run 2 .....	86
5.19 Non-Dimensional Longitudinal Velocity Distributions Near the Outer Bank, Varshney and Grade(14) Run 3 .....	87
5.20 Non-Dimensional Longitudinal Velocity Distributions Near the Outer Bank, Francis and Asfari(4) Run 1 .....	88
5.21 Non-Dimensional Longitudinal Velocity Distributions Near the Outer Bank, Francis and Asfari(4) Run 2 .....	89
5.22 Non-Dimensional Longitudinal Velocity Distributions Near the Outer Bank, de Vriend(15) Run 1 .....	90
5.23 Non-Dimensional Longitudinal Velocity Distributions Near the Outer Bank, de Vriend(15) Run 2 .....	91
5.24 Non-Dimensional Longitudinal Velocity Distributions Near the Outer Bank, Steffler(12) Run 1 .....	92
5.25 Non-Dimensional Longitudinal Velocity Distributions Near the Outer Bank, Steffler(12) Run 2 .....	93

Figure	Page
5.26 Non Dimensional Development of Longitudinal Velocity Near the Outer Bank for Rectangular Channels .....	95
5.27 Non Dimensional Development of Longitudinal Velocity Near the Outer Bank for Trapezoidal Channels .....	96
5.28 Non Dimensional Development of Longitudinal Velocity Near the Outer Bank for Rectangular and Trapezoidal Channels .....	97
5.29 Ultimate Velocity Near the Outer Bank .....	99
5.30 Length Scale for Longitudinal Velocity Development .....	101
5.31 Length Scale for Longitudinal Velocity Development .....	102
5.32 Length Scale for Longitudinal Velocity Development - Log .....	103
6.1 The Estimated Non-Dimensional Longitudinal Velocity Near the Outer Bank .....	107

## List of Symbols

A	a constant in an equation
b	half of the channel mean width
B	channel mean width
C	Chezy coefficient
$C_c$	non dimensional Chezy coefficient
$C_c'$	the suggested critical point for erosion area
$C_z$	non-dimensional Chezy coefficient
$C_z'$	non-dimensional Chezy coefficient in z direction
$C_x$	non-dimensional Chezy coefficient in x direction
D	a term in an equation
f	friction factor
$f_1, g_1$	functions
$F_r$	Froude number
g	acceleration due to gravity
H	water depth
$H_0$	average flow depth
$H'$	non-dimensional depth deviation
h	superelevation
$I_1, J_1$	integral functions
k	coefficient in the length scale equation
K	an integration constant
L	longitudinal velocity development length scale
$L_s$	superelevation development length scale
m	velocity profile exponent
q	a constant in an equation
Q	flow discharge

$r$	local radius of curvature
$R$	the radius of curvature of channel centerline
$R_e$	Reynolds Number
$S$	longitudinal slope of the water surface
$S_b$	longitudinal channel bed slope
$S_t$	transverse slope of the water surface
$U$	longitudinal velocity near outer bend
$U_1$	the minimum velocity near the outer bank
$U_m$	mean velocity
$U_o$	ultimate velocity near the outer bank
$u$	longitudinal velocity
$u_{s0}$	mean surface velocity at a section
$u_{st}$	difference between surface velocity near outer bank and $u_{s0}$
$\bar{u}$	depth averaged velocity
$\bar{u}_c$	depth averaged velocity along channel centerline
$u_*$	the friction velocity
$u_s$	surface velocity in x direction
$u^*$	non-dimensional longitudinal velocity
$v$	vertical velocity
$v_s$	surface velocity in y direction
$w$	lateral velocity
$w_s$	surface velocity in z direction
$w^*$	non-dimensional lateral velocity
$u', w'$	velocity perturbations
$x$	distance from the entrance of the bend into the curve



$x_b$	distance measured from 0.5B downstream of bend entrance
$x'_b$	$x_b$ which is nondimensionalized by $H_0$
$x_c$	distance which measured from the entrance of the bend to the start of erosion control works
$x$	longitudinal co-ordinate
$y$	vertical co-ordinate
$z$	lateral co-ordinate
$\alpha, \beta$	non-dimensional coefficient
$\epsilon$	eddy viscosity
$\xi$	vertical vorticity = $\frac{y}{H}$
$\eta$	lateral vorticity = $\frac{z}{b}$
$\theta$	bend angle
$\kappa$	Von Karman's constant $\approx 0.4$
$\mu$	$(\frac{\bar{u}}{\bar{u}_c})^2$
$\nu$	kinematic viscosity
$\rho$	mass density of water
$\sigma$	non-dimensional downstream coordinate = $x/B$
$\tau$	local shear stress
$\tau_0$	average bed shear stress
$\tau_{x0}$	longitudinal bed shear stress
$\tau_{yz}$	fluid shear stress
$\tau_{z0}$	lateral shear stress

## 1. Introduction .

River bank erosion is a very common and serious problem in curved channels. Thousands of hectares of valuable land are destroyed by bank erosion. In Canada, bank stabilization works involve the expenditure of millions of dollars every year. The immediate practical interest has been in developing methods to stabilize the streams and prevent further progression of the meanders. The design of stabilization works is hampered however at present by a lack of prediction methods for the erosive force of curved channel flows. This leads to costly overdesigned or unreliable protection.

In the past three decades many investigators have contributed their efforts to studying this complicated three dimensional flow phenomenon. However, results from these studies were seldom correlated with each other. This study has tried to combine data from previous significant investigations in order to derive generally applicable results. As a first attempt, the amount of data was reduced by considering only flat bed flume data. In general, more detailed data was available which was obtained under more controlled circumstances.

It is of interest to accomplish the following items :

- (1) Study mechanics of flow behavior in the bend.
- (2) Use the existing data to develop longitudinal distribution curves.

(3) Predict distribution of erosive attack on the banks of curved channels.

(4) Determine the critical points for starting and ending or changing the gradation of side bank protection.

Finally, it is hoped that these findings may ultimately have practical value in determining the degree and areal extent of protective works required to stabilize natural stream channels.

Chapters 2 and 3 of this study review the significant theoretical developments and present a theoretical analysis in which equations which govern the longitudinal velocity distribution through the bend are developed. These equations lead to some understanding the flow characteristics. Chapter 4 reviews the significant experimental investigations of flow in channel bends. Chapter 5 is an analysis of these experiments. The analysis method is to define channel zones, collect data from each experiment, develop longitudinal velocity distribution curves, and compare and correlate the results. Chapter 6 presents an application procedure, which may be used in practical river engineering designs.

## 2. Review of the Significant Theoretical Studies

### 2.1 Introduction

The purpose of this research is to develop some scales useful in the prediction of erosion force on the banks of a curved channel. Therefore, the theoretical study will only focus on the derivation of the longitudinal velocity distribution along the outer banks.

Of the many theoretical analyses in the literature two have been selected because they are relatively simple and essentially one dimensional. The assumptions made in these two models are steady, subcritical flow in alluvial channel bends with uniform sediment and constant width. The radius of the curves are large compared to the width and the longitudinal velocity is large compared with the transverse velocity. The Chezy number  $C$  was assumed the same everywhere. These models were both intended for the prediction of the bed configuration and therefore provided an estimation of the velocity distribution.

#### 2.1.1 Co-ordinate System

The co-ordinate system will be based on Figures 2.1 and 2.2, where  $x$  and  $u$  are the longitudinal direction and velocity,  $z$  and  $w$  are the lateral direction and velocity, and  $y$  and  $v$  are the vertical direction and velocity. The

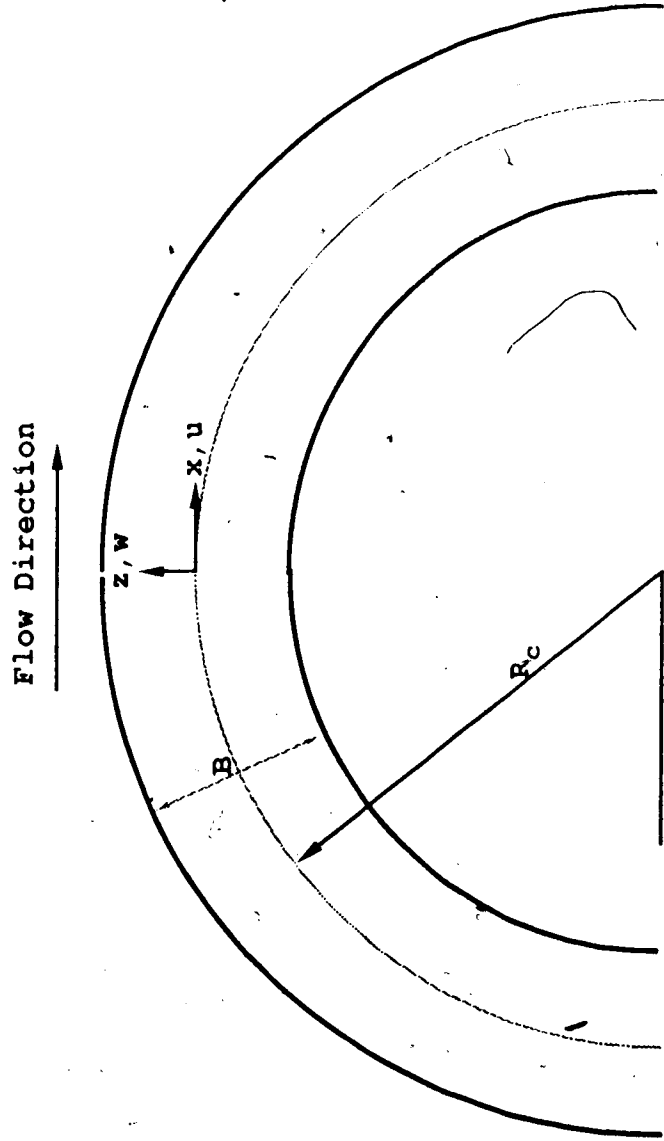


Figure 2.1 Definition Sketch - plan

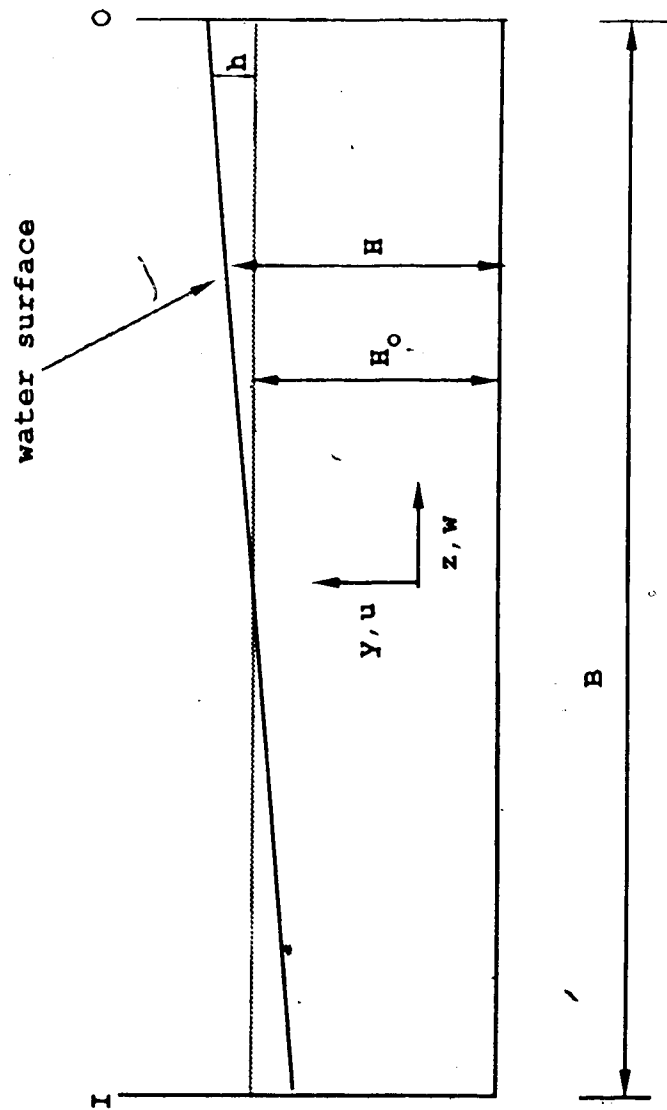


Figure 2.2 Definition Sketch - Cross Section

radius of curvature of the channel centerline is  $R_c$ . The channel width is  $B$  and the average flow depth across the channel is given by  $H_o$ .

The radius of curvature of any point across the channel is given by  $r$  which is related to  $R_c$  and  $z$

$$r = R_c + z \quad [2.1]$$

$h$  (refer to Figure 2.2) is the elevation of the water surface above  $H_o$  for a channel with a flat bed. The depth of flow is represented by  $H$  and is given by:

$$H = H_o + h \quad [2.2]$$

## 2.2 Odgaard (1986)

This theoretical study was for a steady, subcritical, turbulent flow in alluvial channel curves with uniform bed sediment. It was assumed that the banks affected the flow pattern within a distance of about one water depth. Other limitations were:

1. the channel width was constant;
2. the centerline radius of curvature was large compared with channel width;
3. the flow depth was small compared with the width;

4. cross-channel (transverse) velocity components were small compared with longitudinal velocity components;
5. the turbulence was isotropic.

### 2.2.1 Governing Equations

The equations of motion for the longitudinal and transverse velocity components could be given as follows (in the present coordinate system):

$$u \frac{\partial u}{\partial x} + v \frac{\partial u}{\partial y} + w \frac{\partial u}{\partial z} + \frac{uw}{r} = gS_s + \frac{\partial}{\partial y} \left( \epsilon \frac{\partial u}{\partial y} \right) \quad [2.3]$$

$$u \frac{\partial w}{\partial x} - \frac{u^2}{r} = gS_r + \frac{\partial}{\partial y} \left( \epsilon \frac{\partial w}{\partial y} \right) \quad [2.4]$$

where,

$r$  = local radius of curvature

$\epsilon$  = eddy viscosity

$S$  and  $S_r$  = longitudinal and transverse slope of the water surface, respectively.

Under the aforementioned conditions, only one friction (Reynolds Stress) term was considered in each equation; and viscous terms were neglected. The equation of motion for the vertical velocity component was reduced to the hydrostatic condition.



The velocity profile for longitudinal velocity,  $u$ , was assumed to be given by the traditional power law

$$\frac{u}{\bar{u}} = \frac{m+1}{m} \left(\frac{y}{H}\right)^{1/m} \quad [2.5]$$

where

$\bar{u}$  = depth averaged velocity

$H$  = water depth

$m$  = friction parameter (velocity profile exponent)

The parameter  $m$  was related to the shear velocity  $u_*$ , Darcy-Weisbach's friction factor  $f$ , Chezy coefficient  $C$  and non-dimensional conveyance  $C_c$  as

$$m = \frac{\kappa \bar{u}}{u_*} = \kappa \sqrt{\frac{8}{f}} = \kappa C / \sqrt{g} = \kappa C_c \quad [2.6]$$

where

$\kappa$  = Von Karman's constant  $\approx 0.4$

$u_* = \left(\frac{\tau}{\rho}\right)^{0.5}$ ;  $\tau$  = bed shear stress;  $\rho$  = fluid density.

### 2.2.2 Reduction of Equations

The solution strategy for longitudinal velocity distribution consisted of: (1) converting Equation 2.4 into an ordinary differential equation for  $w$  at the water surface  $w_s$ ; (2) converting Equation 2.3 into an ordinary differential equation for  $\bar{u}$ .

With  $\epsilon = \kappa u_s y(1-y/H)$ ; and  $\frac{\partial u}{\partial y} = u_s/(\kappa y)$ , Equation 2.3, taken at water surface  $y = H$  (subscript s denoted the velocity at water surface), was reduced to

$$u_s \frac{\partial u_s}{\partial x} + v_s \frac{\partial u_s}{\partial y} + w_s \frac{\partial u_s}{\partial z} + \frac{u_s w_s}{r} = gS - \frac{u_s^2}{H} \quad [2.7]$$

or, in terms of  $\bar{u}$ , with  $u_s = \kappa \bar{u}/m$ ,  $v_s \approx 0$  and  $w_s = \bar{u}(m+1)/m$

$$\frac{1}{2} \left(\frac{m+1}{m}\right)^2 \frac{\partial \bar{u}^2}{\partial x} + \frac{\kappa^2}{m^2 H} \bar{u}^2 = gS - \left(\frac{m+1}{m}\right) w_s \left(\frac{\bar{u}}{r} + \frac{\partial \bar{u}}{\partial z}\right) \quad [2.8]$$

Along the channel centerline, both  $\bar{u}$  and water depth  $H$  were practically constant (De Vriend and Geldof 1983; Kikkawa, et al 1976; Odgaard 1984; Thorne, et al 1983) and the centerline form of Equation 2.8 became

$$\frac{\kappa^2 \bar{u}_c^2}{m_c^2 H_c} = gS_c - gS'_c \quad [2.9]$$

in which  $gS'_c$  is the last term on the right-hand side of Equation 2.8 taken at  $r=r_c$ . Subscript c denoted the centerline values. By introducing the non-dimensional streamwise coordinate  $\sigma = x/B$ , dividing by  $\bar{u}_c^2$ , and using Equation 2.9, Equation 2.8 took the following form along a path at constant distance from the channel centerline:

$$\frac{d}{d\sigma} \left(\frac{\bar{u}}{\bar{u}_c}\right)^2 + G \frac{H_c}{H} \left(\frac{\bar{u}}{\bar{u}_c}\right)^2 = G \frac{R_c}{r} \left(\frac{m}{m_c}\right)^2 \quad [2.10]$$

in which

$$G = \frac{2\kappa^2}{(m+1)^2} \frac{B}{H_c} \quad [2.11]$$

When  $d\bar{u}^2/d\sigma=0$ , which will occur in the fully developed part of long, constant-radius curves, Equation 2.8 yielded

$$\left(\frac{\bar{u}}{\bar{u}_c}\right)^2 = \left(\frac{m}{m_c}\right)^2 \frac{H}{H_c} \frac{R_c}{r} \quad [2.12]$$

in which  $\bar{u}_c^2 = \frac{m_c^2}{\kappa} g S_o H_c$ .

$$u^* = \frac{\bar{u}}{\bar{u}_c} = \frac{m}{m_c} \left(\frac{H}{H_c} \frac{R_c}{r}\right)^{1/2} \quad [2.13]$$

With  $\mu = \left(\frac{\bar{u}}{\bar{u}_c}\right)^2$ , Equation 2.10 was reduced to:

$$\frac{d\mu}{d\sigma} + k\mu = q \quad [2.14]$$

in which

$$k = G \frac{H_c}{H}$$

$$q = G \frac{R_c}{r} \left(\frac{m}{m_c}\right)^2$$

This analysis can be extended to derive a length scale for longitudinal velocity. Define the non-dimensional development length,  $L$ , as the distance over which the velocity changes to the average of its initial and final

values divided by the channel depth.

The solution of Equation 2.14 is:

$$\mu = Ae^{-kx} + \frac{q}{k} \quad [2.15]$$

For  $x = 0$  at  $0.5B$  downstream of the curve entrance,  $\mu_1$  can be obtained as:

$$\mu_1 = \frac{q}{k} + A \quad [2.16]$$

therefore

$$\frac{U_1}{U_m} = \left( \frac{q}{k} + A \right)^{1/2} \quad [2.17]$$

The ultimate value of  $\mu$ ,  $\mu_u$ , happens as  $x \rightarrow \infty$ , is therefore

$$\mu_u = \frac{q}{k} \quad [2.18]$$

$$\frac{U_u}{U_m} = \left( \frac{q}{k} \right)^{1/2} \quad [2.19]$$

Since  $\frac{U_L}{U_m}$  is the average of  $\frac{U_1}{U_m}$  and  $\frac{U_u}{U_m}$ . Then

$$\frac{U_L}{U_m} = \frac{1}{2} \left( \left( \frac{q}{k} + A \right)^{1/2} + \left( \frac{q}{k} \right)^{1/2} \right) \quad [2.20]$$

Using Equation 2.15

$$\frac{U_L}{U_m} = \left( A e^{-kx_L} + \frac{q}{k} \right)^{1/2} \quad [2.21]$$

Therefore,

$$\frac{1}{2} \left( \left( \frac{Q}{k} + A \right)^2 + \left( \frac{Q}{k} \right)^2 \right) = \left( A e^{kx} + \frac{Q}{k} \right)^2 \quad [2.22]$$

Squaring both sides of the equation gives

$$\frac{1}{4} \left( 2 \frac{Q}{k} + A + 2 \left( \left( A + \frac{Q}{k} \right) \left( \frac{Q}{k} \right) \right)^2 \right) = A e^{kx} + \frac{Q}{k} \quad [2.23]$$

Therefore

$$\begin{aligned} e^{kx} &= \frac{1}{4A} \left( A + 2 \frac{Q}{k} + 2 \left( \left( A + \frac{Q}{k} \right) \left( \frac{Q}{k} \right) \right)^2 \right) = D \\ -kx &= \ln D \\ x &= -\frac{\ln D}{k} \end{aligned}$$

and if  $L = \frac{x_b}{H_c}$ , therefore,

$$L = -\frac{\ln D}{k} \frac{B}{H_c} \quad [2.24]$$

An estimate of  $\frac{U_1}{U_m}$  is given by Steffler(12) as :

$$\frac{U_1}{U_m} = 1 - \frac{B}{2R_c} \quad [2.25]$$

Subsequently, the value A can be determined as

$$A = \left( 1 - \frac{B}{2R_c} \right)^2 - \frac{R_c}{r} \frac{H}{H_c} \left( \frac{m}{m_c} \right)^2 \quad [2.26]$$

Substituting the expressions for A, k, q, G, and m into

Equations 2.17 and 2.19 to define the value  $D$  and  $L$ .

Equation 2.24 becomes

$$L = \frac{\ln D}{2\kappa} \frac{H_1}{H} (\kappa^2 C_s^2 + 2\kappa C_s + 1) \quad [2.27]$$

### 2.3 Engelund (1974)

The study was for firstly, a steady fully developed uniform flow in wide rectangular channel and secondly a developing flow. Only the middle part of the channel, where the vertical velocity components were negligible, was considered because the circulation pattern was unaffected by the existence of side walls. The channel was wide and the mean radius of curvature  $R_c$ , was assumed large as compared with the channel width.

#### 2.3.1 Governing Equations

The equations of motion for the longitudinal and transverse velocity components were previously given as Equation 2.3 and 2.4. The velocity profile for longitudinal velocity,  $u$ , was assumed to be given by a quadratic profile with wall slip.

#### 2.3.2 Reduction of Equations

Under the above developed flow assumptions, the flow equations were reduced to

$$-\frac{u^2}{r} = -\frac{\partial}{\partial r}(gh) + \epsilon \frac{\partial^2 w}{\partial y^2} \quad [2.28]$$

$$gS + \epsilon \frac{\partial^2 u}{\partial y^2} = 0 \quad [2.29]$$

where

$h$  = the superelevation and the vertical coordinate was considered positive downwards.

Except for wall region, the equation of continuity was

$$\frac{\partial}{\partial r}(rw) = 0 \quad [2.30]$$

The physical meaning of Equation 2.28 and 2.29 was easily realized. The left hand side of Equation 2.28 was the centrifugal force per unit mass, which was mainly balanced by the pressure gradient and friction term on the right hand side. Equation 2.29 was reduced to the shear stress and weight terms. However, note that for simple geometrical reasons the slope,  $S$ , must follow the law:

$$Sr = S_c R_c \quad [2.31]$$

in which  $S_c$  = the slope at the middle of the channel,

$r = R_c$ .

To solve the flow equations, the following substitutions were introduced

$$u = \frac{UH}{r} f\left(\frac{Y}{H}\right) \quad [2.32]$$

$$w = U \sqrt{\frac{\bar{R}_c}{r}} \phi\left(\frac{Y}{H}\right) \quad [2.33]$$

$$h = -\frac{aU^2}{g} \frac{R_c}{r} \quad [2.34]$$

in which  $U$  = some reference velocity, for instance, taken as the surface velocity in the middle of the stream; and  $a$  = a nondimensional factor which was determined by the last boundary condition. The eddy viscosity,  $\epsilon$ , was assumed to vary as  $u$ , so that

$$\epsilon = \epsilon_0 \sqrt{\frac{\bar{R}_c}{r}} \quad [2.35]$$

After insertion in the flow equations, the following pair of ordinary differential equations were obtained

$$f'' = \frac{Hu_s}{\epsilon_0} (a - \phi^2) \quad [2.36]$$

$$\phi'' = -\frac{gHS}{\epsilon U} \quad [2.37]$$

in which the primes indicated derivation with respect to the variable,  $\eta = \frac{Y}{H}$ . The surface velocity,  $u_s$ , varied with  $r$ , but if the channel width was small compared with the radius of curvature, this variation might be neglected.



After integration Equation 2.37 became

$$\phi = \int 6.5 \frac{u_s}{U} (1-\eta)^2 \quad [2.38]$$

Equation 2.38 was inserted into Equation 2.36, which was then integrated twice, taking account of the boundary conditions as follows

1. The shear stress must vanish at the water surface

$$f'(1) = 0 \quad [2.39]$$

2. In a steady and uniform transverse circulation the total flux through a vertical must vanish, thus

$$\int_0^1 f(\eta) d\eta = 0 \quad [2.40]$$

Then the function,  $f$ , is found to be given by

$$\frac{\epsilon_0}{Hu_s} f(\eta) = \frac{1}{2}(1-\eta)^2(a-1) + \frac{1}{6} \beta(1-\eta)^4 - \frac{1}{30} \beta^2(1-\eta)^6 + K \quad [2.41]$$

in which

$K =$  an integration constant.

$$\beta = 6.5 \frac{u_s}{U}$$

To obtain an improved description of the flow in a meander bend with a variable radius of curvature, the

coordinates  $x$  and  $y$ , defined previously were applied, and it was still assumed that the channel walls are fixed and the superelevation small. The longitudinal component of the flow equation was assumed as

$$\bar{u} \frac{\partial \bar{u}}{\partial x} = - \frac{\partial}{\partial x} (gh) - \frac{\bar{u}^2 r}{C_*^2 H R_c} \quad [2.42]$$

To proceed further Equation 2.42 was linearized by

$$\bar{u} = U_m (1 + u') \quad [2.43]$$

and assuming  $u'$  to be so small that second and higher-order terms were neglected. Similarly, the local depth,  $H$ , was written as

$$H = H_0 (1 + \xi) \quad [2.44]$$

in which  $\xi$  was also assumed to be a small quantity. Substitution of Equation 2.44 into Equation 2.42 for a constant radius single bend resulted in the following first-order differential equation.

$$\frac{du'}{dx} + ku' = q \quad [2.45]$$

in which

$$k = \frac{2}{C_*^2 H}$$

$$q = \frac{2}{C_*^2 H} \xi$$

The solution of Equation 2.45 can be written as below:

$$u' = \frac{q}{k} + A e^{-kx_b} \quad [2.46]$$

when  $x_b=0$ ,  $u' = \xi + A$ ; the minimum velocity  $\frac{U_1}{U_m} = 1 + \xi + A$ .  
If  $x_b \rightarrow \infty$ ,  $u' \approx \xi$ , therefore the flow is in the ultimate condition. The average of these two velocities is

$$\frac{A}{2} = A e^{-kx_b} \quad [2.47]$$

$$-\ln 2 = -\frac{2}{C_*^2 H} x_b \quad [2.48]$$

let  $L = \frac{x_b}{H_0}$ . Therefore the length scale is given by

$$L = \frac{\ln 2}{2} \frac{H}{H_0} C_*^2 \quad [2.49]$$

## 2.4 Conclusion

Both the analyses of Odgaard and Engelund provide estimates of the development length for longitudinal velocity distribution and for the ultimate (developed) velocity near the outer bank. Since neither analysis included the effect of the secondary flow on velocity redistribution this fully developed velocity is

underestimated. It is also uncertain whether the secondary flow affects the development length. In the next chapter an analysis is attempted which addresses these concerns.

### 3. Theoretical Analysis

#### 3.1 Introduction

The flow in a meandering channel is complicated by its curvilinear characteristics. It is difficult to fully understand with the existing knowledge. The previous analyses did not take into account the effect of secondary flow. In particular, they predict a virtually uniform cross sectional distribution in the fully developed situation for rectangular channels. Experiments, however, indicate a significant skewing towards the outside bank. Therefore, it would be of value to attempt further analysis.

Using a similar method to Odgaard(9) and Engelund (3) (in Chapter 2), equations are developed to predict the high velocity areas in a curved channel for practical engineering designs. This research will be focused on the deviation of the longitudinal velocity from the mean channel value. Therefore once the velocity equations are derived they will be simplified by elimination of mean surface velocity and mean depth of the cross-section and their corresponding equations. The remaining equations are linearized by noting that the distribution parameters and mean lateral velocity are small compared to the mean velocity and depth. The final result is a set of first-order linear differential equations.

### 3.2 Governing Equation

The channel geometry and co-ordinate system in this chapter is as shown in Figures 2.1 and 2.2 and as used previously in Chapter 2.

#### 3.2.1 General Assumptions

In order to limit the problem, the distribution of velocities, shear stresses and depth at a section are assumed to be similar from section to section. Previous experimental data indicated that this is only approximately true.

#### 3.2.2 Equations of Motion

The longitudinal velocity in the bend can be derived from Navier-Stokes equations. Once derived the equations are further simplified by elimination of mean velocity at a section,  $u_{so}$ , and mean depth at a section,  $H_0$  and their corresponding equations.

$$u \frac{\partial u}{\partial x} + v \frac{\partial u}{\partial y} + w \frac{\partial u}{\partial z} + \frac{uw}{r} = - \frac{1}{\rho} \frac{\partial P}{\partial x} + \frac{1}{\rho} \frac{\partial \tau_{xy}}{\partial y} + gS \quad [3.1]$$

$$u \frac{\partial v}{\partial x} + v \frac{\partial v}{\partial y} + w \frac{\partial v}{\partial z} = - \frac{1}{\rho} \frac{\partial P}{\partial y} + \frac{1}{\rho} \frac{\partial \tau_{yy}}{\partial y} - g \quad [3.2]$$

$$u \frac{\partial w}{\partial x} + v \frac{\partial w}{\partial y} + w \frac{\partial w}{\partial z} - \frac{u^2}{r} = - \frac{1}{\rho} \frac{\partial P}{\partial z} + \frac{1}{\rho} \frac{\partial \tau_{zy}}{\partial y} \quad [3.3]$$

$$\frac{\partial u}{\partial x} + \frac{\partial v}{\partial y} + \frac{\partial w}{\partial z} = 0 \quad [3.4]$$

for a shallow flow, Equation 3.2 reduces to :

$$\frac{\partial P}{\partial y} = -\rho g$$

$$P = -\rho g(H-y) \quad [3.5]$$

Substitute Equation 3.5 into Equation 3.1 and 3.3, and change to conservation form

$$\frac{\partial u^2}{\partial x} + \frac{\partial uv}{\partial y} + \frac{\partial uw}{\partial z} + \frac{uw}{r} = -g \frac{\partial H}{\partial x} + \frac{1}{\rho} \frac{\partial \tau_{xy}}{\partial y} + gS \quad [3.6]$$

$$\frac{\partial uw}{\partial x} + \frac{\partial vw}{\partial y} + \frac{\partial w^2}{\partial z} - \frac{u^2}{r} = -g \frac{\partial H}{\partial z} + \frac{1}{\rho} \frac{\partial \tau_{yz}}{\partial y} \quad [3.7]$$

Using boundary conditions

$$u = v = w = 0 \text{ at } y = 0$$

$$v|_H = \frac{dH}{dt} \text{ at } y = H$$

Integrate with respect to  $y$  from 0 to  $H$ . Equation 3.4 is reduced to

$$\frac{\partial}{\partial x} \int_0^H u \, dy + \frac{\partial}{\partial z} \int_0^H w \, dy = 0 \quad [3.8]$$

By the top boundary condition, Equation 3.6 is reduced to

$$\begin{aligned} & \frac{\partial}{\partial x} \int_0^H u^2 \, dy + \frac{\partial}{\partial z} \int_0^H uw \, dy + \int_0^H \frac{uw}{r} \, dy \\ & = -g H \frac{\partial H}{\partial x} - \frac{\tau_{x0}}{\rho} + g S H \end{aligned} \quad [3.9]$$

and Equation 3.7 is reduced to

$$\begin{aligned} & \frac{\partial}{\partial x} \int_0^H uw \, dy + \frac{\partial}{\partial z} \int_0^H w^2 \, dy - \int_0^H \frac{u^2}{r} \, dy \\ & = -g H \frac{\partial H}{\partial z} - \frac{\tau_{z0}}{\rho} \end{aligned} \quad [3.10]$$

Next, integrate across the channel for  $z$  from  $z = -b$  to  $b$ .

Equation 3.8 becomes

$$\int_{-b}^b \frac{\partial}{\partial x} \int_0^H u \, dy \, dz + \int_{-b}^b \frac{\partial}{\partial z} \int_0^H w \, dy \, dz = 0 \quad [3.11]$$

It is assumed that there is no lateral inflow from the channel side boundary, and since the flow discharge is also assumed to be constant, Equation 3.11 becomes

$$\frac{d}{dx} \int_{-b}^b \int_0^H u \, dy \, dz = 0 \quad [3.12]$$



Similarly, Equation 3.9 is reduced to

$$\begin{aligned} & \frac{d}{dx} \int_{-b}^b \int_0^H u^2 dy dz + 2 \int_{-b}^b \int_0^H \frac{uw}{R} dy dz \\ &= -\frac{g}{2} \frac{d}{dx} \int_{-b}^b H^2 dz - \int_{-b}^b \frac{\tau_{x0}}{\rho} dz + g S \int_{-b}^b H dz \end{aligned} \quad [3.13]$$

and Equation 3.10 becomes

$$\begin{aligned} & \frac{d}{dx} \int_{-b}^b \int_0^H u w dy dz - \int_{-b}^b \int_0^H \frac{H u^2}{R} dy dz \\ &= -\frac{g}{2} \left[ H^2 \right]_{-b}^b - \int_{-b}^b \frac{\tau_{z0}}{\rho} dz \end{aligned} \quad [3.14]$$

If Equation 3.8 is multiplied by  $z$  and integrated with respect to  $z$  from  $-b$  to  $b$ , the mass moment distribution can be obtained by

$$\frac{\partial}{\partial x} \int_{-b}^b \int_0^H z u dy dz = \int_{-b}^b \int_0^H w dy dz \quad [3.15]$$

Repeat the same process with Equation 3.9 to procure the moment of momentum distribution

$$\begin{aligned} & \frac{\partial}{\partial x} \int_{-b}^b \int_0^H z u^2 dy dz - \int_{-b}^b \int_0^H u w dy dz \\ &= -\frac{g}{2} \frac{d}{dx} \int_{-b}^b z H^2 dz - \int_{-b}^b z \frac{\tau_{x0}}{\rho} dz + g S \int_{-b}^b z H dz, \end{aligned} \quad [3.16]$$

Multiply Equation 3.7 by  $y$  and integrate with respect to  $y$  from 0 to  $H$  and  $z$  from  $-b$  to  $b$  the equation 3.7 becomes

$$\begin{aligned} \frac{d}{dx} \int_{-b}^b \int_0^H y u w \, dy \, dz + \int_{-b}^b \int_0^H \frac{\gamma u^2}{R} \, dy \, dz \\ = \frac{g}{6} \left[ H^3 \right]_{-b}^b - \int_{-b}^b \int_0^H \tau_{yz} \, dy \, dz \end{aligned} \quad [3.17]$$

### 3.2.3 Summary of the Motion Equations in Integral Forms

1. Equation 3.12

$$\frac{d}{dx} \int_{-b}^b \int_0^H u \, dy \, dz = 0$$

2. Equation 3.13

$$\begin{aligned} \frac{d}{dx} \int_{-b}^b \int_0^H u^2 \, dy \, dz + \int_{-b}^b \int_0^H \frac{uw}{R} \, dy \, dz \\ = -\frac{g}{2} \frac{d}{dx} \int_{-b}^b H^2 \, dz - \int_{-b}^b \frac{\tau_{x0}}{\rho} \, dz + g S \int_{-b}^b H \, dz \end{aligned}$$

3. Equation 3.14

$$\begin{aligned} \frac{d}{dx} \int_{-b}^b \int_0^H u w \, dy \, dz - \int_{-b}^b \int_0^H \frac{H u^2}{R} \, dy \, dz \\ = -\frac{g}{2} \left[ H^2 \right]_{-b}^b - \int_{-b}^b \frac{\tau_{z0}}{\rho} \, dz \end{aligned}$$

4. Equation 3.15

$$\frac{\partial}{\partial x} \int_{-b}^b \int_0^H z u dy dz = \int_{-b}^b \int_0^H w dy dz$$

5. Equation 3.16

$$\begin{aligned} \frac{\partial}{\partial x} \int_{-b}^b \int_0^H z u^2 dy dz &= \int_{-b}^b \int_0^H u w dy dz \\ &= -\frac{g}{2} \frac{d}{dx} \int_{-b}^b z H^3 dz - \int_{-b}^b z \frac{\tau_{x0}}{\rho} dz + g S \int_{-b}^b z H dz \end{aligned}$$

6. Equation 3.17

$$\begin{aligned} \frac{d}{dx} \int_{-b}^b \int_0^H y u w dy dz &= \int_{-b}^b \int_0^H \frac{y}{R} u^2 dy dz \\ &= \frac{g}{6} \left[ H^3 \right]_{-b}^b - \int_{-b}^b \int_0^H \tau_{yz} dy dz \end{aligned}$$

### 3.2.4 Similarity Hypothesis

#### 3.2.4.1 Assumptions

Let  $\eta = \frac{y}{H}$ ,  $\zeta = \frac{z}{b}$ . Using a similarity hypothesis assume:

1.  $u = (u_{s0} + u_{sb} g_1(\zeta)) f_1(\eta)$
2.  $H = H_0 + h_b^4 g_2(\zeta)$
3.  $w = \bar{w} + w_s f_2(\eta)$

4.  $u_{sc}, u_{sb}, \bar{w}, w_s, H_0, h_1$  are functions of 'x' only.
5. Also  $u_{sb}$  is less than  $u_{sc}$ ,  $\bar{w}$  &  $w_s$  is much smaller than  $u_{sc}$ ,  $h_1$  is much smaller than  $H_0$ .
6.  $\frac{\tau_{xy}}{\rho} = (u_{sc} + u_{sb} g_1(\xi))^2 C_{tx}$
7.  $\frac{\tau_{xz}}{\rho} = (u_{sc} + u_{sb} g_1(\xi)) (\bar{w} + w_s) C_{tz}$
8.  $\frac{\tau_{xy}}{\tau_{xz}} = f_1(\eta)$

Also define

$$I_1 = \int_0^1 f_1(\eta) d\eta$$

$$I_2 = \int_0^1 f_1(\eta)^2 d\eta$$

$$I_3 = \int_0^1 f_1(\eta) f_2(\eta) d\eta$$

$$I_4 = \int_0^1 \eta f_1(\eta) d\eta$$

$$I_5 = \int_0^1 \eta f_1(\eta) f_2(\eta) d\eta$$

$$I_6 = \int_0^1 \eta f_1(\eta)^2 d\eta$$

$$I_7 = \int_0^1 f_3(\eta) d\eta$$

$$J_6 = \int_{-1}^1 \xi g_1(\xi) d\xi$$

$$J_7 = \int_{-1}^1 \xi g_2(\xi) d\xi$$

## 3.2.4.2 Formulation

With the above assumptions Equation 3.12 becomes

$$\frac{d}{dx} \int_b^b \int_0^H (u_{so} + u_{sb} g_1(\zeta)) f_1(\eta) dy dz = 0 \quad [3.18]$$

Substitute  $\eta$  and  $\zeta$  into Equation 3.18 to obtain the following equation.

$$\frac{d}{dx} \int_{-1}^1 b (u_{so} + u_{sb} g_1(\zeta)) (H_o + h_b g_2(\zeta)) \int_0^1 f_1(\eta) d\eta d\zeta = 0 \quad [3.19]$$

Finally, the equation becomes,

$$\frac{d}{dx} (2 b u_{so} H_o + J_3 u_{sb} h_b) = 0 \quad [3.20]$$

Ignore any of  $u_b$ ,  $h_b$ ,  $\bar{w}$ ,  $w_s$  in quadratic or higher order combination, then Equation 3.20 becomes

$$\frac{d}{dx} (u_{so} H_o) = 0 \quad [3.21]$$

Similarly, after substitutions and simplifications, Equations 3.13 to 3.17 are reduced to:

$$I_2 \frac{d}{dx} (2u_{so}^2 H_o) = -g \frac{d}{dx} H_o^2 - 2C_{fx} u_{so}^2 + 2gSH_o \quad [3.22]$$

$$\begin{aligned} & \frac{d}{dx} (u_{so} H_o) (I_1 \bar{w} + I_4 w_s) - \frac{I_2}{r} u_{so}^2 H_o \\ & = - \frac{g H_o h_b}{b} - C_{fz} u_{so} (-\bar{w} + w_s) \end{aligned} \quad [3.23]$$

$$I_1 \frac{d}{dx} (J_6 H_o u_{sb} + J_7 h_b u_{so}) = 2 \bar{w} \frac{H_o}{b} \quad [3.24]$$

$$\begin{aligned} & I_2 \frac{d}{dx} (J_7 h_b u_{so}^2 + 2J_6 H_o u_{sb} u_{so}) - \frac{2}{b} (I_1 \bar{w} + I_4 w_s) u_{so} H_o \\ & = - g J_7 \frac{d}{dx} h_b H_o - 2J_6 C_{fx} u_{so} u_{sb} + J_7 g S h_b \end{aligned} \quad [3.25]$$

$$\begin{aligned} & \frac{d}{dx} (2H_o^2 u_{so}) (I_4 \bar{w} + I_5 w_s) - 2 \frac{I_6}{r} H_o^2 u_{so}^2 \\ & = - \frac{g}{b} H_o^2 h_b - 2I_7 C_{fz} (-\bar{w} + w_s) H_o u_{so} \end{aligned} \quad [3.26]$$

Further simplify by assuming  $u_{so}$ ,  $H_o$  are constant and equal to the initial value of flow velocity and depth (as a uniform flow). By referring to Equations 3.21 and 3.22, which describes a backwater curve, the value of  $H_o$  and  $u_{so}$  can be determined as below:

$$H_o = \frac{C_{fx} u_{so}^2}{gS} \quad [3.27]$$

and

$$u_{so} H_o = \frac{Q}{2b} = \text{constant} \quad [3.28]$$

The remaining four equations (Equation 3.23 to 3.26) are

nondimensionalized by  $u_{so}$  or  $H_o$  and also nondimensionalize  $x$  with  $R_c$ . In addition, each equation is multiplied by  $\frac{R_c}{u_{so} H_o}$ . Finally, Equations 3.23 to 3.26 become

$$\begin{aligned} & \frac{d}{dx'} (J_{10} I_1 \bar{w}' + I_3 w_s') - I_2 \frac{R_c}{r} \\ &= -\frac{h_b'}{F_r^2} \frac{R_c}{b} - C_{fz} (-J_{10} \bar{w}' + w_s') \frac{R_c}{H_o} \end{aligned} \quad [3.29]$$

$$\frac{d}{dx'} (J_6 u_{sb}' + J_7 h_b') = 2 J_{10} \frac{\bar{w}'}{I_1} \frac{R_c}{b} \quad [3.30]$$

$$\begin{aligned} & \frac{d}{dx'} (h_b' J_7 + 2 J_6 u_{sb}') - \frac{2}{I_2} (J_{10} I_1 \bar{w}' + I_3 w_s') \frac{R_c}{b} \\ &= -\frac{J_7}{I_2 F_r^2} \frac{d}{dx} h_b' - \frac{2 J_6}{I_2} C_{fx} u_{sb}' \frac{R_c}{H_o} + \frac{J_7}{I_2} C_{fx} h_b' \frac{R_c}{H_o} \end{aligned} \quad [3.31]$$

$$\begin{aligned} & 2 \frac{d}{dx'} (J_{10} I_4 \bar{w}' + I_5 w_s') - 2 I_6 \frac{R_c}{r} \\ &= -\frac{h_b'}{F_r^2} \frac{R_c}{b} - 2 I_7 C_{fz} (-J_{10} \bar{w}' + w_s') \frac{R_c}{H_o} \end{aligned} \quad [3.32]$$

where

$$h_b' = \frac{h_b}{R_c} = h'$$

$$\bar{w}' = \frac{\bar{w}}{u_{so} J_{10}}$$

$$u_{sb}' = \frac{u_{sb}}{u_{so}} = u'$$

$$x' = \frac{x}{R_c}$$

$$w_s' = \frac{w_s}{U_{s0}} = w'$$

$$F_r^2 = \frac{U_{s0}^2}{gR_c}$$

These four equations are a set of solvable equations for the developing flow in a curved channel. To solve this set of equations, the distributions  $f_1$  and  $g_1$  may be obtained from experimental data or expressions derived for developed flow. The parameters  $F_r$ ,  $\frac{R_c}{b}$ ,  $\frac{R_c}{H_o}$ ,  $\frac{R_c}{r}$  are specified by upstream conditions and channel geometry.  $C_{fx}$  and  $C_{fz}$  must be evaluated experimentally or from a more sophisticated turbulence model. They may be found to be functions of the other parameters.

In the case of developed flow when  $\frac{d}{d\theta}(\cdot) = 0$  and  $\bar{w} = 0$  Equations 3.29 to 3.32 can be reduced to:

$$I_2 \frac{R_c}{r} = \frac{h'}{F_r} \frac{R_o}{b} + \frac{R_c}{H_o} C_{fz} w' \quad [3.33]$$

$$- 2 \frac{R_c}{b} I_3 w' = - 2 J_6 \frac{R_c}{H_o} C_{fx} u' + J_7 \frac{R_c}{H_o} C_{fx} h' \quad [3.34]$$

$$2 I_6 \frac{R_c}{r} = \frac{h'}{F_r^2} \frac{R_c}{b} + 2 I_7 \frac{R_c}{H_o} C_{fz} w' \quad [3.35]$$

By solving Equations 3.33 and 3.35, the result can be obtained as:

$$(I_2 - \frac{2}{3} I_6) \frac{H_o}{R_c} = (1 - \frac{2}{3} I_7) C_{fz} w' \quad [3.36]$$



$$(2I_7 I_2 - 2I_6) \frac{b}{R_c} = (2I_7 - 1) \frac{h'}{F_r^2} \quad [3.37]$$

therefore the secondary flow is given by

$$w' = \frac{(I_2 - 0.67I_6)}{(1 - 0.67I_7)} \frac{1}{C_{tz}} \frac{H_0}{R_c} \quad [3.38]$$

and the superelevation is given by

$$h' = \frac{2(I_7 I_2 - I_6)}{(2I_7 - 1)} F_r^2 \frac{b}{R_c} \quad [3.39]$$

Equation 3.40 gives the longitudinal velocity perturbation

$$u' = \frac{I_3}{J_6 C_{fx}} \frac{H_0}{b} w' + \frac{h'}{2} \quad [3.40]$$

therefore

$$u' = f\left(\frac{H_0}{R_c}, \frac{B}{2R_c}, F_r\right) \quad [3.41]$$

Therefore the parameters  $F_r$ , curvature, aspect ratio, are the variables of the function of the longitudinal velocity. The function  $g_1(\xi)$  represents the non-dimensional longitudinal velocity distribution across a channel. For a simple linear variation

$$g,(\xi) = \xi \quad [3.42]$$

and

$$u' = 1 + u' \xi \quad [3.43]$$

$u'$  is the non-dimensional ultimate cross sectional velocity distribution.

The comparison of these three theoretical analysis (Odgaard, Englund and the present analysis) and one of Steffler's experiments is shown in Figure 3.1. It has shown that the present analysis method is most close to the experimental result. (The exponential distribution is used for  $f(\eta)$  as detailed in the next section)

### 3.2.5 Length Scale for Developing Flow

The rearrangement of Equation 3.31 will give

$$\frac{du'}{dx'} + k u' + q = 0 \quad [3.44]$$

where

$$1. \quad k = \frac{C_{fx} R_c}{I_2 H_o}$$

$$2. \quad q = \frac{2}{I_2} (J_{10} I_1 \bar{w}' + I_3 w'_s) \frac{R_c}{b} + \frac{J_7}{I_2} C_{fx} h'_b \frac{R_c}{H_o}$$

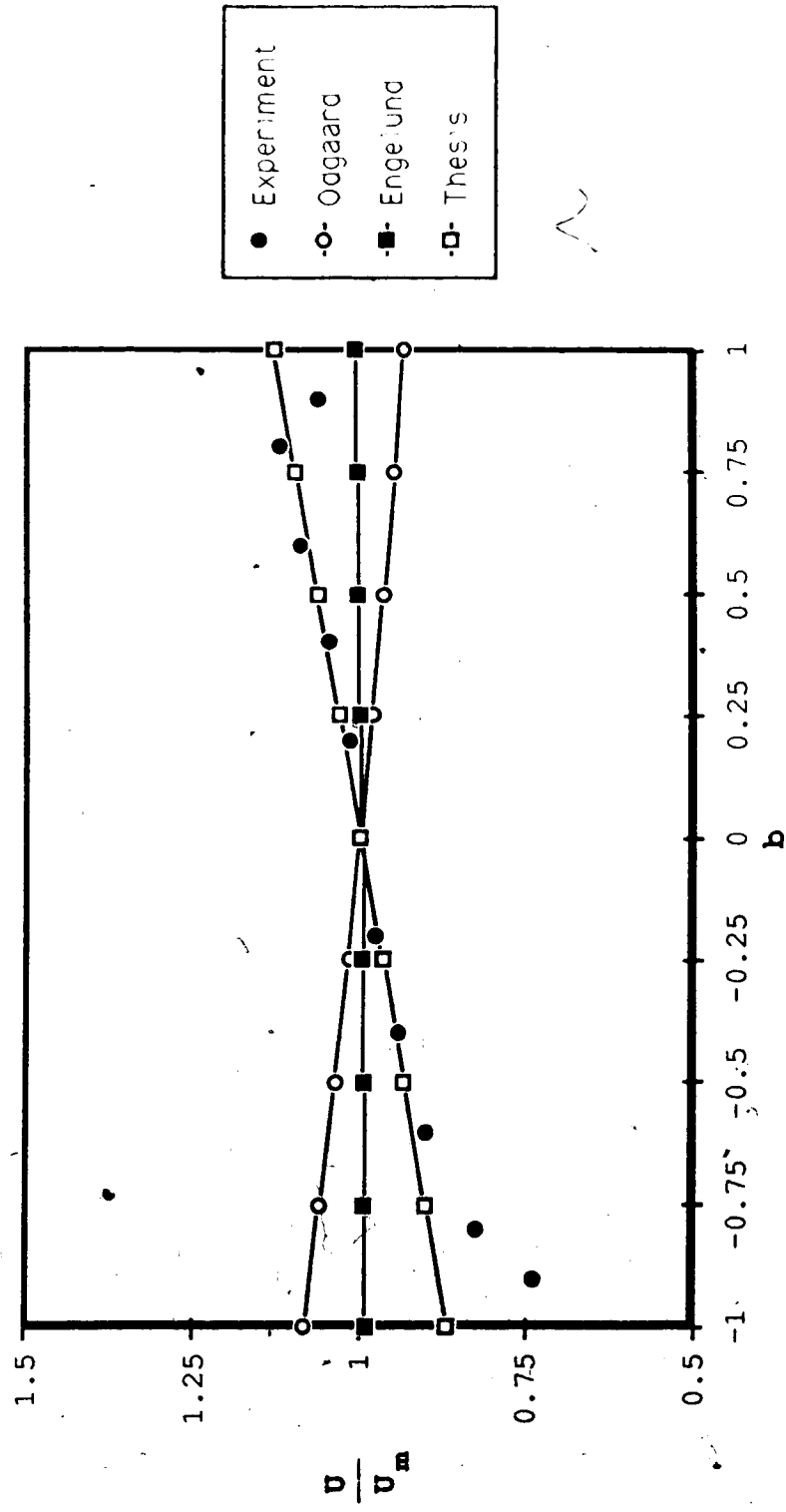


Figure 3.1 Comparison of the Ultimate Cross Sectional Velocity Distributions.

Therefore, the value of  $u'$  can be solved as

$$u' = \frac{q}{k} + A e^{-kx'} \quad [3.45]$$

in which  $q$  is not a function of  $u'$ . It may be assumed as a constant in this solution and should be negative.

Velocity distributions, presented by most studies, indicated an initial shift in longitudinal maximum velocity toward the inside of the bank, followed by the outward shift of the maximum longitudinal velocity. In other words, the minimum velocity would happen in the outer bank near the entrance of the bend. It is assumed that this minimum velocity,  $U_i$ , happens at the location of  $x_b=0$

$$U_i = U_m \left( 1 + \frac{q}{k} + A \right) \quad [3.46]$$

The ultimate velocity,  $U_u$ , occurs when  $x_b \rightarrow \infty$ .

$$U_u = U_m \left( 1 + \frac{q}{k} \right) \quad [3.47]$$

The average velocity of  $U_i$  and  $U_u$  is named  $U_L$ . It is located at the non-dimensional distance  $x'_L$  ( $L = \frac{x'_L R_c}{H_o}$ ). Therefore,

$$U_L = U_m \left( 1 + \frac{q}{k} + A e^{-kx'_L} \right) \quad [3.48]$$

$$U_L = \frac{U_i + U_o}{2} \quad [3.49]$$

then,

$$-kx'_L = \ln 0.5 \quad [3.50]$$

$$L = - \frac{\ln 0.5 R_c}{k H_o} \quad [3.51]$$

If  $k = \frac{C_{fx} R_c}{I_2 H_o}$ , therefore

$$L = - \frac{\ln 0.5}{C_{fx}} I_2 \quad [3.52]$$

in which  $I_2 = \int_0^1 f_1(\eta)^2 d\eta$ .

Recall from assumption 6 of section 3.2.5,  $C_{fx} = \frac{I_1^2}{C_s^2}$ .

Thus

$$L = -\ln 0.5 \frac{I_2}{I_1^2} C_s^2 \quad [3.53]$$

The value of  $I_1$  and  $I_2$  are defined as follow

$$f_1 = \eta^{1/m}$$

therefore

$$I_1 = \int_0^1 \eta^{1/m} = \frac{m}{m+1} \quad [3.54]$$

$$I_2 = \int_0^1 \eta^{2/m} d\eta = \frac{m}{m+2} \quad [3.55]$$

Therefore

$$L = -\ln 0.5 \frac{(m+1)^2}{m(m+2)} C_*^2 \quad [3.56]$$

in which  $m = \kappa C_*$ .

### 3.3 Conclusion

The three theoretical analyses (Odgaard, Englund, present analysis) are based on similar assumptions:

1. The ratio of radius of curvature to channel width is large.
2. Steady uniform subcritical flow in a wide rectangular channel.
3. Chezy number  $C$  is assumed the same everywhere.
4. Transverse velocity is small compared with longitudinal velocity.

The assumptions unique to each analysis are:

1. Odgaard
  - a. The channel bed was assumed immobile.
  - b. The turbulence was isotropic.
  - c. Velocity profile for longitudinal velocity was assumed to be given by the traditional power law.

- d. Flow depth distributions were a simple relationship between transverse surface velocity and transverse slope of bed.
  - e. The radial variation of  $u$  in the fully developed flow is a linear.
2. Engelund
- a. The channel bed was assumed to be composed of uniform sediment.
  - b. Secondary flow was unaffected by the side wall.
  - c. The velocities in transverse and longitudinal components were based on the given equations.
  - d. The radial variation of  $u$  in the fully developed flow is a straight line.
3. Present analysis
- a. The model is restricted to a rectangular wide channel, however, it may be extended for use in other cases.
  - b. Vertical and lateral distributions of lateral and longitudinal velocity and bed stress were assumed similar.

Longitudinal velocity profile for fully developed flow predicted by the three methods are compared with one of Steffler's experiments(12) in Figure 3.1. It is found that the present analysis method is closest to the experimental result. This is because only the present analysis considers the effect of secondary flow.

Three length scale equations 2.27, 2.49 and 3.56 are plotted in Figure 3.2. It is found the length scale is roughly proportional to  $C_1$ . Odgaard and present analysis give close results for a practical range of  $C_1$  while Engelund's results are significantly lower. In view of the assumptions made in these derivations, these results must be checked with experimental data.



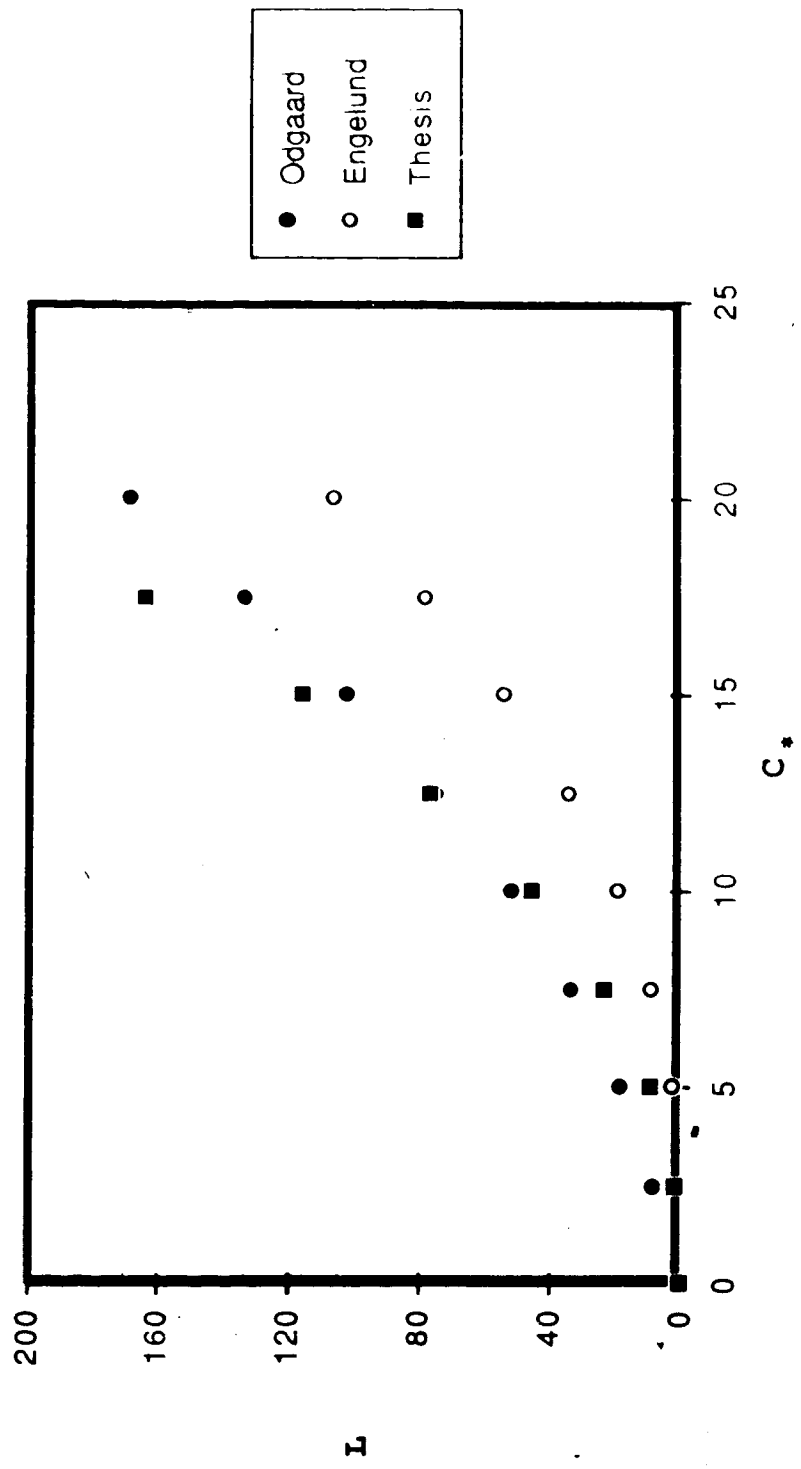


Figure 3.2 Comparison of the Three Length Scales

## 4. Review of Significant Experimental Studies

### 4.1 Introduction

The experimental studies of curved channel flow done by six researchers have been chosen for analysis. This data relates to flat bed channels and was chosen because there is more detailed data available, the data is more reliable and is generally characterized by fewer parameters. For the purpose of this analysis, descriptions of apparatus, results and conclusions will be reviewed.

### 4.2 Ippen and Drinker (1962)

The experiments were conducted in two trapezoidal flumes. In both channels the general arrangement was the same; consisting of a 6 meter long straight approach section; a single curve with a  $60^\circ$  central angle, and a 3 meter long straight exit section. The side slopes were 2:1 and the channels were constructed with horizontal inverts along all radial sections. A smooth entrance transition from the stilling basin at the upstream end of the approach channel reduced the tendencies for local separation. The flow depth was controlled by an adjustable sluice gate mounted at the exit section.

The centerline slope of each flume was 0.00055. The bottom width of the larger flume was 0.6 meters and the radius of the curve centerline was 1.5 meters. For the

smaller flume, the base width was 0.3 meters, and the curve centerline radius was 1.78 meters.

#### 4.2.1 Analysis of the Experimental Results

Some asymmetry of the velocity, shear stress, and water-surface configuration was found at station 1 test section (about 66cm upstream of the bend entrance). However the flow pattern in the bend was not caused by the upstream distortion of the flow.

The velocity distribution was according to the free-vortex (irrotational) motion for the flow through the upstream portion of the curve (stations 3-5). The free-vortex pattern broke down in the downstream portion of the curve and established a high velocity zone near the outer bank. It was caused by two major factors and depends on the stream curvature :

1. The helicoidal motion tended to move the high velocity fluid continuously toward the outer bank.
2. The separation zone that originated at the inside of the curve reduced the effective area of the section, resulting in acceleration of the constricted stream and a deflection of the flow away from the inner bank. For increased curvature, runs 1-4, the separation zone was strongly developed on the inner bank.

The flow velocity was asymmetrical in a long straight reach below the curve. The channel was too short to permit

the flow to return to normal, indicating that such a return would be fairly gradual. Therefore, a considerable length of straight channel downstream of the curve would be required.

For all seven contours of relative bed stress intensity were presented. From these diagrams velocities near the outer bank were derived by interpolating the shear half way up the outer bank. The outer bank relative velocity selected for further analysis is equal to the square root of the relative stress.

#### 4.2.2 The Experimental Conclusions

A few important conclusions were found in this investigation of the flow through a  $60^\circ$  curved trapezoidal channel.

1. Shear stress in the curved reach increased with increasing stream curvature. With a larger curvature the location of shear maxima was found in the inner bank following the entrance of the curve and near the outer bank below the exit of the curve. With lower curvature the increased shear stresses appear along the outer bank in the downstream portion of the curve.
2. The relative shear pattern was found to be independent from the flow depth and velocity but not the stream geometry.
3. This investigation showed the importance of the boundary shear stress which plays a significant role in stream

erosion and deposition and thus provides valuable design information in stream bank protection and river training.

4. Additional studies were deemed desirable to evaluate the effects of the central angle of the curve, boundary roughness, and curve combination on the maximum shear rates and their locations. "

#### 4.3 Yen (1965)

The experiment was conducted in a flume which had two identical  $90^\circ$  curves of trapezoidal section. These were set in a reversed direction and connected by a 4.27 meter straight reach. The side slope of the channel was 1:1. The bottom width of the channel was 1.83 meters and the centerline radius was 8.53 meters. A 15 cm high tail-gate was built at the end of the channel so that backwater could be controlled.

The boundary shear measurements were obtained by a Preston tube which was connected to a modified micromanometer. The outside and inside diameters of the tube were 3.18 mm and 2.44 mm respectively, and the measurements were taken at the cross sections spaced every  $11.25^\circ$  in the bend.

A Pitot tube was set in a plane parallel to the bed. It was a standard (0.47625 cm) Prandtl-type pitot but a 0.55563 cm) Prandtl-type pitot was used when the flow was slower. In

either case the Prandtl-type tube was connected to two manometers. One was a water manometer to measure piezometric head and velocity head, the other was a micromanometer for the local velocities below 2.54 cm.

#### 4.3.1 Analysis of the Experimental Results

The radial distribution of the average longitudinal velocity over a vertical was fairly uniform in the straight reach upstream of the curve entrance. However, as the flow entered the curve, it was found that the velocity in the outer bank was slower than it was in the inner bank. This phenomenon was explained by the residual spiral motion from the preceding curve, and was indicated by the longitudinal slope of the water surface. The radial distribution of the depth averaged velocity followed approximately that of a free vortex pattern. This increased velocity near the inner bank continued until a point between sections  $11.25^\circ$  and  $22.5^\circ$  of the curve was reached.

Following the section at  $22.5^\circ$ , the maximum average velocity of a section gradually shifted outward. Downstream from Section  $67.5^\circ$ , the depth of the flow near the inner bank started to increase. Downstream of Section  $78.75^\circ$ , the flow depth decreased near the outer bank.

The velocity distribution in the exit section of the bend was fairly uniform. It may have been due to the fact that the flow was not fully developed. However, no

measurements were taken after the exit of the curved channel in this experiment.

In the experimental runs, as the width-depth ratio decreased, the non-dimensional velocity distribution tended to be slightly higher near the central region of the channel, and lower near the banks, owing to the stronger spiral motion, and the relatively higher bank resistance. The superelevation was small compared to the depth of flow; hence, the non-dimensional velocity distribution was not changed by the Froude number, and was only slightly affected by the width-depth ratio. The trace of the maximum surface velocity was almost the same as the average velocity. In the downstream half of the bend the former was slightly closer to the outer bank. The trace of the maximum velocity near the bottom in the downstream half of the bend was much closer to the inner bank. This difference in traces of the maximum velocity at different depths was explained by the momentum transfer due to spiral motion.

The experimental results showed that the change of width-depth ratio slightly alters the distribution of boundary shear. The trace of the maximum boundary shear, starting from the upstream of the curve entrance was located very near the toe of the inner bank. Subsequently, the trace followed an almost circular arc with its center coinciding with the center of the bend until the downstream portion of the curve, where the trace moved outward gradually with the

decreasing boundary shear stress. At the exit section of the bend, the point of maximum boundary shear stress was inside the centerline of the section. The boundary shear stress distribution was quite uniform, and was closely related to the velocity distribution. The higher boundary shear prevailed near the inner bank. This phenomenon had also been observed in natural rivers and some experimental models.

The spiral motion has an upward direction and thus it stabilized the bank. On the other hand, at the outer bank the spiral motion had a downward direction which created the erosion. Even though the boundary shear stress was not maximum on the outer bank the downward direction of the spiral motion would cause the most serious erosion.

The outer bank velocity selected for further analysis was the velocity at mid-depth half way up the bank.

#### 4.3.2 The Experimental Conclusions

1. Since the boundary shear stress was proportional to the velocity gradient, the redistribution of shear stress was closely related to the velocity distribution.
2. The spiral motion and the superelevation are two of the most evident characteristics of the flow and the effect of the bend extends both upstream and downstream.
3. The highest velocity occurred very near the inner bank around the entrance of the bend and gradually shifted



outward with distance downstream until around the exit of the bend where the flow distribution changed to being fairly uniform.

4. The flow pattern was a function of the width-depth ratio but not Froude number.
5. Due to the direction of the spiral motion, the most serious scour area occurred not in the inner bank, but at the outer bank near the exit of the bend.
6. The fully developed bend flow was not obtained in this experiment.
7. This experiment also indicated that the spiral motion becomes stronger as the radius-depth ratio decreases and that the flow in the central region becomes independent when the width-depth ratio is greater than about 12.

#### 4.4 Varshney and Grade (1974)

The experiment was conducted in a 0.6 meter wide and 0.76 meter deep rectangular flume with cement plastered walls. A 6 meter straight length of channel preceded and followed the 180° bend. The bed of the flume was cement plastered and coated with different sand grains.

A uniform flow was ensured by adjusting the depth of flow to be constant near the entrance and exit reach of the flume. The shear stress distribution was measured by a Preston tube of 0.635 cm with a static pressure probe placed above it. The pressure difference,  $P - P_0$ , between the

Preston tube and the pressure probe was observed at various sections 1.5 meters apart in the straight channel, and at every  $10^\circ$  in the bend portion. At each section the shear was measured every 7.6 cm from the outer wall.

#### 4.4.1 Analysis of the Experimental Results

The observed shear distribution showed that the value of the local shear ratio was larger at the inner bank than the outer bank for some distance downstream of the entrance of the bend.

The flow in the beginning portion of the curve followed the free vortex law. Then, the trend of higher longitudinal velocity shifted to the other side of the wall at the exit of the bend.

The local maximum shear was found at some distance downstream of the bend. Subsequently, the shear decreased at the outer bank, and increased at the inner bank as the flow tended to return to uniform across the channel.

The relationship between  $R_c/B$  and dimensionless shear distribution was obtained in different cases for a constant Reynolds number of  $0.455 \times 10^5$  and  $B/H_0$  equal to 4 and 8. It indicated that the maximum value of the shear ratio at the exit section decreased with an increasing value of  $R_c/B$ .

The outer bank relative shear stress selected for further analysis was derived by interpolating the shear

half way up the outer bank. The relative velocity is equal to the square root of the relative velocity.

#### 4.4.2 The Experimental Conclusions

1. The velocity distribution near the exit section of the bend followed the forced vortex law .
2. For rigid boundary bends, the maximum value of  $(\tau_r/\tau)$  occurred near the outer side of the exit. The value was found to dependent primarily on  $R_c/B$ ,  $B/H_o$ ,  $B$  and Reynolds number for constant value of  $\theta$ .

#### 4.5 Francis and Asfari (1970)

The experiment was conducted in a concrete rectangular channel of width 0.61 m. It consisted of a 180° bend with the central radius equal to 1.83 meters, and two straight channels upstream and downstream of the bend. The length of the straight channel was 44 times the depth and was thus probably long enough to ensure that a fully developed velocity distribution was able to occur before the bend started. Wooden barriers were used to form two other narrow channels; with  $B/R_c = 0.154$  (channel II), and  $B/R_c = 0.127$  (channel III) respectively. The tangential velocity was measured in channel I and channel III by a miniature current meter, whose rotor was 1 cm in diameter. The limitation of such an instrument in areas of high velocity gradient were realised.

The discharge of channels I and III were  $0.044 \text{ m}^3/\text{sec}$  and  $0.0275 \text{ m}^3/\text{sec}$  respectively. The flow depth in both the channels at  $30^\circ$  into the curve was 7.6 cm. The longitudinal velocities were measured at 0.5 m before the entrance of the bend at every  $15^\circ$  around the bend and after the exit of the bend. On each section the velocity was taken at 65 points for channel I and at 30 points for channel III.

#### 4.5.1 Analysis of the Experimental Results

The experimental results showed that the region of maximum tangential velocity in channel I near the inner side was between the entrance and  $45^\circ$  into the curve. Afterward, the velocity maximum started to shift toward the outer side of the channel. The overall maximum local velocity was found to be near the outer bank and below the water surface at some distance downstream from the bend exit. In the case of channel III, it was found that the region of maximum velocity was near the centerline at the bend entry (not at the inner bank of the bend). The maximum velocity started to shift towards the outer side of the channel in the region of bend angle about  $15^\circ$  to  $30^\circ$  with increasing magnitude. The overall local maximum velocity prevailed at the outer bank some distance downstream of the bend exit.

The outer bank velocity selected for further analysis was the velocity at mid-depth half way up the bank.

#### 4.5.2 The Experimental Conclusions

The maximum measured velocities in channel I increased towards the outer side. This effect was due to high velocities at the inside of the bend at entry, and seem to be associated with the sharper curvature and larger B/H<sub>o</sub> ratio of this channel. This effect was not found in channel III with milder curvature. Thus, with the sharper curvature there might be a local distortion of the velocity distribution at entry, irrespective of the length of the straight approach channel, and it affected the entire bend.

#### 4.6 de Vriend and Koch (1977)

The experiment was conducted in a 38 meter long straight concrete channel, followed by a 90° bend with a radius of a curvature of 50 meters. The cross-section of the channel was rectangular, 6 meters wide, with a maximum depth of 0.3 meters. The channel was horizontal in the straight channel portion and had a longitudinal slope of  $3 \times 10^{-10}$  along the channel axis of the curve portion.

The discharges were 0.61 m<sup>3</sup>/s and 0.305 m<sup>3</sup>/s. The depth of the flow at the upstream end of the channel was kept constant at about 0.25 meters. Therefore, the average velocities were 0.4 m/s and 0.2 m/s respectively.

#### 4.6.1 Analysis of the Experimental Results

For both discharges the vertical distributions of the normalized velocity were similar in the various measuring stations. Only the distribution in the verticals  $D_013$  (near the inner bank at about  $60^\circ$  into the bend) tended to deviate from the other ones. The reason for this phenomenon can be explained as the influence of the helical flow on the main velocity. The helical flow caused a velocity reduction in the upper part of the flow and an increase of the velocity in the lower part. The helical circulation was more significant in the downstream portion than that in the entrance of the bend. The helical circulation was in an outward direction in the upper half of the flow, pushing the lower half of the flow in an inward direction. Dye injected near the outer wall showed this circulation developed shortly after the beginning of the bend, reached its maximum between the cross-sections  $C_0$  and  $D_0$ , and then decreased slowly until it had vanished around the exit of the bend.

At the entrance, the flow appeared non-uniform. In the first part of the bend the velocity maximum was found to lie near the inner wall, but gradually shifted towards the outer wall while moving further downstream. The shifting of the velocity maximum, and the increase of the inner wall influence, tended to take place over a shorter longitudinal distance at the lower discharge.

The outer bank velocity selected for further analysis was the average velocity over first vertical profile (1.2 depths from the side bank) in each section.

#### 4.6.2 The Experimental Conclusions

1. The vertical distributions of the main velocity were very similar throughout the flow field, except close to the side wall in the curved part of the channel. There, the main velocity was further reduced in the upper part of the flow, whereas it was higher in the lower part of the flow. The deviations were explained by the advective influence of the helical flow on the main flow, which was not accounted for in the logarithmic law.
2. The measurement of the helical velocities was not accurate enough to deduce the similarity of the individual vertical distribution. When all the experimental results were plotted on one figure, most points turned out to be spread around a distinct vertical distribution curve, except for those close to the outer wall. These deviated from the other distributions, indicating existence of a counter rotation.
3. The observed depth-velocity field showed two features: The point of its maximum in a cross-section lies near the inner wall first, and after it enters the bend and then gradually shifts toward the outer bank in the area further downstream. These phenomena were attributed to

the advective influence of the helical flow on the main flow.

#### 4.7 Steffler (1984)

The experiment was conducted in a rectangular flume consisting of a straight section 13.4 m long and a single bend of 3.66 m centerline radius with an arc of  $270^\circ$  (distance 17.2 m), followed by a 2.4 m straight exit section. The channel was 1.07 m wide and 0.2 m deep with an adjustable slope set at 1/1,200 for both experiments.

The flume was composed of galvanized sheet metal with plexiglass inserts at the measurement locations. The experimental data was measured by a Laser Doppler Anaemometer. The laser beams entered the flow from the bed of the flume which allowed the measurement of the longitudinal and lateral velocity components. In the first run, the flow depth was 0.061 m and main velocity was 0.36 m/s. In the other run the flow depth was 0.085 m and main velocity was 0.42 m/s.

##### 4.7.1 Analysis of the Experimental Results

The parameter difference in both runs was not large enough to result in any significant qualitative difference. In the first two sections before the entry of the bend, the velocity had an almost uniform lateral distribution with only the two outermost profiles noticeably different. Just



past the entry of the bend, it showed the velocity larger on the inside of the channel than on the outer bank. As the flow travels further down to about the fourth section (30° into curve) the velocity on the outer bank increased, and the one in the inner bank slowed down. In the fifth and sixth section the flow became almost uniform again (the sixth section was 90° into the bend). In the eleventh section (about 250° into the bend), the flow showed the velocity increased at the outer bank and decreased at the inner bank. Just past the twelfth section (the exit of the bend), it showed a sudden increase of velocity skewness from the previous section and in the thirteenth section an even larger variation. The obtained velocity profiles are significantly different from the one in the straight channel. This was due to the effect of the secondary flow.

The outer bank velocity selected for further analysis was the depth averaged velocity near the outer bank (1.5 depths away from wall for the first run and 1.2 depths away from wall for the second run) in each section.

#### **4.7.2 The Experimental conclusions**

The lack of prediction methods for the developing and developed longitudinal velocity distribution was identified as the most important gap in the present knowledge.

#### 4.8 Conclusions

The selected experimental investigations, covering a wide range of curvatures, aspect ratios and Reynold's numbers, show common trends and conclusions regarding the development of longitudinal flow in a curved channel.

Curvature affects the flow of water in several ways. These effects include superelevation, secondary flow, and longitudinal velocity redistribution. The superelevation of water surface in a channel curve leads to two occurrences of longitudinal increase in depth: along the outer bank of the curve as the water rises entering the curve, and at the curve exit along the inner bank where the water level recovers to normal depth. For bends of large curvature, separation may develop in these two areas and water surface may slope upstream locally.

Some of fluid in the curved channel, especially near the bed, moves slower than the average velocity. Since it is slower, it lacks the apparent centrifugal force to resist the imposed pressure gradient of the water surface slope. It is, therefore, accelerated inward until friction provides a balancing force. Fluid moving faster than average (near the water surface) would experience an opposite effect and be accelerated outward. The net result is a circulation over the flow cross-section, superimposed on main longitudinal flow. The secondary velocities increased with increasing

ratios of depth to radius,  $\frac{H_c}{R_c}$ .

The higher velocities were found at the inner bank near the entrance of the bend, and at the outer bank near the exit of the bend. Bed and bank shear stresses were generally found to correlate well with the local flow velocity.

The investigators attempted to understand the phenomena and proposed theoretical explanations of flow in curved channels. As a result, under some assumptions, the superelevation and secondary flow phenomena can be well explained. However, the flow development and the longitudinal velocity redistribution are not well understood. There is still need for further research in order to predict the extent of the higher velocity area. It should be possible to use the experimental data and theoretical analysis to establish some scales. The scales will depend on non-dimensional flow and geometrical parameters. It may be possible to observe a similarity of the variation of non-dimensional longitudinal velocity in the outer bank. The scales may be a reference for river engineers to determine critical points in the curved channel.

## 5. Analysis of Existing Experiments

### 5.1 Introduction

In the past years many experimental studies on curved channels have been done. However, an attempt to find general relationships from these experiments to establish some scales and empirical correlations has not been made. Using the selected experiments (Chapter 4) some scales for predicting the variation of non-dimensional velocity in the outer bank are presented. The procedure adopted in this research is as follows:

1. Data collection : recording the detailed data from each chosen experiment.
2. Definition of channel zones : The velocity maximum is shifted by different physical phenomena in different parts of the channel, suggesting a simplified analysis for each zone.
3. Analysis : the analysis is to be derived from the data and some appropriate theory. The theoretical results provide guidelines for correlating the empirical data.

### 5.2 Data Collecting Procedure

As a preliminary study, this research was limited to simple rectangular and trapezoidal cross section channels and bends of constant radius. More controlled, detailed and

reliable experiments were available in this class.

1. To simplify the analysis and restrict the range of parameters to physically realistic situations.  
Experiments were chosen that met certain requirements:
  - a. The channel width was constant.
  - b. The centerline radius of curvature was larger than its width.
  - c. The channel width was more than twice the water depth.
  - d. The data was presented in sufficient detail.
2. Due to the fact that most papers did not present original data, data often had to be derived from either the figures of shear stress distribution or relative velocity distribution.
3. The main purpose of this research is bank erosion protection. Therefore, the only data considered were those on the outer and inner banks.
4. In each experimental apparatus, aspect ratio, width to radius of curvature ratio, discharge, Froude number, radius of curvature to depth ratio and Reynold's number were recorded.
5. The Macintosh spreadsheet software EXCEL was used to record and graph the data and to perform the non-dimensional correlations.

### 5.3 Definition of Zones for a Curved Channel

From the general conclusions of the experimental study, it is possible to describe the mechanics of flow and shear stress redistribution. Consider the shear stress distributions from four different cases as shown in Figures 5.1 to 5.4. It may be observed that the shear stress is symmetrical about the axis at the entrance. When the flow goes through the curve, the expected tendency towards a free vortex pattern is found in the initial portion. The higher shear stress is found on the inner bank and lower shear stress is found on the outer bank. Further downstream the shear stress shifts to the opposite banks. In Figure 5.2, the shear stress shifting is not as apparent as the other three figures. This is likely due to the fact that the flow was not fully developed.

From the point of view of vorticity the phenomenon may be explained as follows. Initially the flow is uniform across the channel (neglecting the side wall region). Its vertical vorticity is therefore zero. After entering the bend, the flow is constrained to move concentrically but with zero vorticity which leads to the free vortex pattern. Further downstream the flow gains vertical vorticity from the tilting of the bed vorticity by the secondary flow and the shear stress profile skews to the opposite bank.

The subdivision of a bend is based on the realization that there are distinct physical processes dominant in each

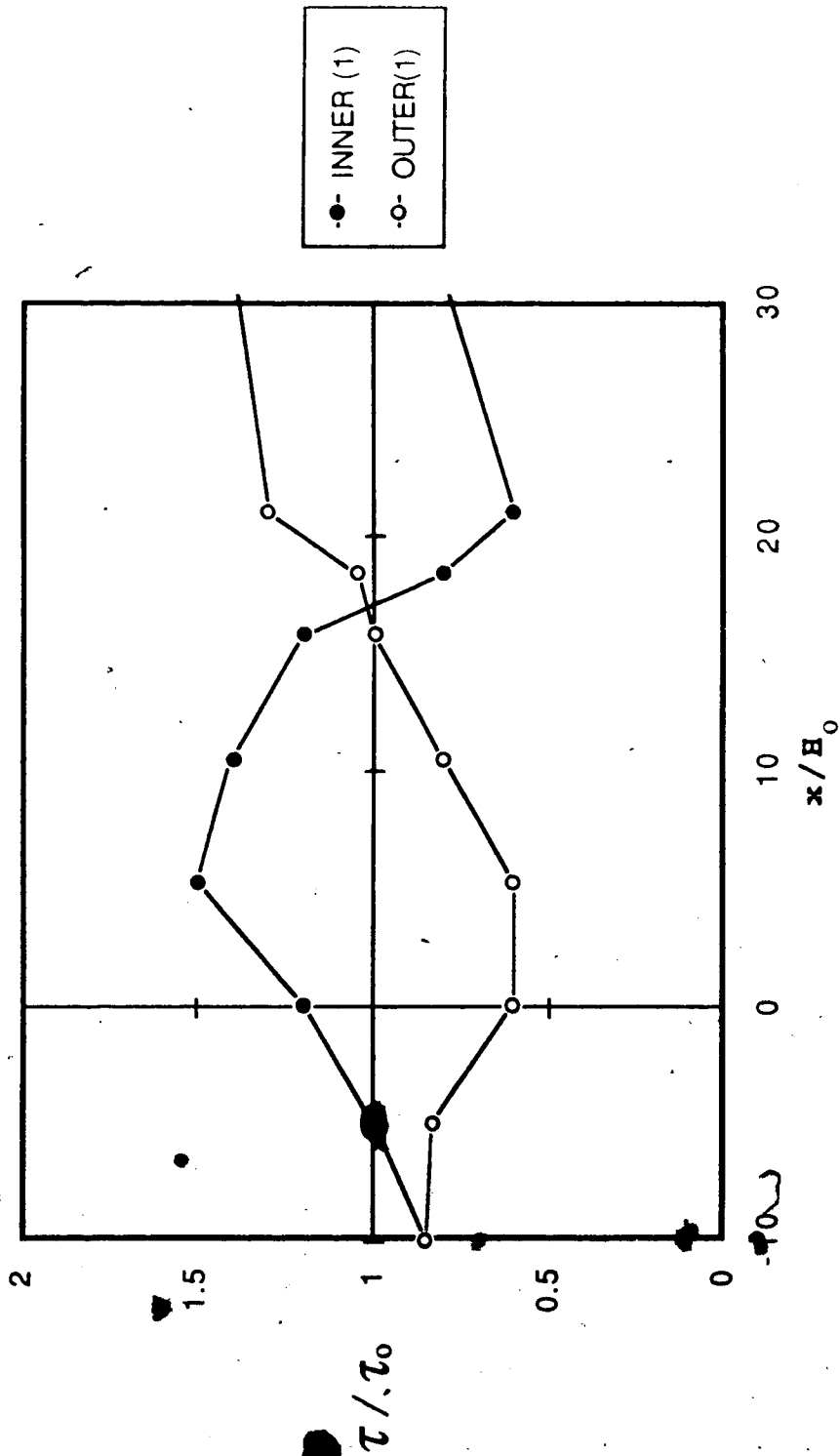


Figure 5.1 Non-Dimensional Shear Stress Distributions Near the Banks, adapted from Ippen & Drinker(6) Run 1.

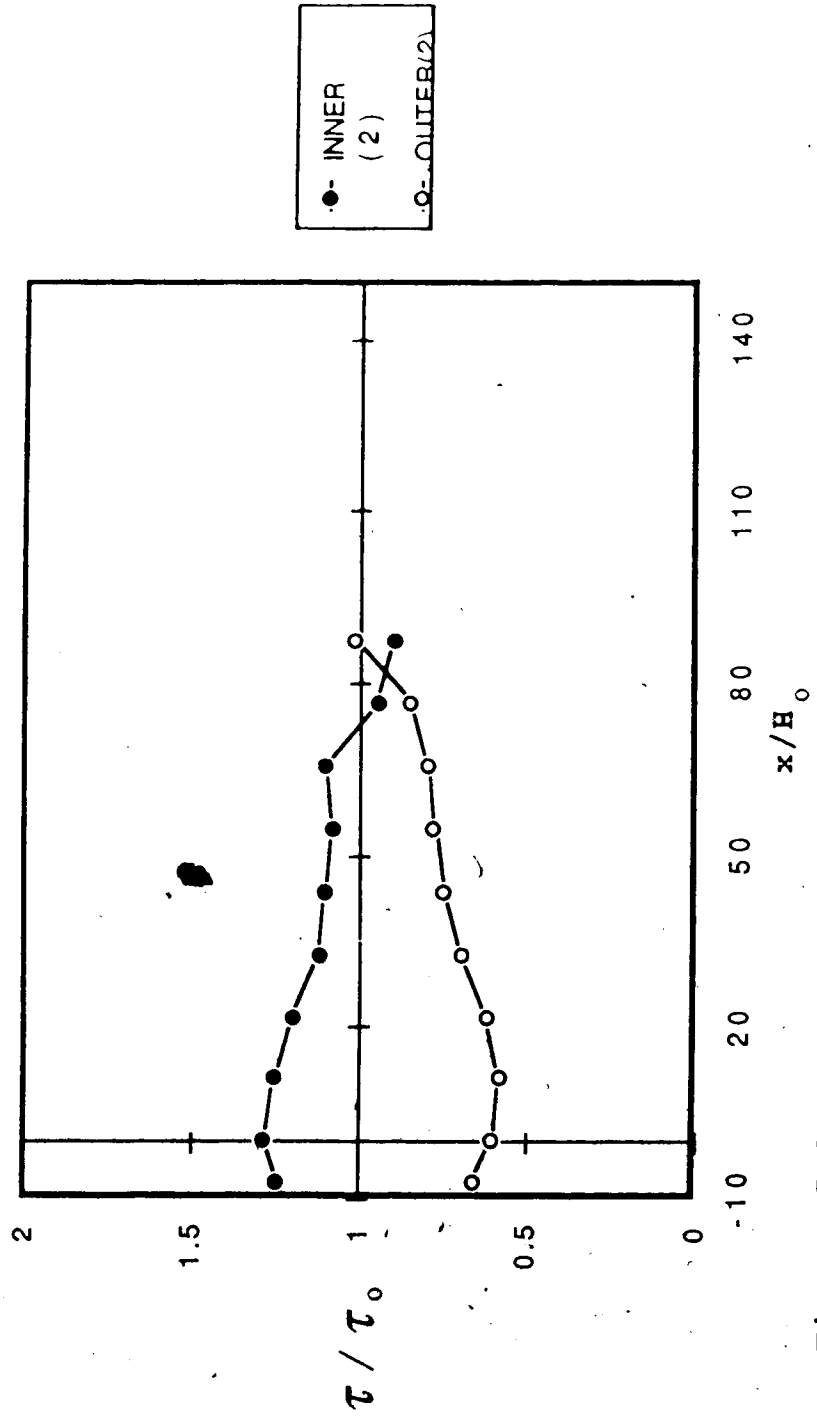


Figure 5.2 Non-Dimensional Shear Stress Distributions Near the Banks, adapted from Yen(16) Run 2.



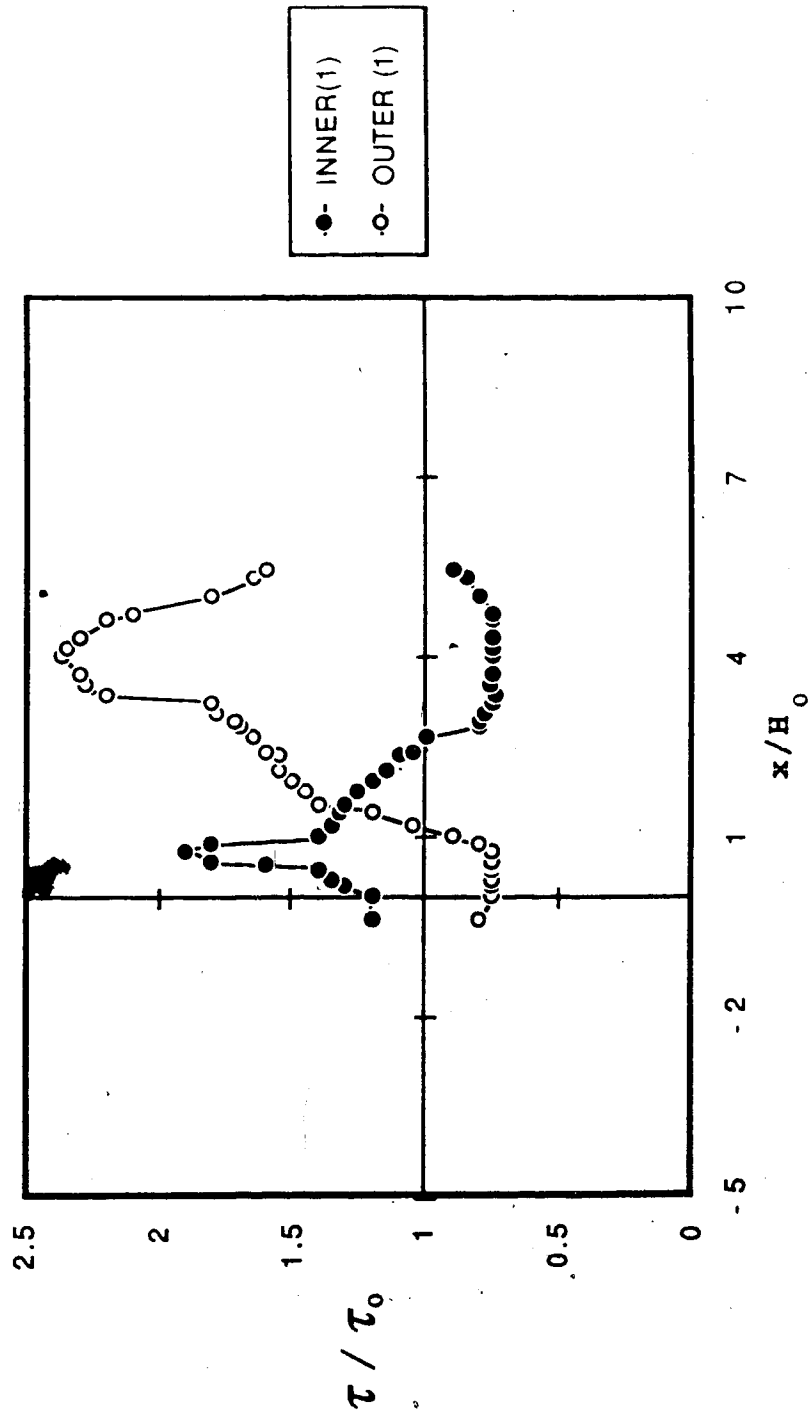


Figure 5.3 Non-Dimensional Shear Stress Distributions Near the Banks, adapted from Varshney & Grade(11) Run 1.

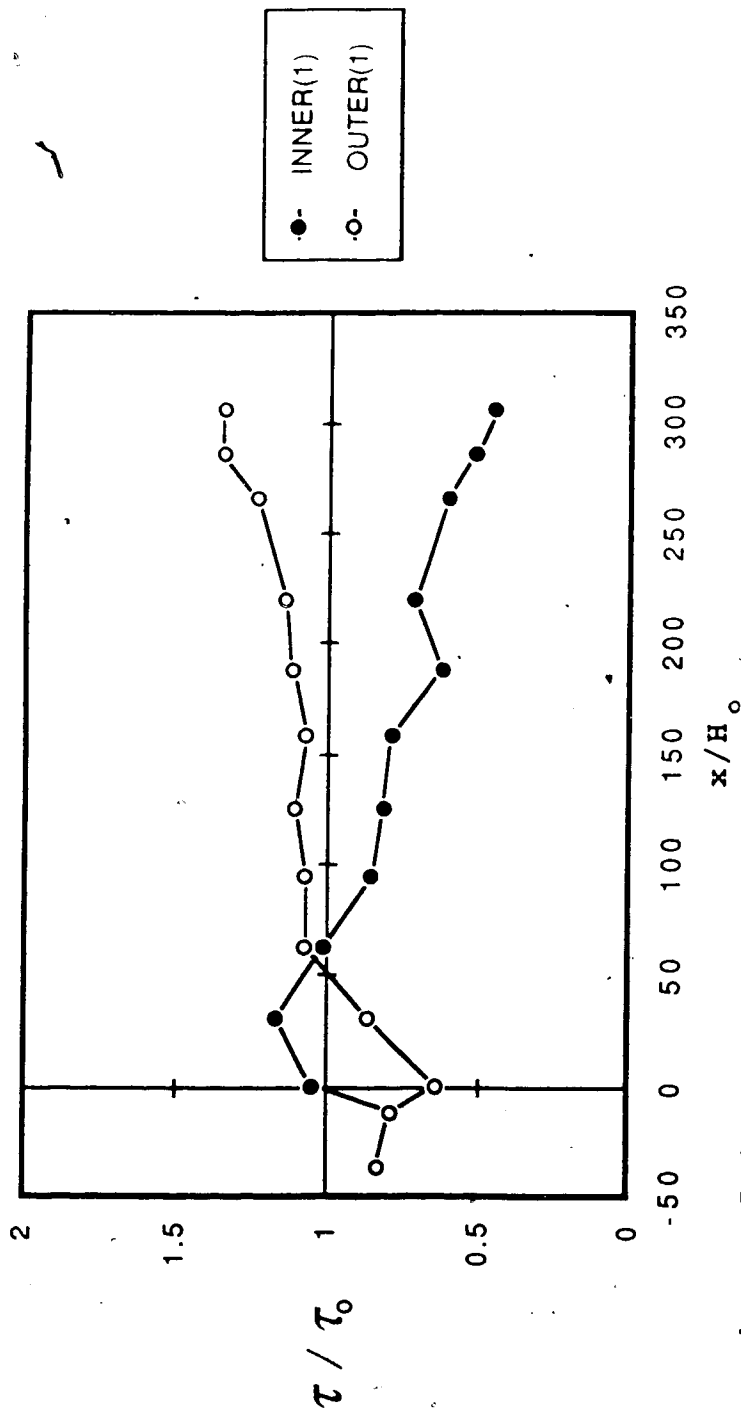


Figure 5.4 Non-Dimensional Shear Stress Distributions Near the Banks, adapted from Steffler(12) Run 1.

zone. Figure 5.5 shows this subdivision. Zone I is an initial zone. Zone II is a secondary flow zone. Zone III is a recovering zone. Zone IV is a relaxing zone.

An analysis of each zone is presented below.

### 5.3.1 Zone I

Zone I is an entrance zone. It displays an essentially potential flow behavior. The critical parameters here are channel width (B) and radius of curvature ( $R_c$ ). The channel width for a trapezoidal channel was taken to be the average of the top and bottom width.

From all the analyses of the results of past investigations, it was found that the minimum velocity ( on the outer bank ) occurred close to a distance of B/2 downstream from the bend entrance and the velocity was reasonably well predicted by (Steffler, 1984)

$$\frac{U_i}{U_u} = 1 - \frac{B}{2R_c} \quad [5.1]$$

where

$U_u$  = the upstream average velocity

$U_i$  = minimum velocity

B = the channel width

$R_c$  = the radius of the curvature

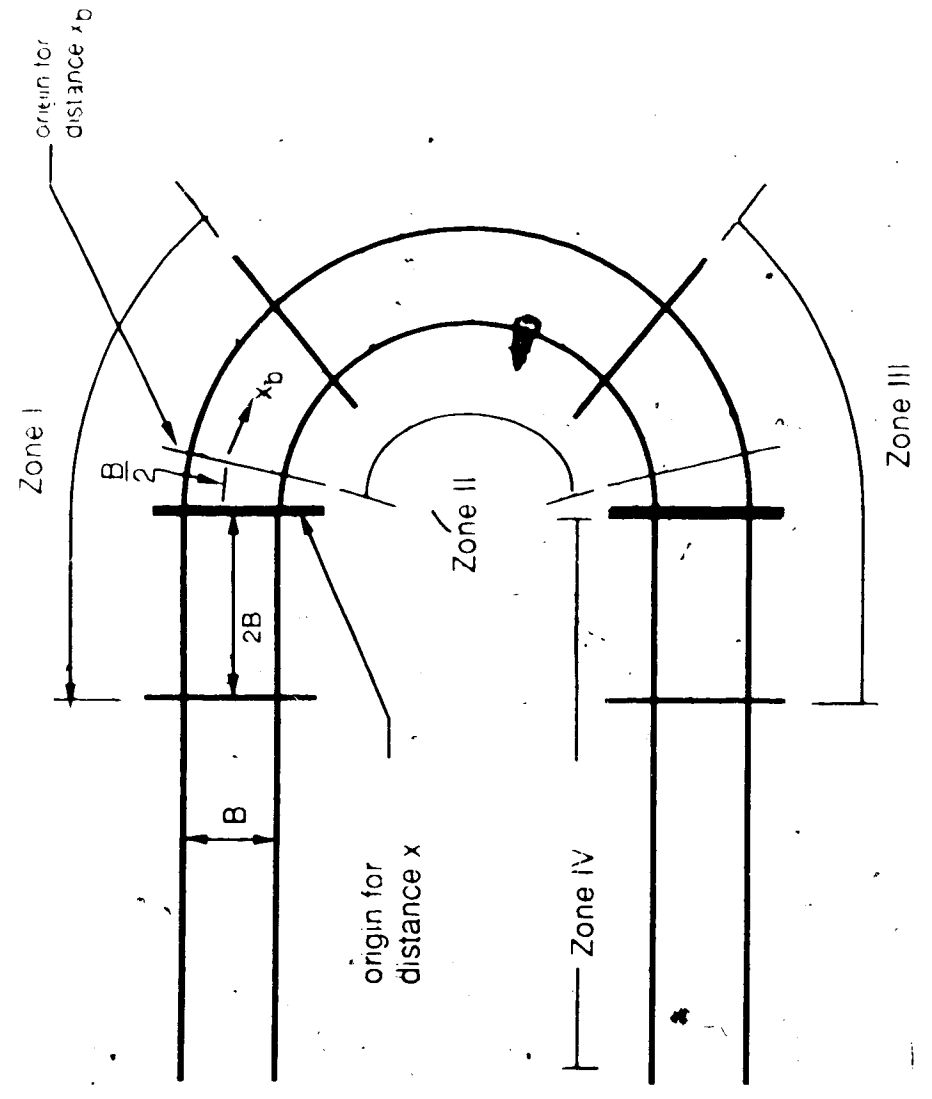


Figure 5.5 Definition of Zones for a Curved Channel.

The value of  $U_1$  obtained here may, in fact, be used as an estimate for the starting velocity in Zone II. Zone I in the analysis extended from  $-2B$  to  $+2B$  (set 0 at entrance). Steffler, Rajaratnam and Peterson (1985) estimate the distance between the points in which 5% and 95% of the final value of its superelevation due to the change of the curvature. They presented

$$L_s = 2.66 b (1 - F_1)^{-2} \quad [5.2]$$

where

$b$  = the half of the channel width( $B$ ).

$F_1$  = Froude number

$L_s$  = the distance between the points in which 5% and 95% of the final value of its superelevation.

Since  $L_s$  is approximately equal to  $B$ , most of the variation is captured within the reach  $-0.5B$  to  $+0.5B$ .

### 5.3.2 Zone II

Zone II starts from  $x = 0.5B$ . It is characterized by a transition to a new equilibrium cross-channel velocity distribution balancing bed slope, friction, and secondary flow effects. The rate of change of this distribution seems to depend on how far out of equilibrium the channel is at any given location. This leads to an exponential decay type of transition. The bend entrance disturbs the flow (causes  $U$  to fall to  $U_1$ ) which then recovers over some distance to a new

equilibrium value  $U_0$  (ultimate velocity). Unfortunately, most bends studied (and perhaps most natural bends) end before this final equilibrium value is approached. The values for  $U_0$  used in most cases in this study were obtained by extrapolating a best fit exponential curve and estimating the asymptotic value. The development length scale  $L$  was taken as the non-dimensional distance, from the start ( $0.5B$  downstream from the entrance) of Zone II to the point where  $U = 0.5(U_1 + U_0)$  on the best fit curve. The scale  $L$  is chosen because it is relatively easy to measure with some confidence. Using these development length scales the similarity curve below was obtained

$$\frac{U - U_1}{U_0 - U_1} = f\left(\frac{x'_b}{L}\right) \quad [5.3]$$

where  $x'_b = x_b/H_0$ .

The chosen non-dimensionalization forces all the curves to pass through the point  $(0.0, 0.0)$  and  $(1.0, 0.5)$  and so a good fit is to be expected. The point  $(0.0, 0.0)$  is at a distance of  $B/2$  downstream of the bend entrance and its velocity  $U$ , is about minimum or 'initial' velocity,  $U_1$ .

### 5.3.3 Zone III

Zone III is similar in behavior to Zone I, except that the rapid velocity shift is now towards the outer bank of the channel. The magnitude and length of this transition

should be identical to those of Zone I. Unfortunately, most experiments end abruptly at the exit and confirmation is difficult. This is, however a critical region, where the attack velocities and shear stresses are largest. The velocity jump here should be added to the velocity obtained from the zone II curve at the point indicated by the end of the bend (not  $U_0$  unless the actual bend is very long) to obtain the maximum attack velocity on the outer bank.

#### 5.3.4 Zone IV

Strictly speaking there should be a Zone IV, starting downstream of the bend exit, considered in determining the end, or downsizing, of bank protection. This zone would be similar to zone II, with  $U_0$  set to  $U_m$ . The value of  $L$  might be somewhat different since the radius of the curvature would now be infinite. Presumably, the same curve would apply and may also be truncated by the beginning of a new bend (likely in the opposite direction). Unfortunately, at this time very limited data exists.

### 5.4 Analysis of Results

Table 5.1 and Table 5.2 summarize the experimental parameters from the selected investigations.

Table 5.1 Data for Rectangular Channels

RESEARCHER	$U_1/U_m$ (1)	$U_1/U_m$ (2)	L (3)	B/H <sub>o</sub> (4)	B/R <sub>c</sub> (5)	R <sub>c</sub> /B (6)	C <sub>f</sub> (7)	R <sub>c</sub> /H <sub>o</sub> (8)	H <sub>o</sub> /R <sub>c</sub> (9)
STEFFLER 1	0.820	1.063	32.00	17.54	0.292	3.43	16.00	60.07	0.017
STEFFLER 2	0.820	1.030	27.00	12.54	0.292	3.43	16.00	42.95	0.023
VARSHNEY 1	0.792	1.350	1.30	2.26	0.333	3.00	12.20	6.79	0.147
VARSHNEY 2	0.842	1.096	8.96	9.16	0.333	3.00	12.00	27.51	0.036
VARSHNEY 3	0.825	1.442	2.35	2.85	0.333	3.00	12.00	8.56	0.117
de VRIEND 1	0.900	1.083	53.00	23.62	0.120	8.33	15.40	196.83	0.005
de VRIEND 2	0.875	1.092	64.86	23.62	0.120	8.33	7.20	196.83	0.005
FRANCIS 1	0.845	1.185	20.78	8.00	0.333	3.00	14.70	24.02	0.042
FRANCIS 2	0.965	1.129	14.00	3.30	0.127	7.88	15.14	25.98	0.038



Table 5.2 Data For Trapezoidal Channels

RESEARCHER	$U_i/U_m$ (1)	$U_u/U_m$ (2)	$L$ (3)	$B/H_0$ (4)	$B/R_c$ (5)	$R_c/B$ (6)	$C_f$ (7)	$R_c/H_0$ (8)	$H_0/R_c$ (9)
IPPEN 1	0.815	1.090	6.00	9.90	0.500	2.00	17.53	19.800	0.0505
IPPEN 2	0.700	1.170	8.50	8.12	0.530	1.89	21.07	15.321	0.0653
IPPEN 3	0.770	1.180	4.00	9.75	0.570	1.75	20.88	17.105	0.0585
IPPEN 4	0.590	1.072	3.60	5.94	0.600	1.67	22.36	9.900	0.1010
IPPEN 5	0.850	1.167	11.50	7.98	0.230	4.35	18.27	34.696	0.0288
IPPEN 6	0.900	1.190	7.90	5.97	0.260	3.85	21.25	22.962	0.0436
IPPEN 7	0.910	1.220	4.90	5.02	0.290	3.45	22.30	17.310	0.0578
YEN 1	0.770	1.085	33.68	17.99	0.226	4.42	22.00	79.602	0.0126
YEN 2	0.750	1.030	23.50	12.99	0.232	4.31	22.20	55.991	0.0179
YEN 3	0.805	1.000	17.58	8.99	0.240	4.17	22.66	37.458	0.0267

#### 5.4.1 Initial Velocity

An evaluation was made of the relative minimum velocity on the outer bank,  $\frac{U_1}{U_m}$ . The variation of the ratio  $\frac{U_1}{U_m}$  with the curvature  $\frac{B}{R_c}$ , which is shown in Figure 5.6, clearly indicates a decreasing minimum velocity with increasing curvature.

According to the theoretical analysis the relationship between  $\frac{U_1}{U_m}$  and  $\frac{B}{R_c}$  was presented as Equation 5.1. The data selected from the experiments of many researchers, have been plotted on Figure 5.6, which indicated those are in good agreement with Equation 5.1; especially for rectangular channels. The reason that the data of trapezoidal channels shows some scatter might be due to ambiguity in defining the widths of those channels. Therefore, the minimum velocity which occurs close to a distance of  $\frac{B}{2}$  downstream from the bend entrance is well predicted by Equation 5.1

#### 5.4.2 Non-Dimensional Longitudinal Velocity Distribution

##### Near the Outer Bank in Zone II

Figures 5.7 to 5.25 indicate the relative velocities near the outer bank in zones II, which are affected by the free and forced vortex motions in the bend. The variation of the velocity is characterized by a transition to a new equilibrium ( $U$  falls to  $U_i$  and attempts to rise to  $U_o$ ). However, most experiments end before this final equilibrium

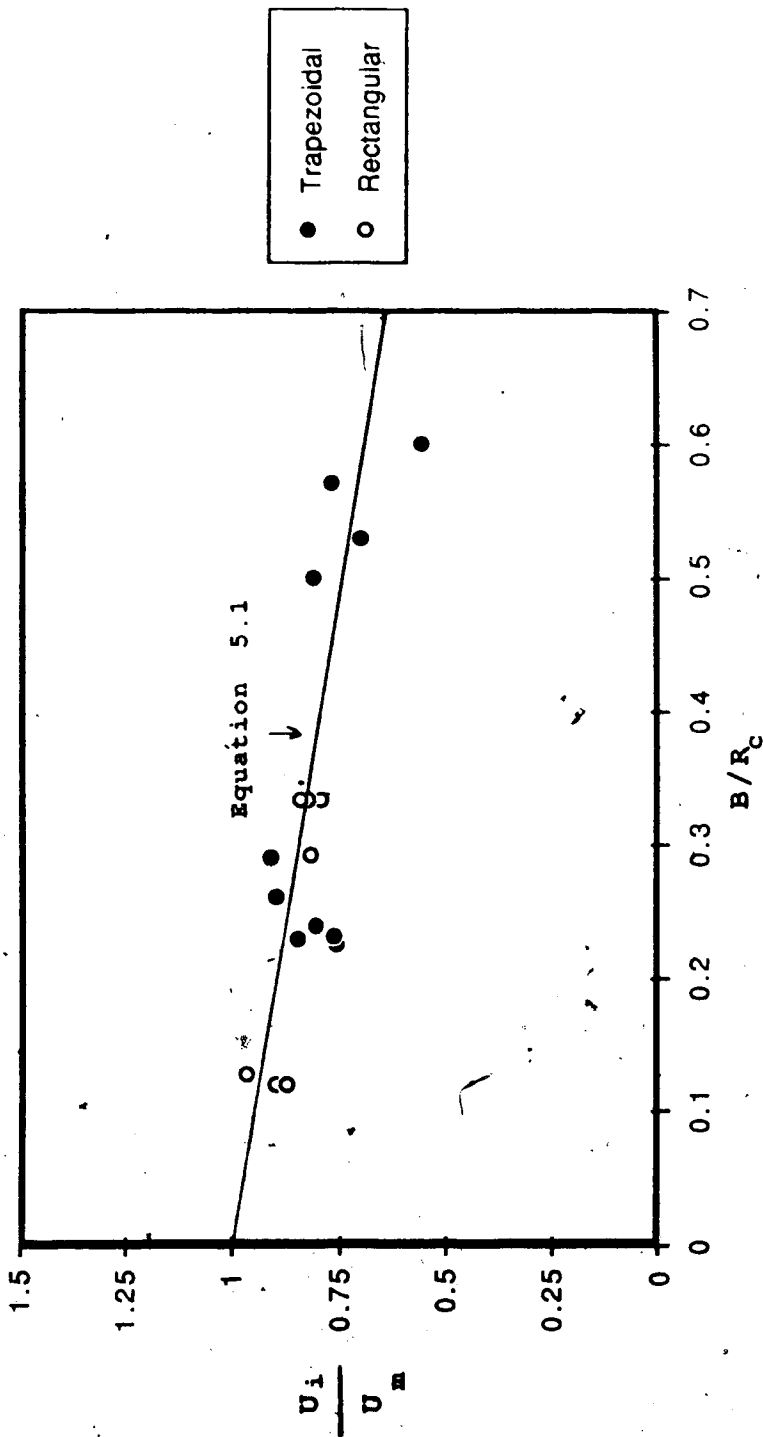


Figure 5.6 Minimum Velocity Near the Outer Bank

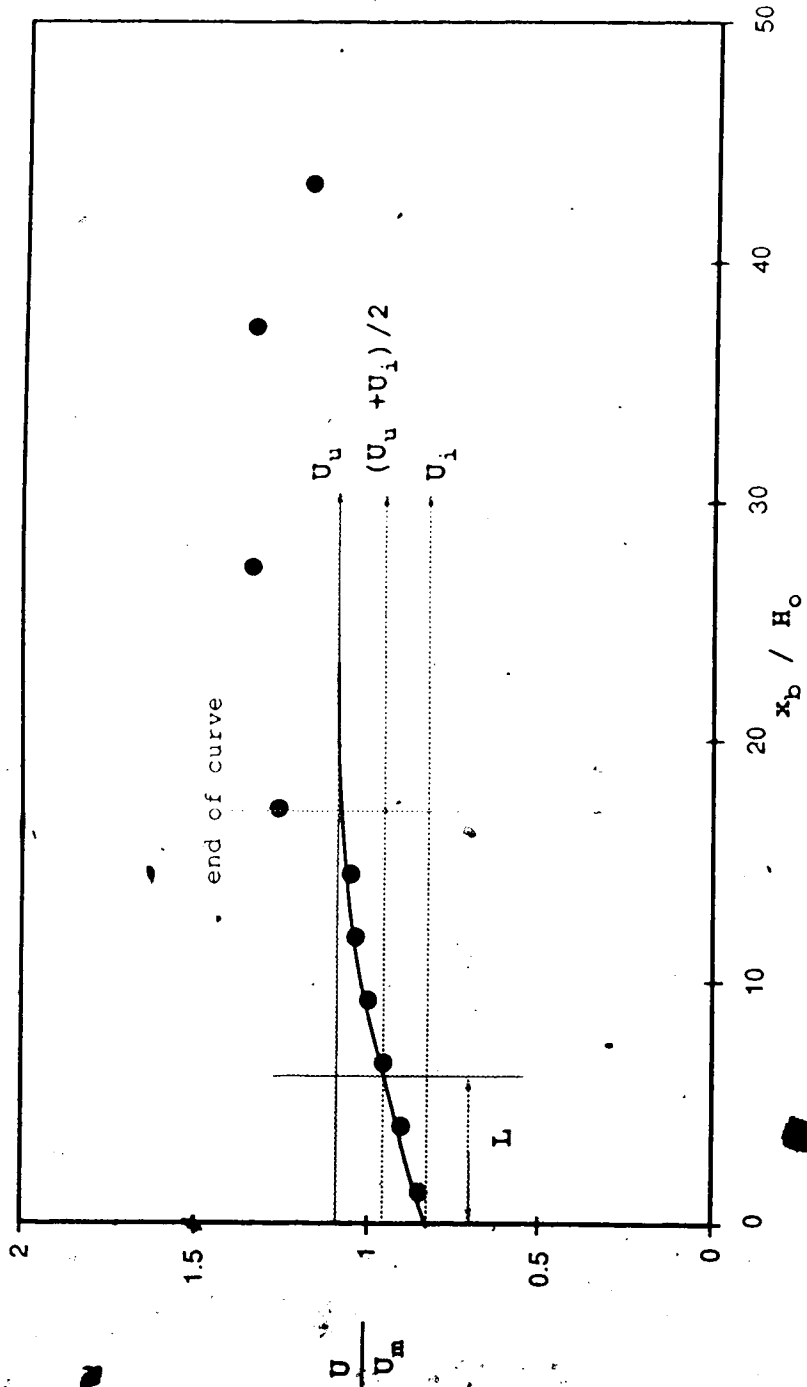


Figure 5.7 Non-Dimensional Longitudinal Velocity Distribution Near the Outer Bank, adapted from Ippen & Drinker (6) Run 1.

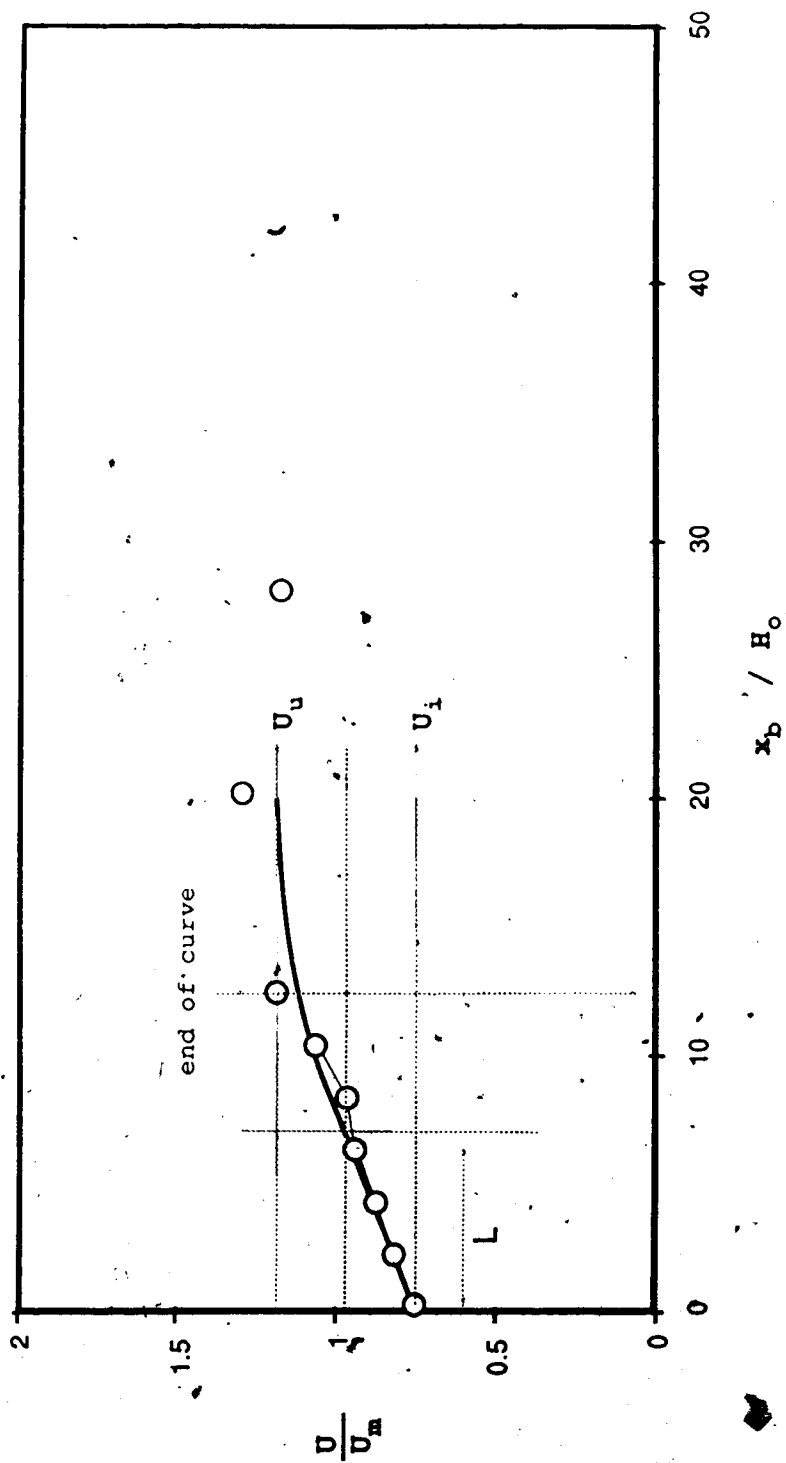


Figure 5.8 Non-Dimensional Longitudinal Velocity Distribution Near the Outer Bank, adapted from Ippen & Drinker (6) Run 2.

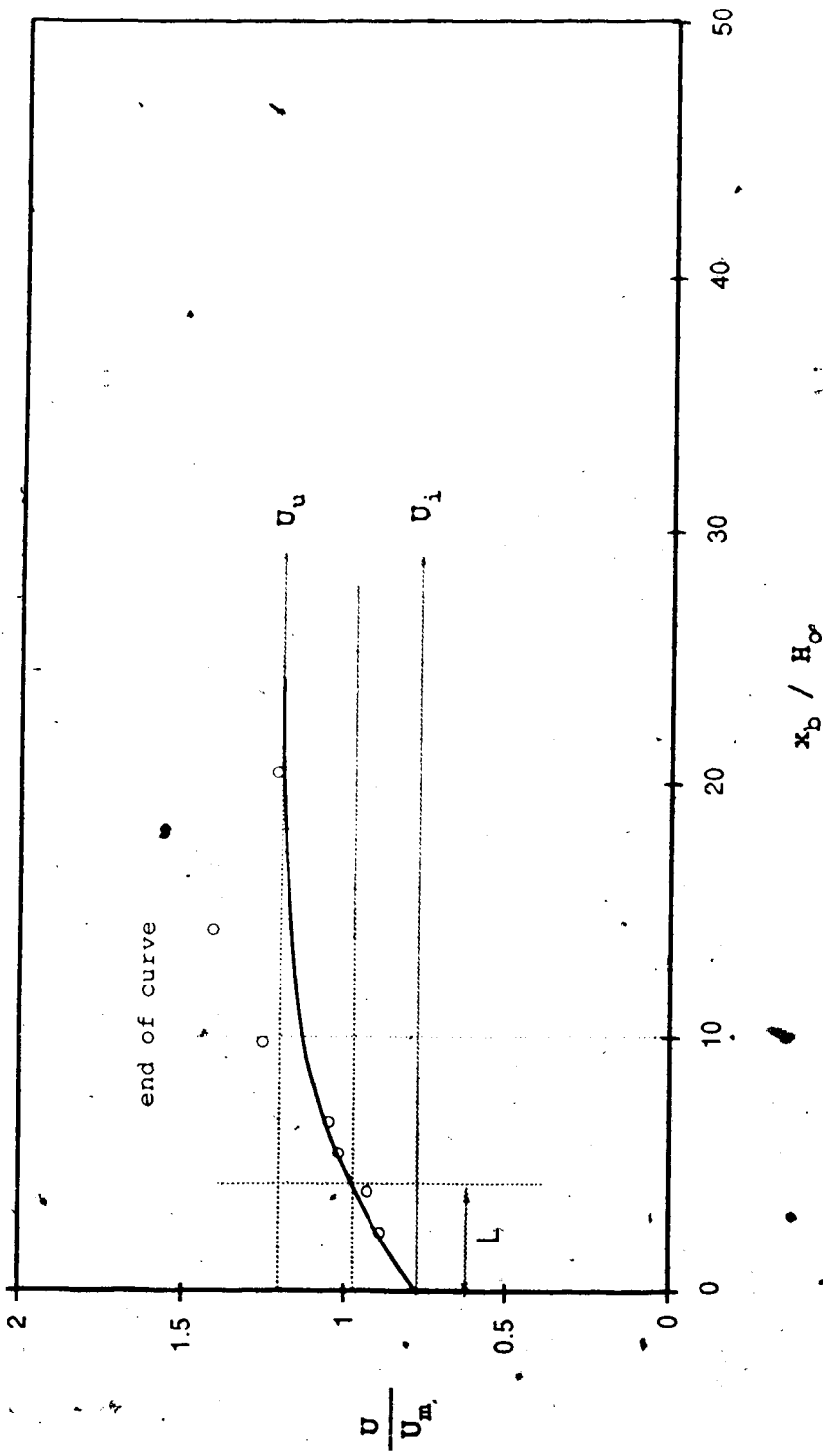


Figure 5.9 Non-Dimensional Longitudinal Velocity Distribution Near the Outer Bank, adapted from Ippen & Drinker(6) Run 3.

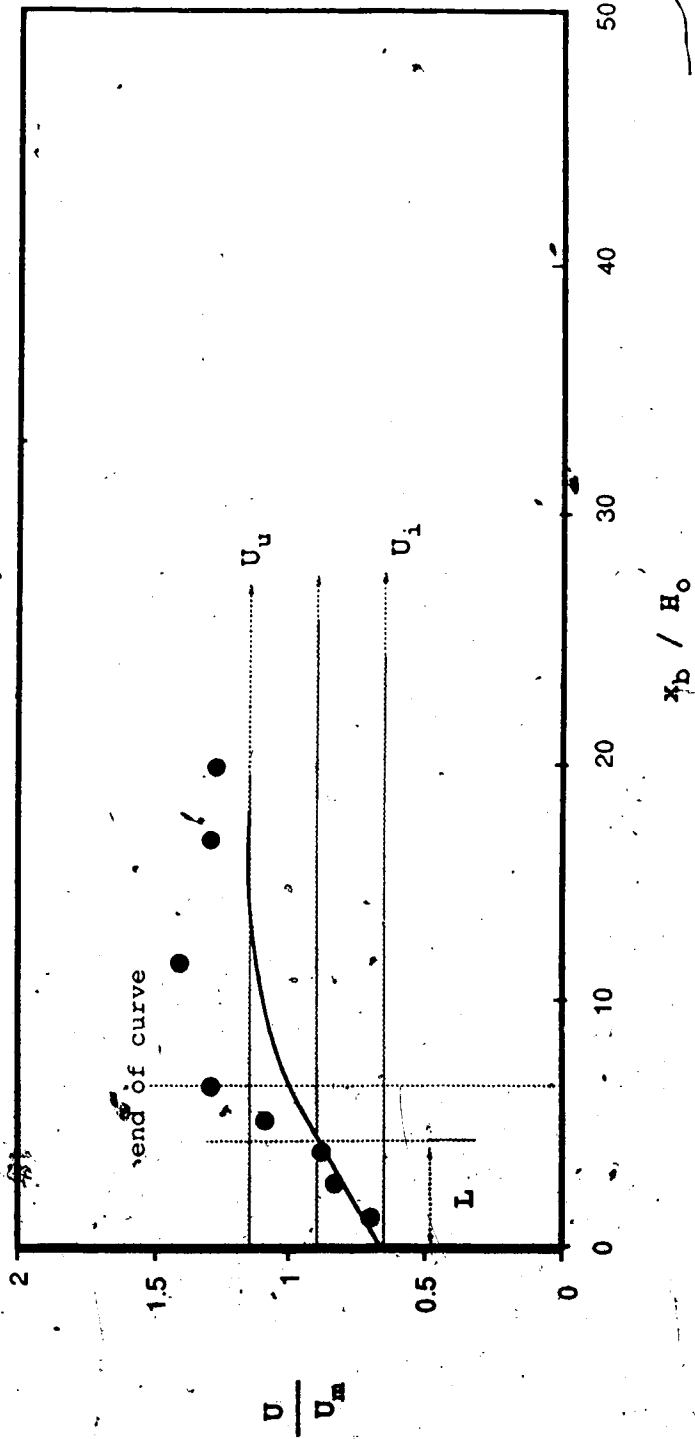


Figure 5.10 Non-Dimensional Longitudinal Velocity Distribution Near the Outer Bank, adapted from Ippen & Drinker (6) Run 4.

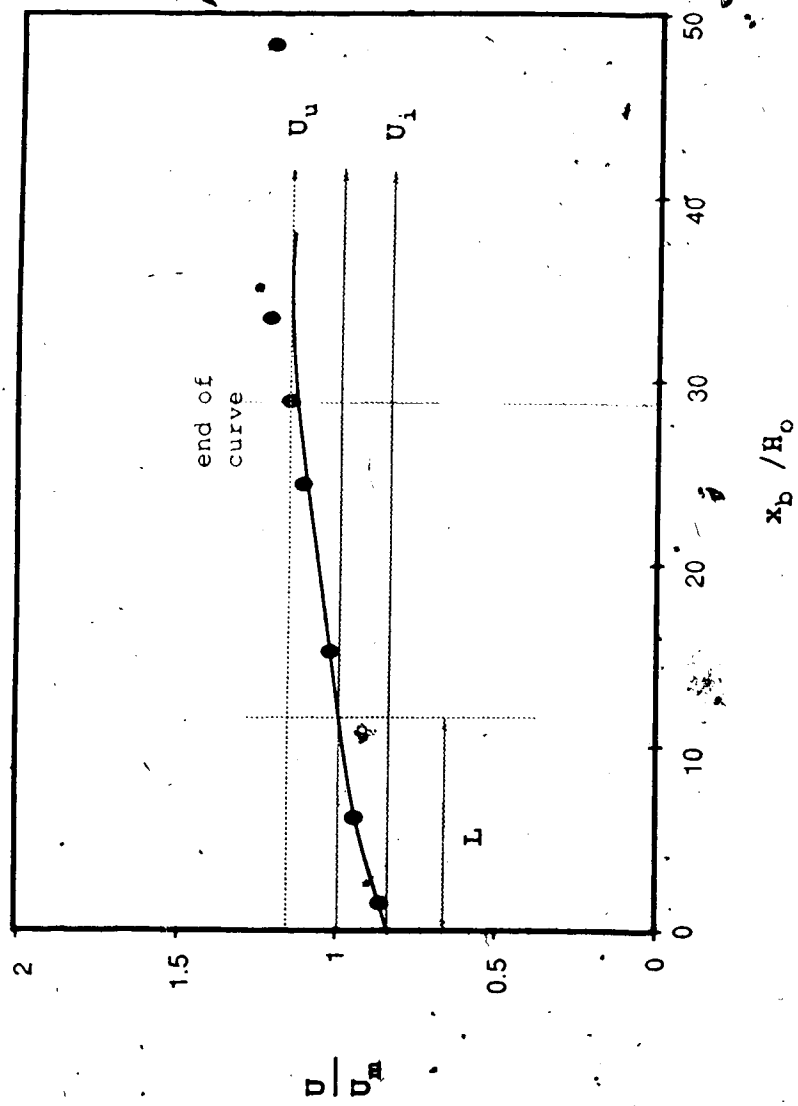


Figure 5.11 Non-Dimensional Longitudinal Velocity Distribution Near the Outer bank, adapted from Ippen & Drinker(6) Run 5.



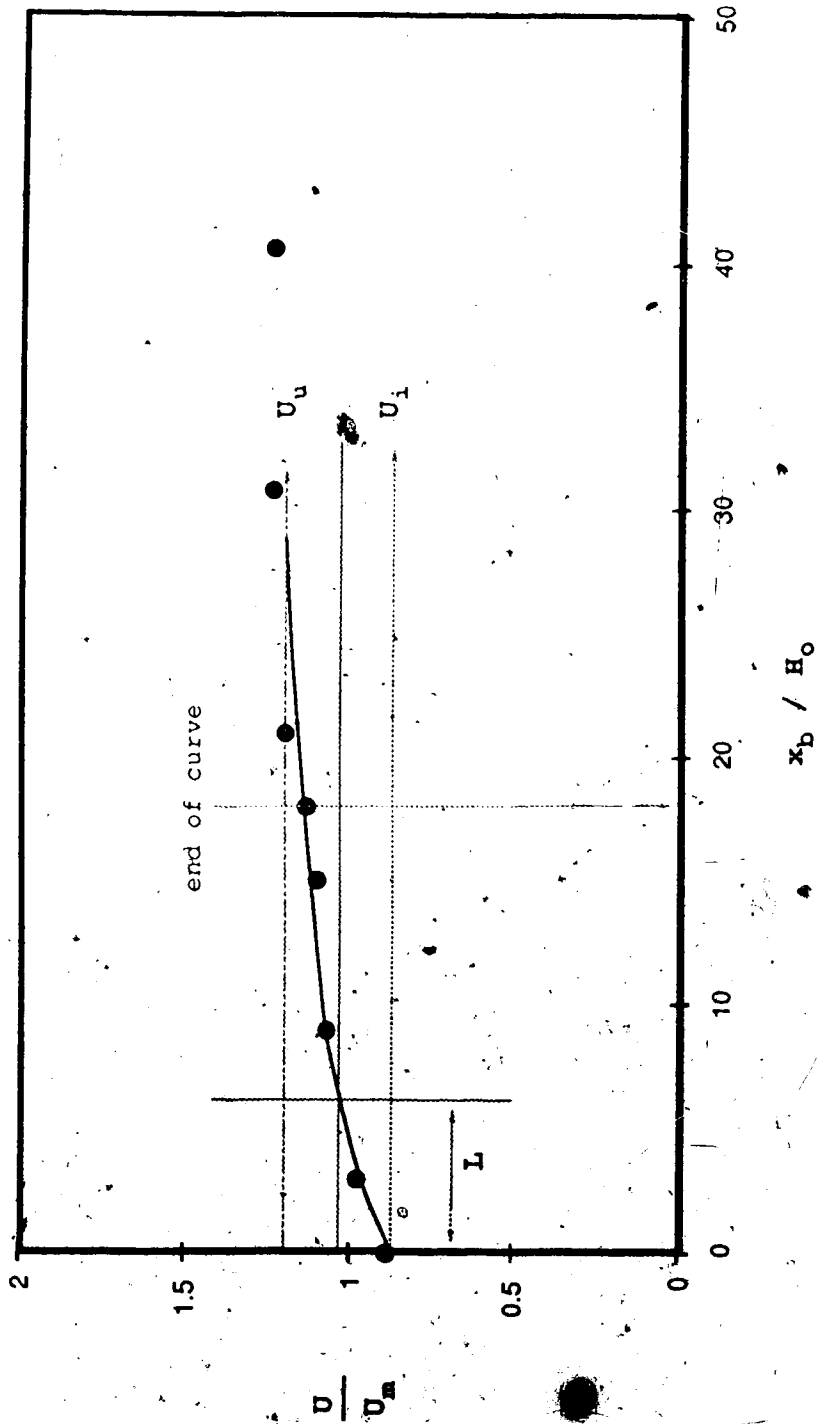


Figure 5.12 Non-Dimensional Longitudinal Velocity Distribution Near the Outer bank, adapted from Rippen & Drinker (6) Run 6.

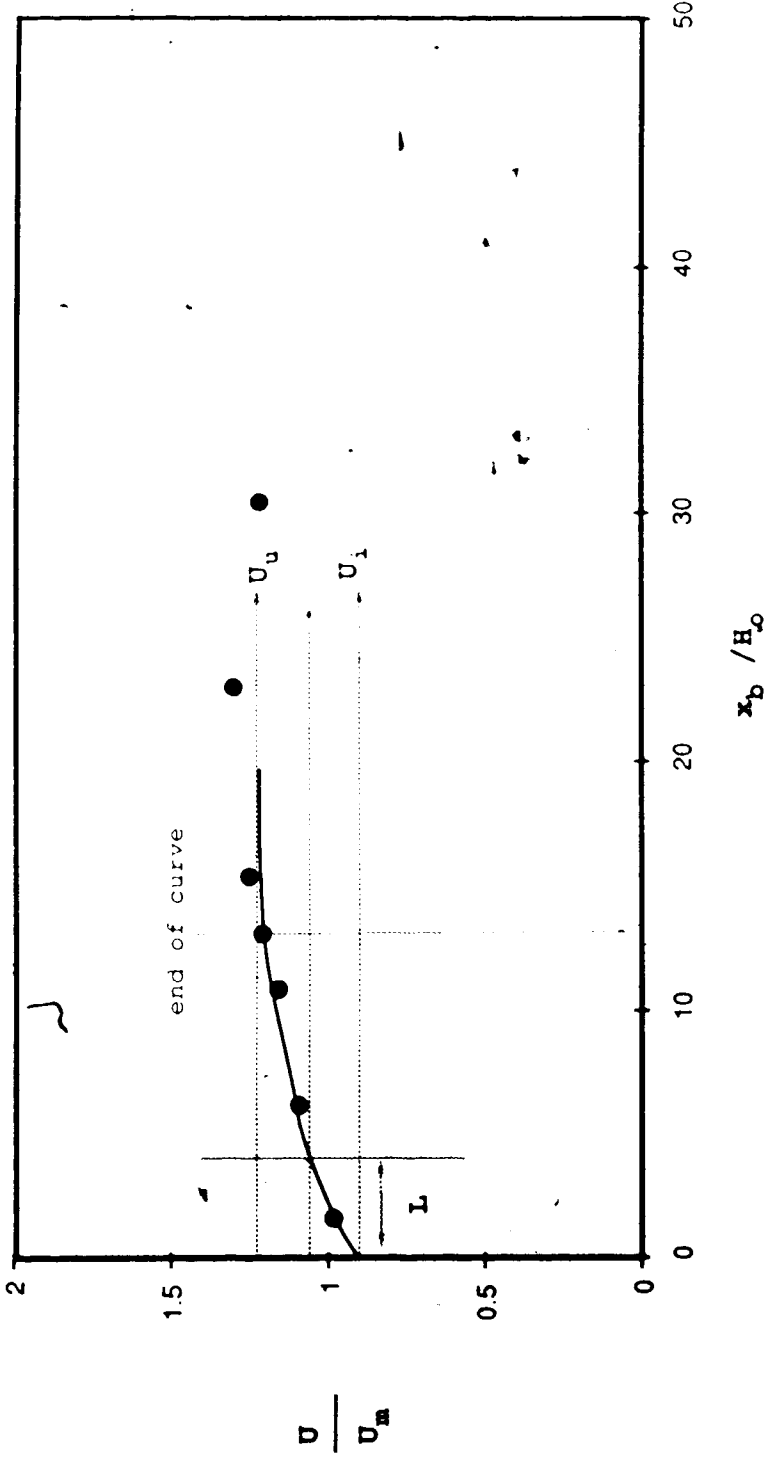


Figure 5.13 Non-Dimensional Longitudinal Velocity Distribution Near the Outer Bank, adapted from Ippen & Drinker (6) Run 7.

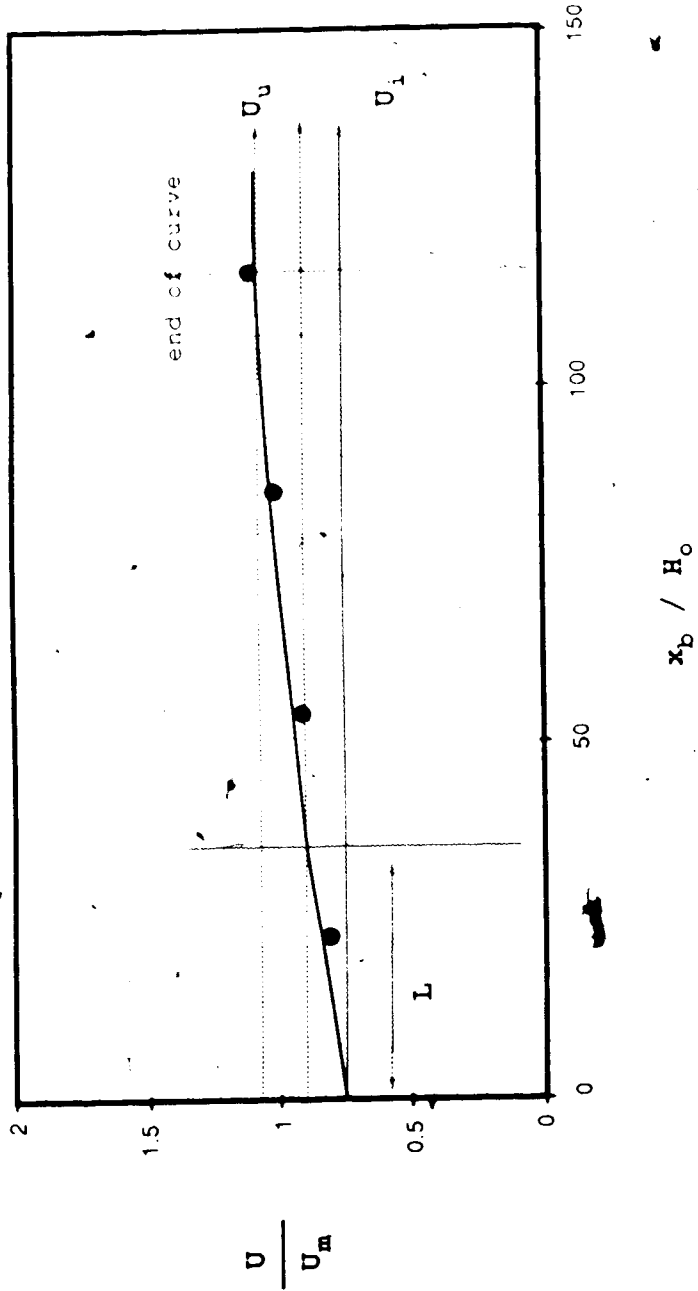


Figure 5.14 Non-Dimensional Longitudinal Velocity Distribution Near the Outer Bank, adapted from Yen(17) Run 1.

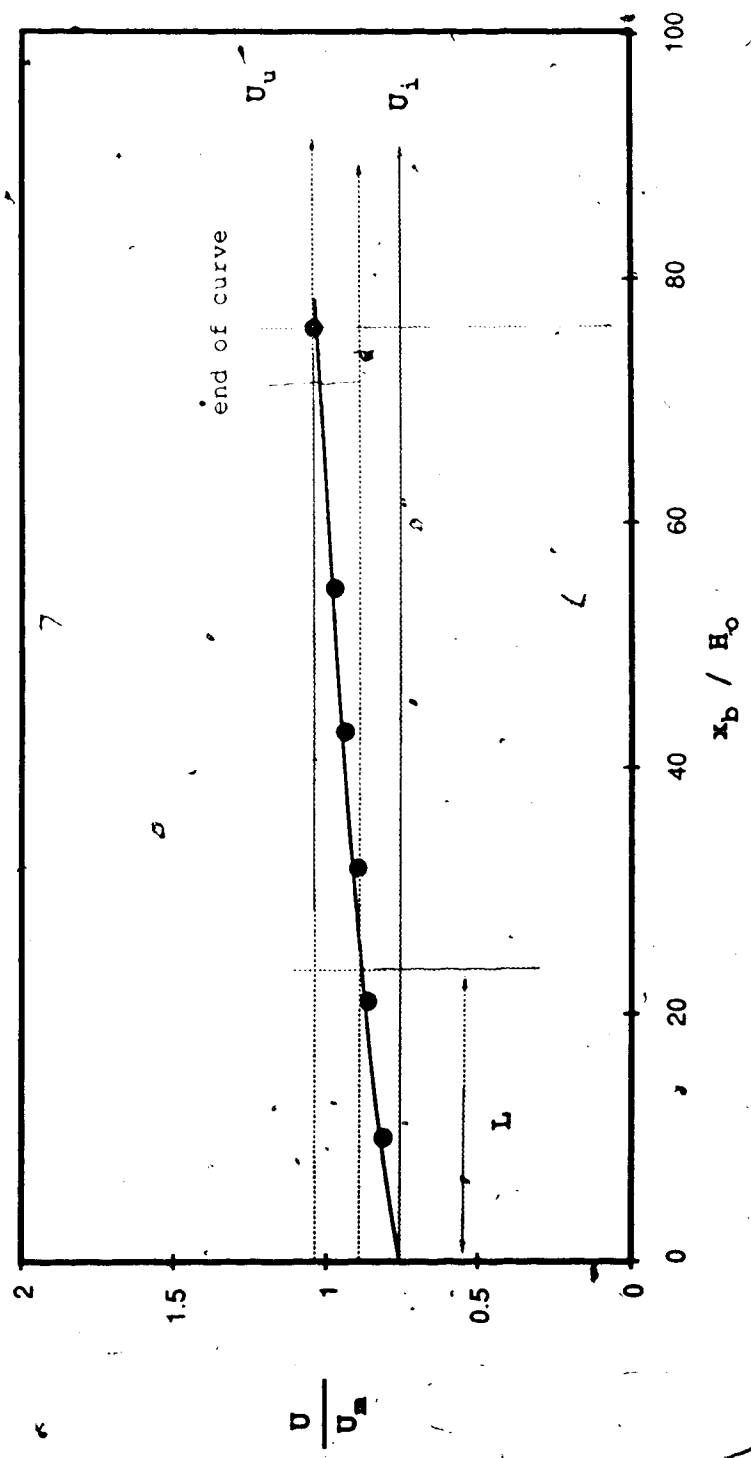


Figure 5.15 Non-Dimensional Longitudinal Velocity Distribution Near the Outer Bank, adapted from Yen(17) Run 2.

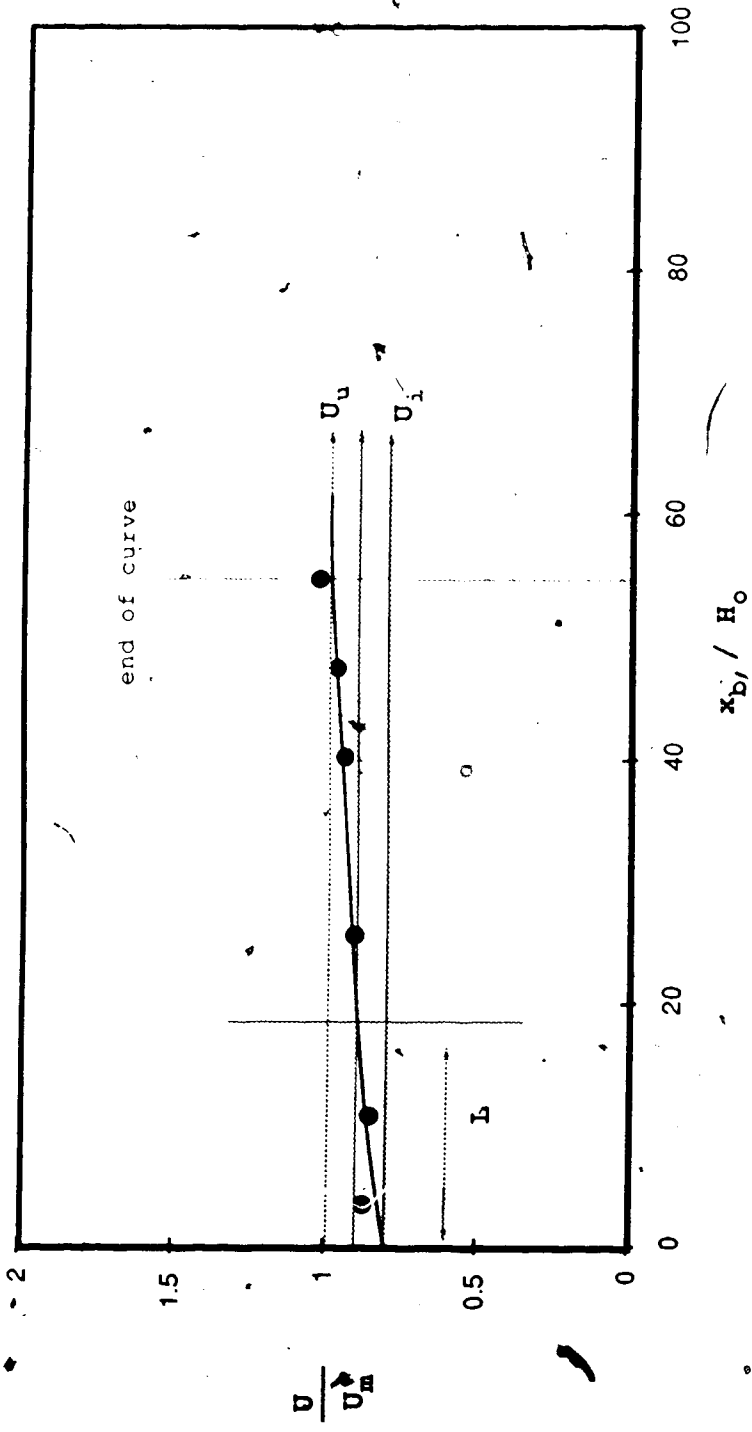
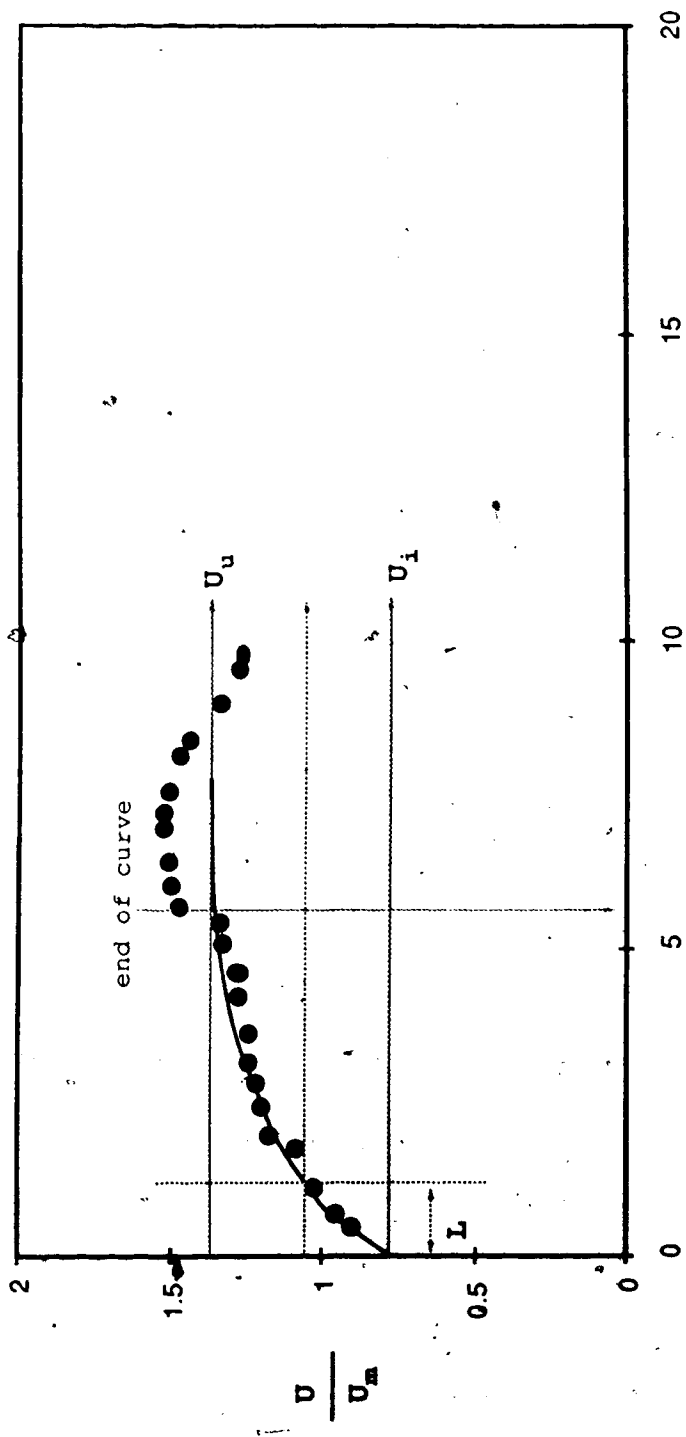


Figure 5.16 Non-Dimensional Longitudinal Velocity Distribution Near the Outer Bank, adapted from Yen(17) Run 3.



**Figure 5.17** Non-Dimensional Longitudinal Velocity Distribution Near the Outer Bank, adapted from Varshney & Grade (11) Run 1.

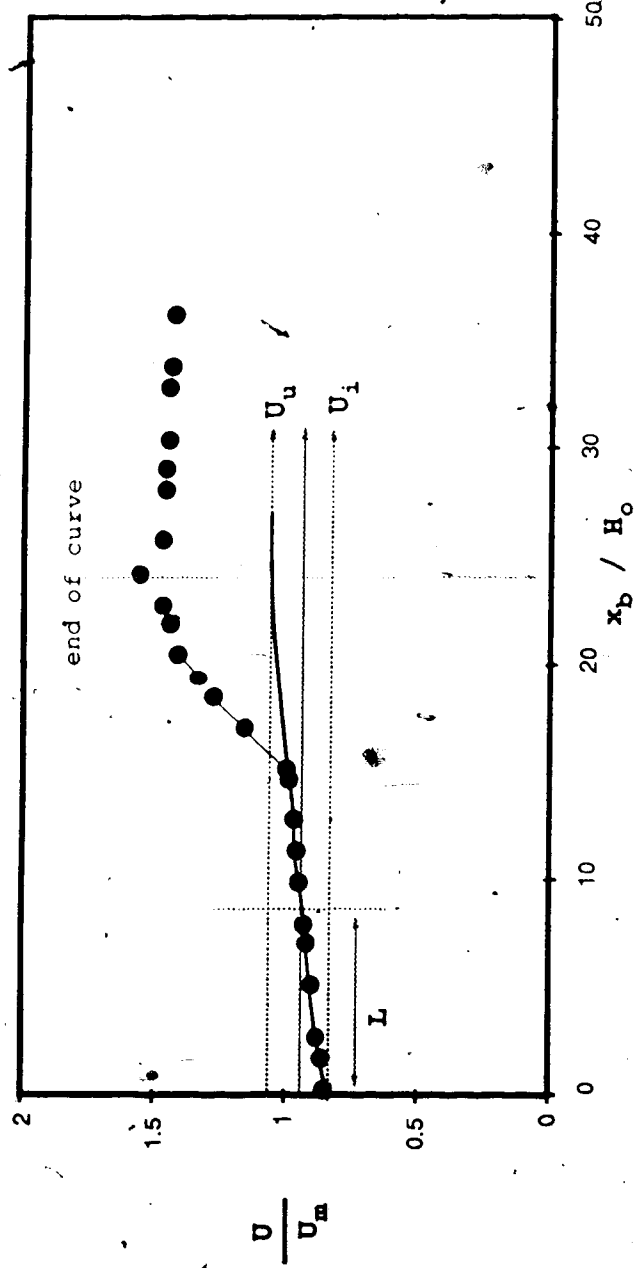


Figure 5.18 Non-Dimensional Longitudinal Velocity Distribution Near the Outer Bank, adapted from Varshney & Grade (11) Run 2.

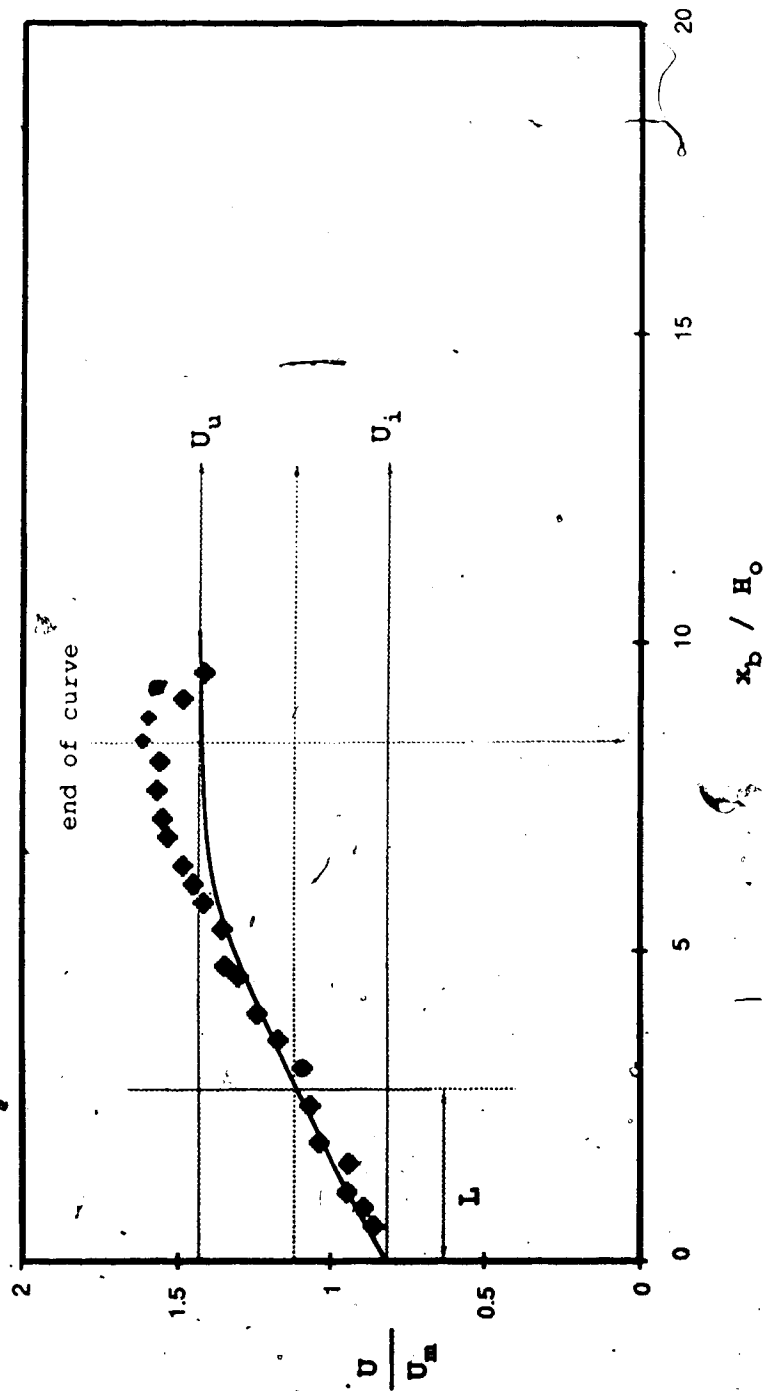


Figure 5.19 Non-Dimensional Longitudinal Velocity Distribution Near the Outer Bank, adapted from Varshney & Grade(11) Run 3.



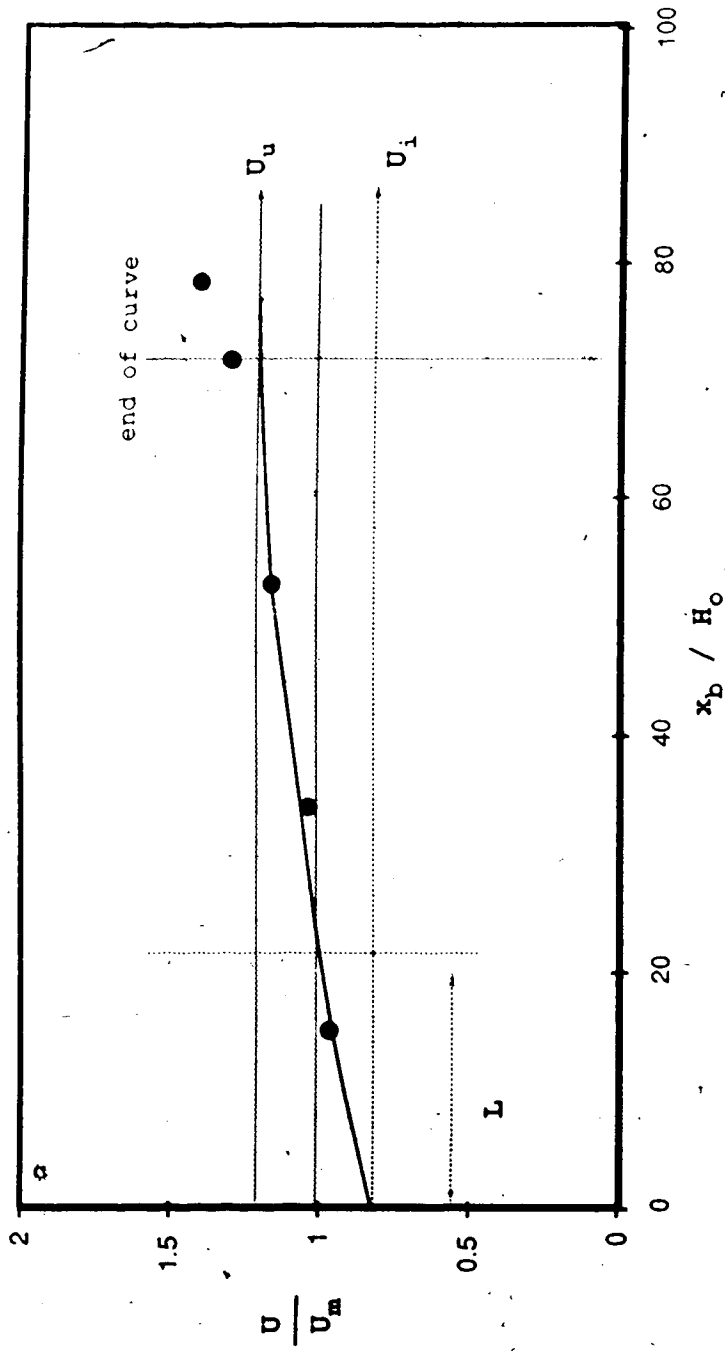


Figure 5.20 Non-Dimensional Longitudinal Velocity Distribution Near the Outer Bank, adapted from Francis & Asfari (4) Run 1&2.

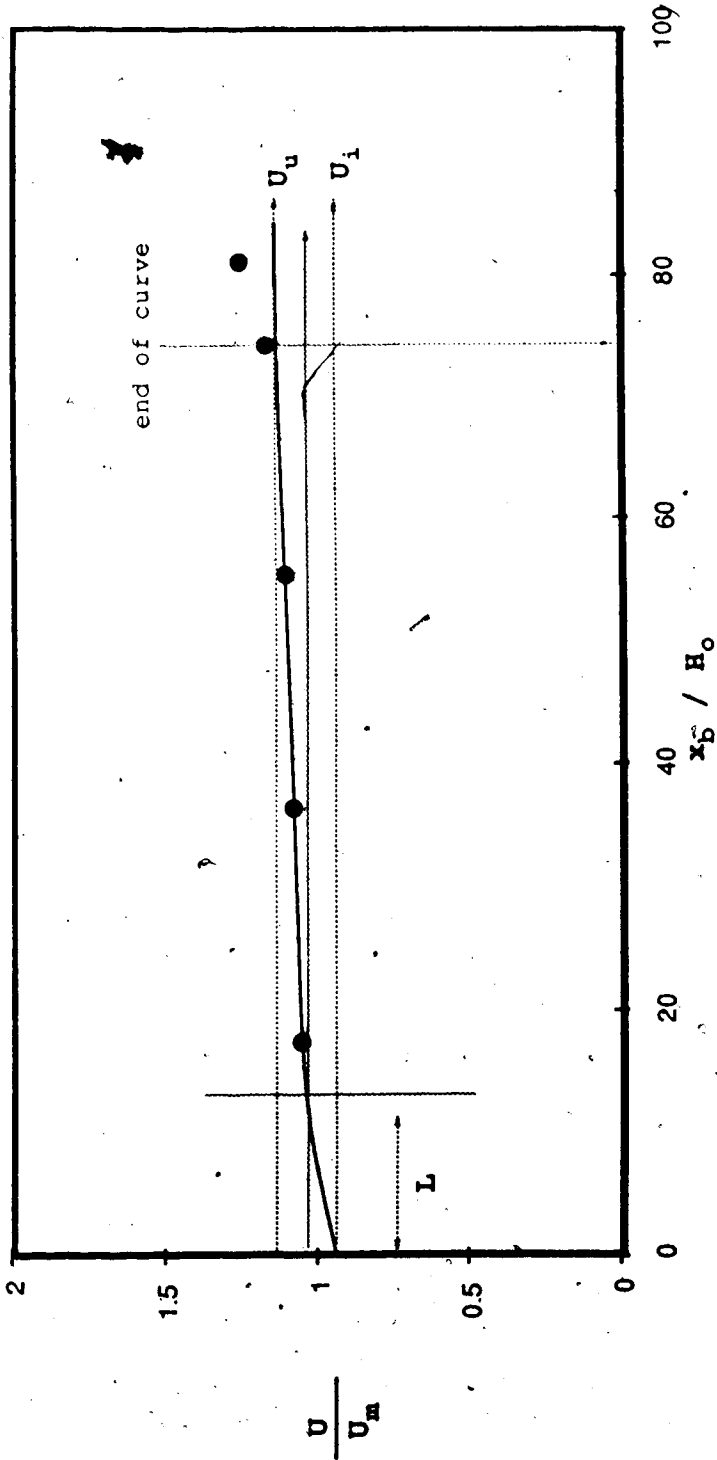


Figure 5.21 Non-Dimensional Longitudinal Velocity Distribution Near the Outer Bank, adapted from Francis & Asfari(4) Run 2

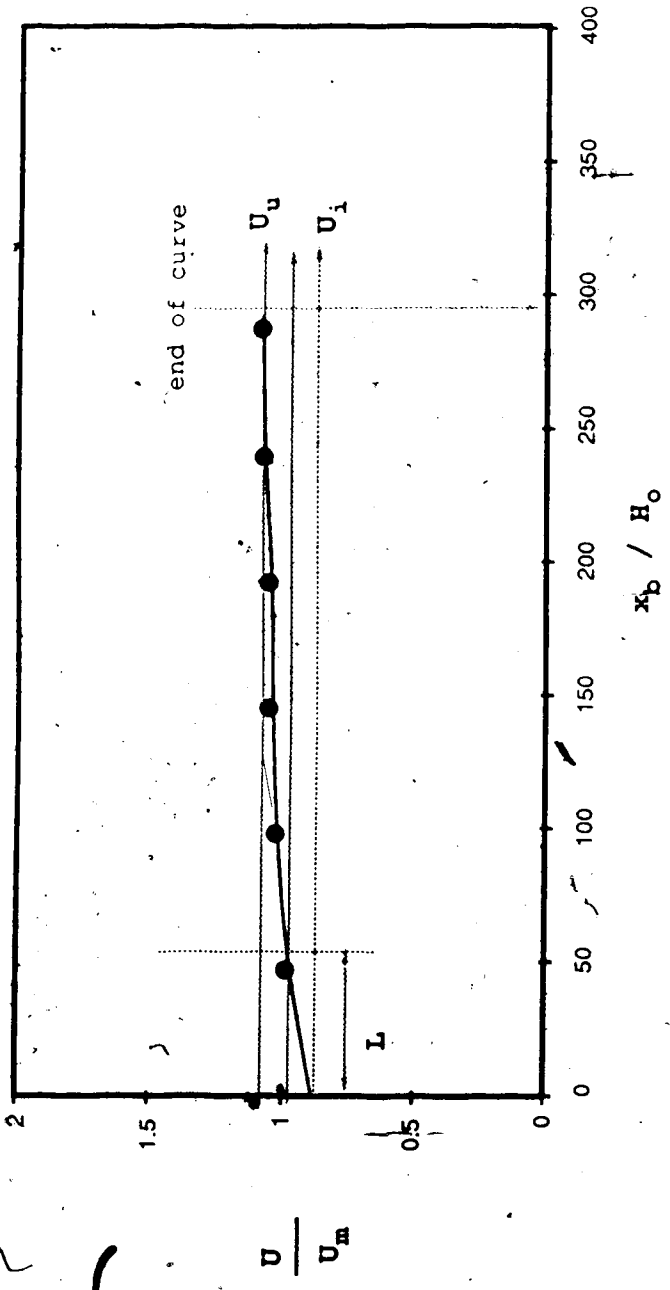


Figure 5.22 Non-Dimensional Longitudinal Velocity Distribution Near the Outer Bank, adapted from de Vriend(14) Run 1

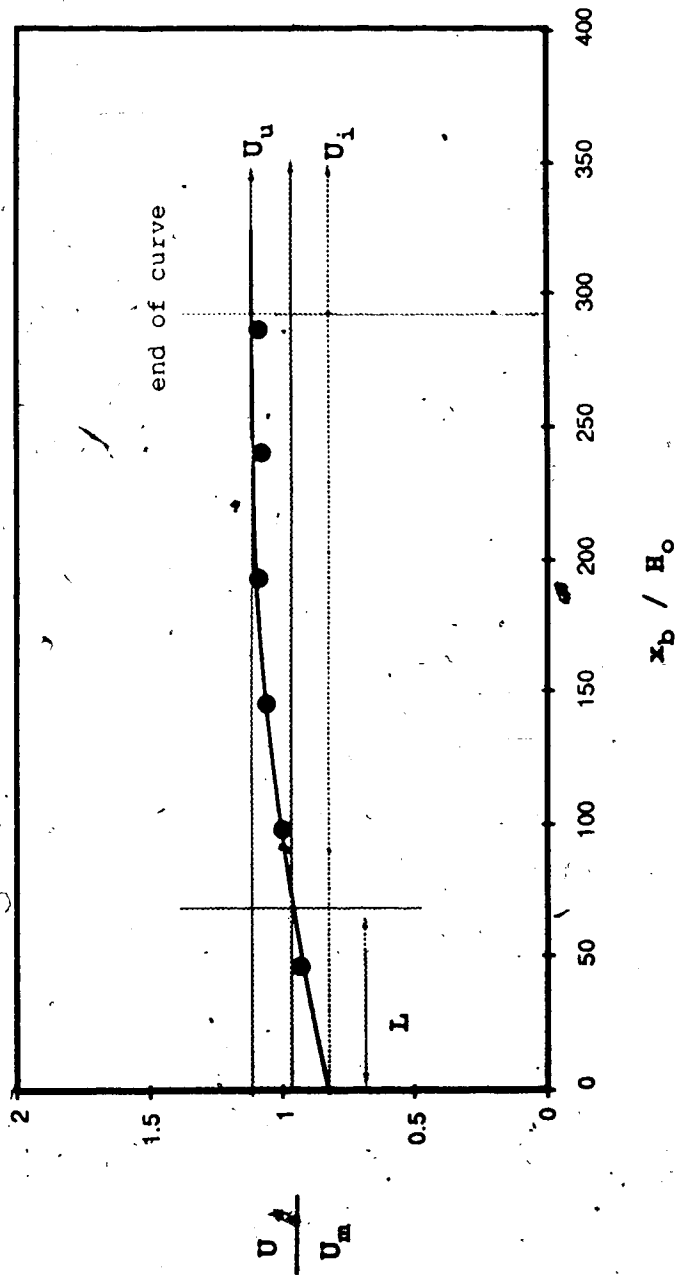


Figure 5.23 Non-Dimensional Longitudinal Velocity Distribution Near the Outer Bank, adapted from de Vriend(14) Run 2.

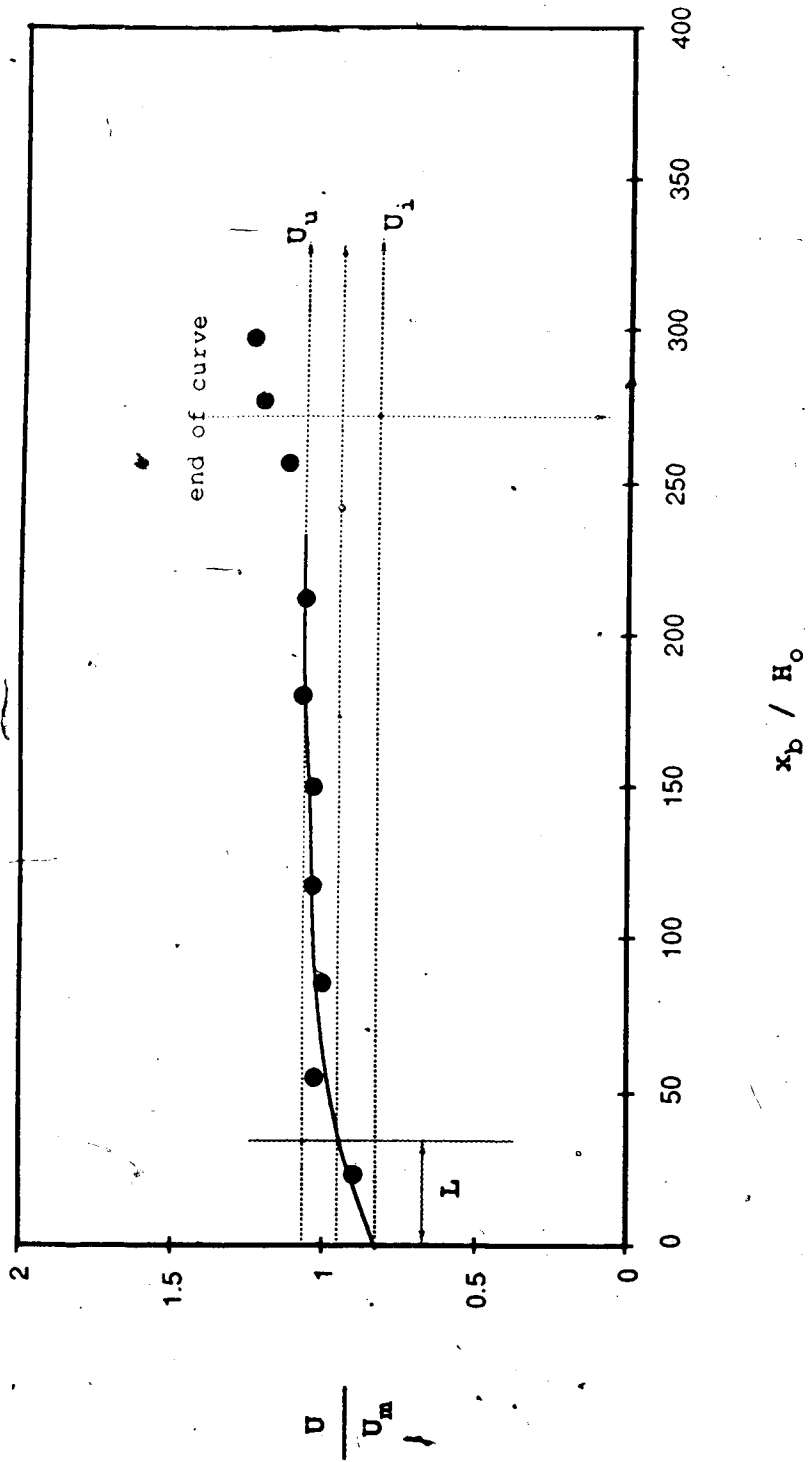


Figure 5.24 Non-Dimensional Longitudinal Velocity Distribution Near the Outer Bank, adapted from Steffler(12) Run 1.

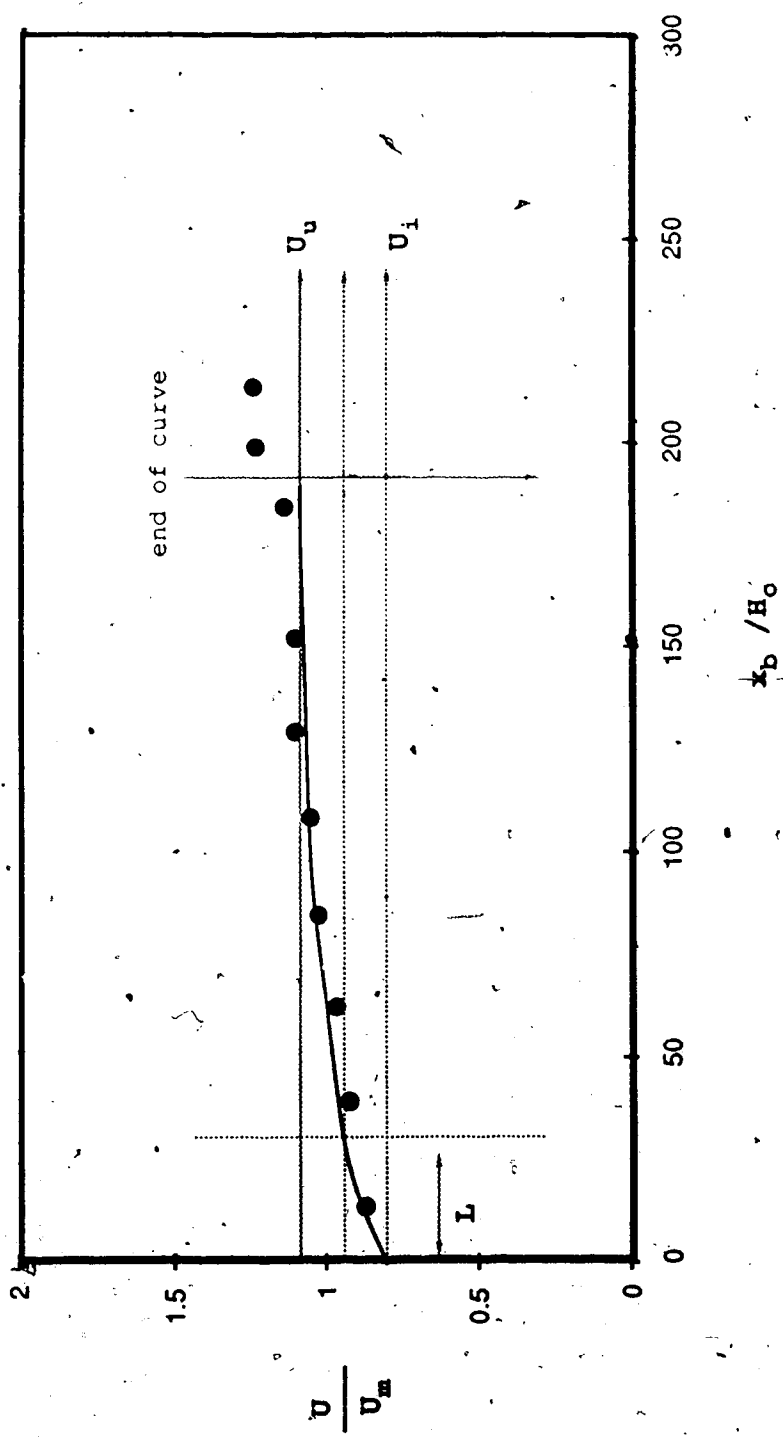


Figure 5.25 Non-Dimensional Longitudinal Velocity Distribution Near the Outer Bank, adapted from Steffler(12) Run 2.

value of  $U_u$  is reached. Thus, the ultimate velocity is obtained by extrapolating a best fit exponential type curve. Points near the end of the curve were not included due to exit effects. The value of the  $L, U_1, U_u$  is shown in each figure.

#### 5.4.3 Non-Dimensional Development of Longitudinal Velocity near The Outer Bank

Figure 5.26 which is based on the data from Table 5.1 indicates the non dimensional velocity perturbation near the outer bank in a rectangular curved channel against non-dimensional distance ( $\frac{x'_b}{L}$ ). Figure 5.27 is for trapezoidal channels. Figure 5.28 is a combination of Figures 5.26 and 5.27. It shows the best fit curve of each data set which behaved as expected between point(0,0) and point(0.5,1.0). Beyond the point(0.5,1.0) these curves show some scatter. Therefore, for design purposes it is recommended that the practical engineer decide the appropriate curve between the defined upper and lower limit.

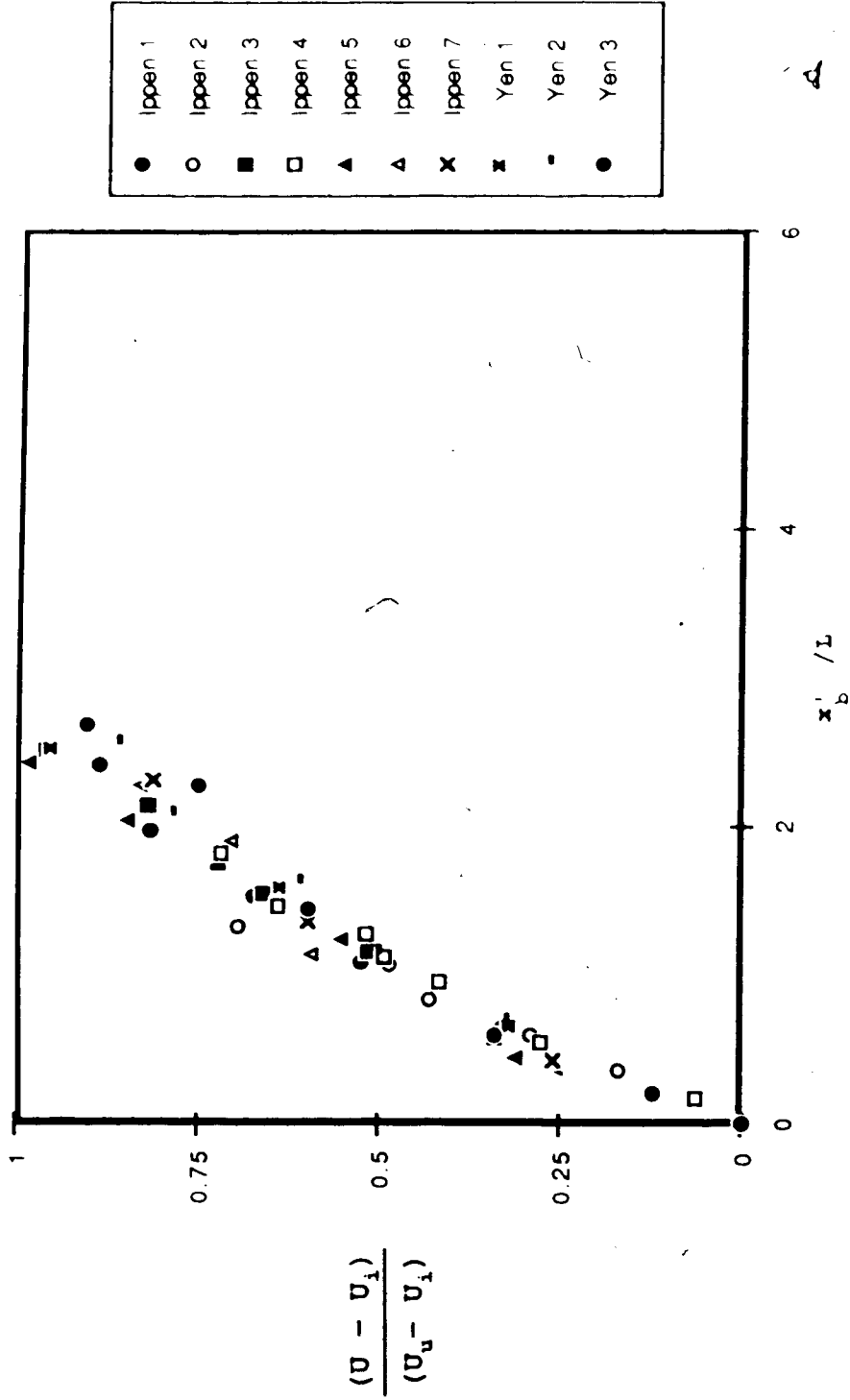


Figure 5.27 Non-Dimensional Development of Longitudinal Velocity Near the Outer Bank for Trapezoidal Channels



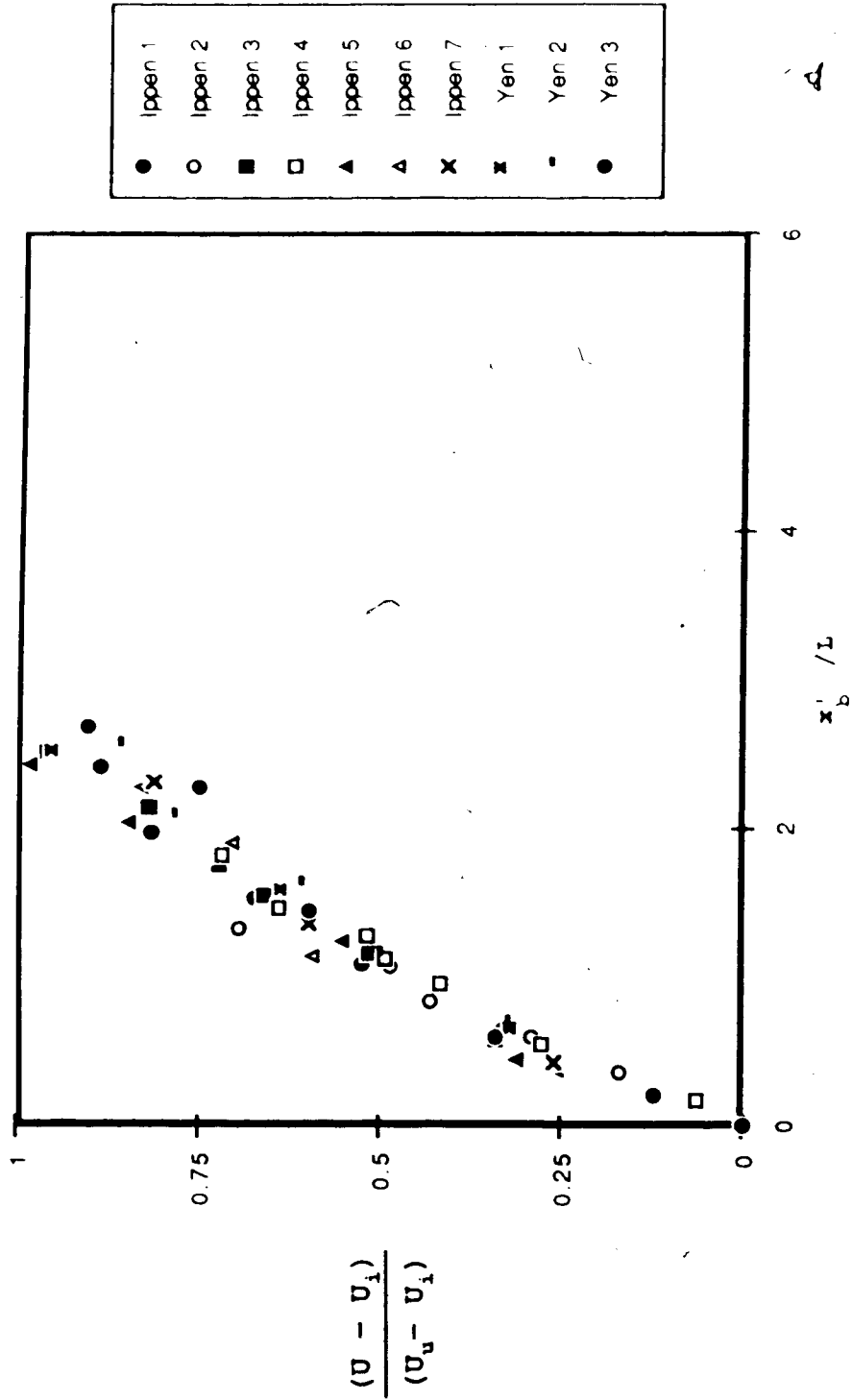


Figure 5.27 Non-Dimensional Development of Longitudinal Velocity Near the Outer Bank for Trapezoidal Channels

1 e

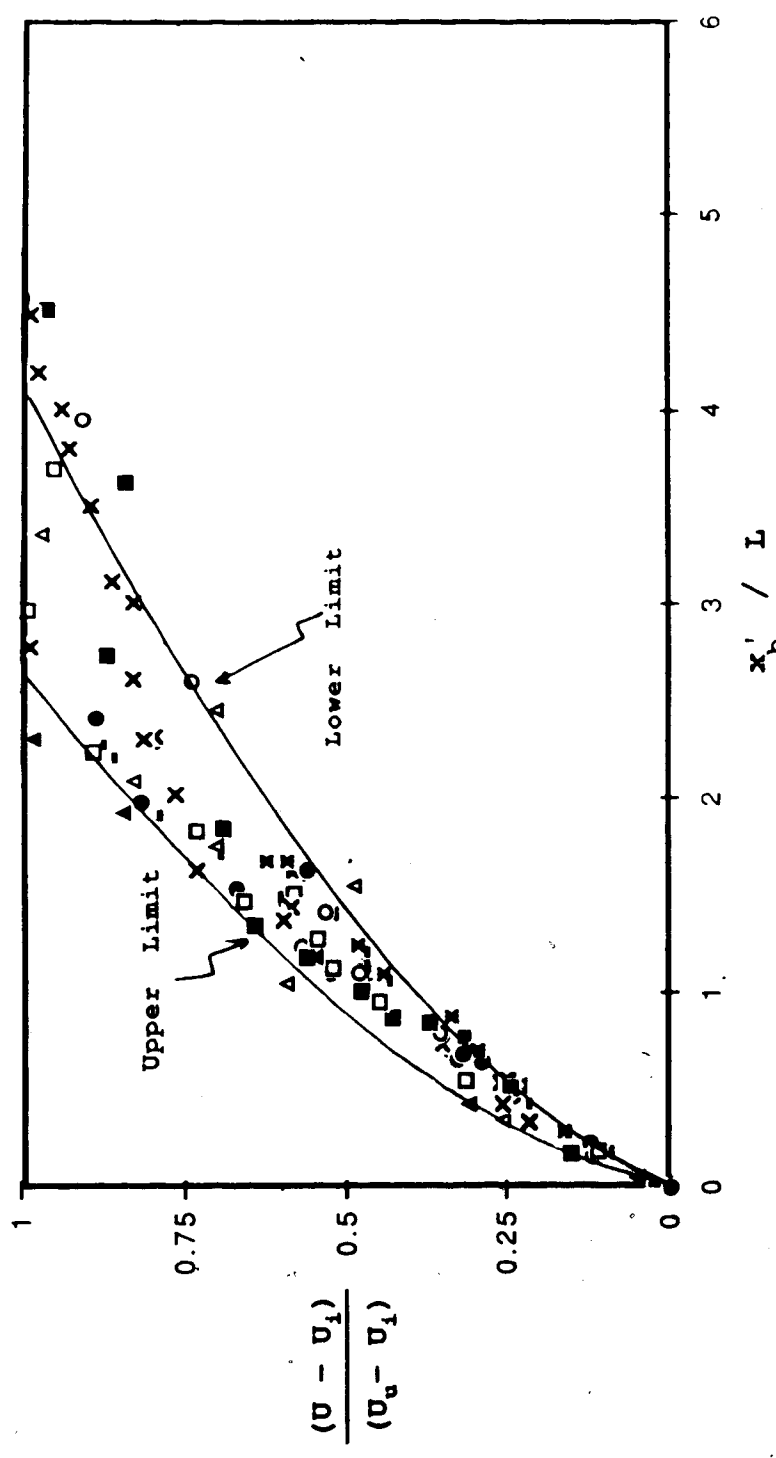


Figure 5.28 Non-Dimensional Development Velocity Near the Outer Bank for Rectangular and Trapezoidal Channels.

#### 5.4.4 Ultimate Velocity

Figure 5.29 indicates that the relative ultimate velocity ( $\frac{U_u}{U_m}$ ) decreases with increasing aspect ratio ( $\frac{B}{H_o}$ ). The visual trend line in Figure 5.29 indicates that when the aspect ratio is less than 10, the ultimate velocity will be decreased. However, if the aspect ratio is larger than 10, there is no significant difference between the ultimate velocity and the mean velocity.

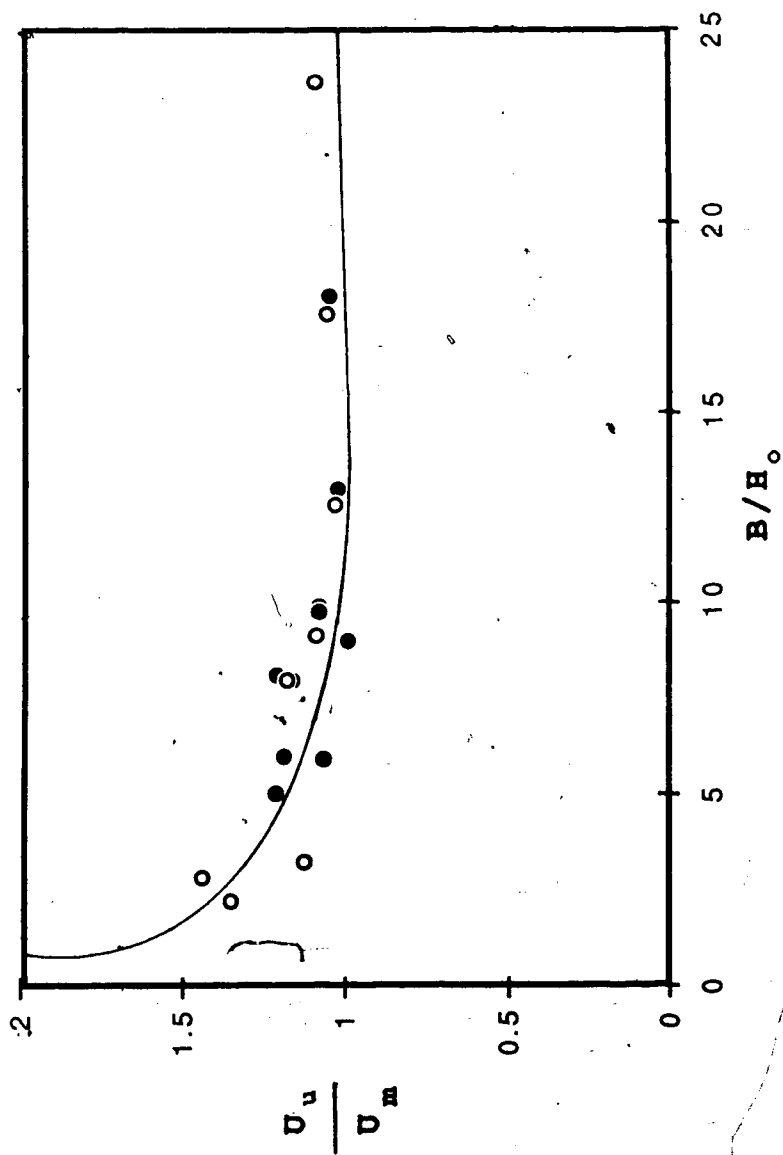
#### 5.4.5 Development Length Scale

Figure 5.30 and 5.31 display the relationship between length scale,  $L$ , and curvature,  $\frac{H_o}{R_c}$  and  $\frac{R_c}{H_o}$  respectively. This data is also shown in log-log form on Figure 5.32. An equation can be derived from the log-log plot as shown below:

$$L = 0.72 \left( \frac{H_o}{R_c} \right)^{-1.12} + A \quad [5.4]$$

It appears that the secondary flow which is directly related to  $\frac{H_o}{R_c}$  has a dominating effect on the development length. Only for very mild curvature ratios do the actual development lengths approach the values given by the theoretical analyses (Chapters 2 and 3).

Equation 5.4 has been developed from selected experimental data. In order to generalize the relationships



● Trapezoidal  
○ Rectangular

Figure 5.29 Ultimate Velocity Near the Outer Bank.

of those variables to represent natural channels further research, is essential.

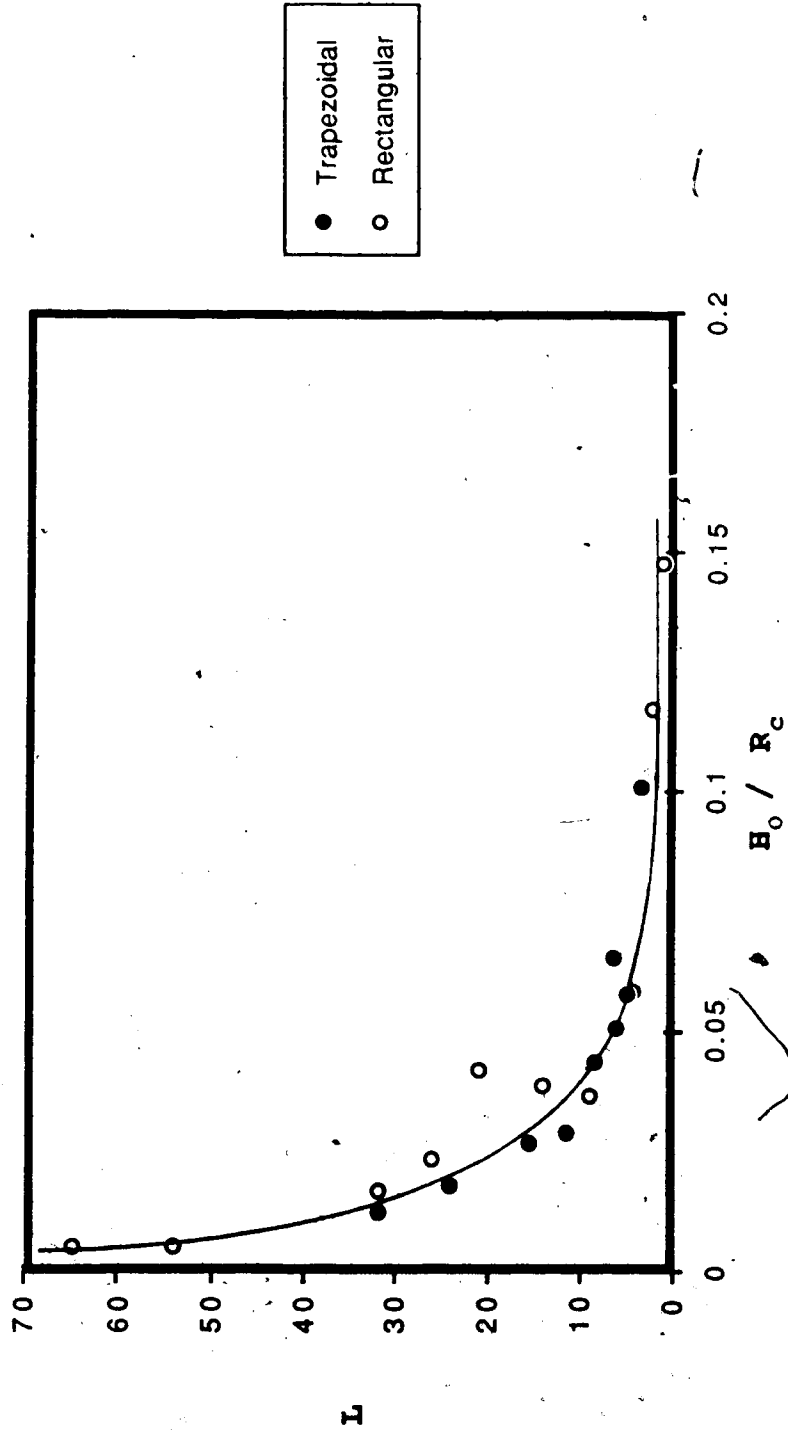


Figure 5.30 Length Scale for Longitudinal Velocity Development

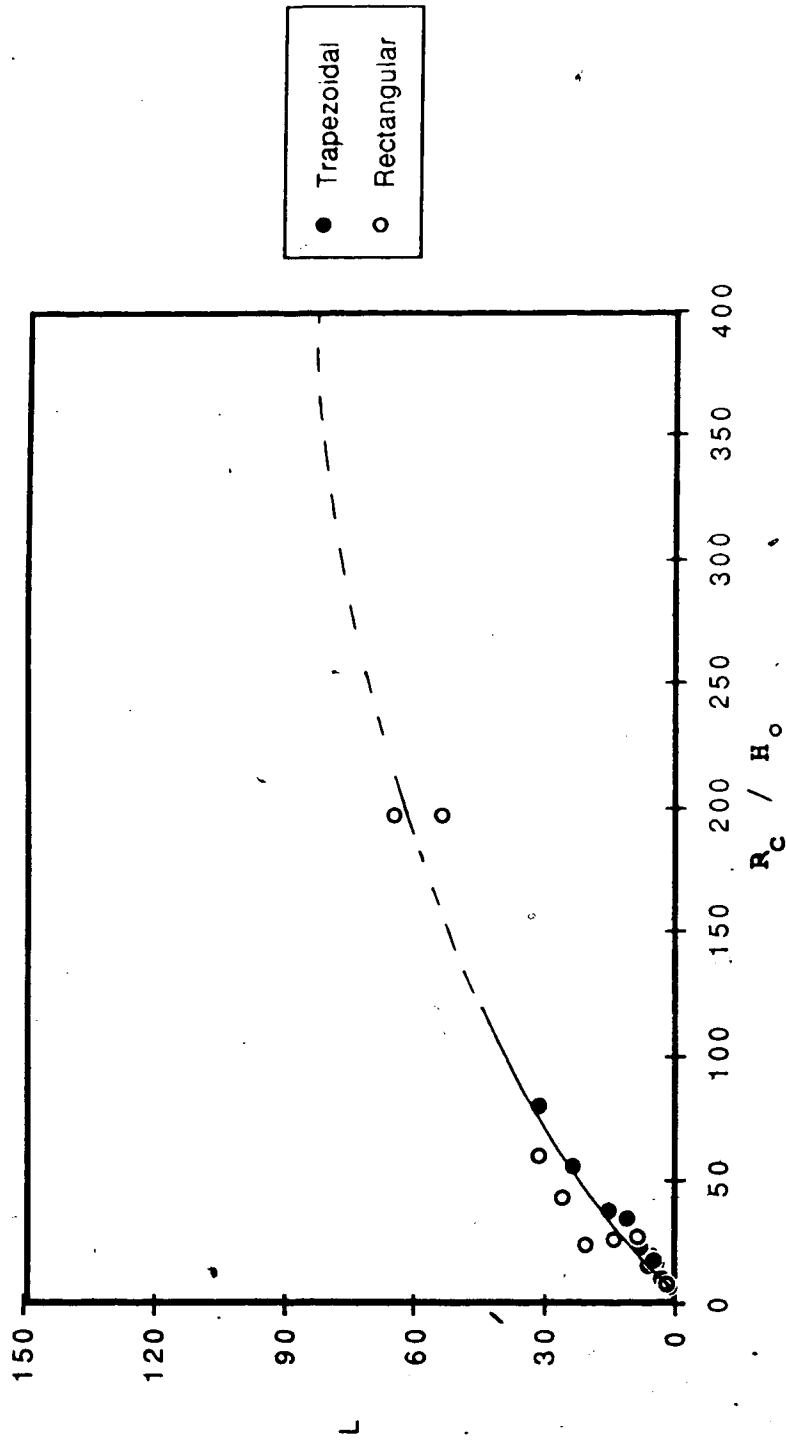


Figure 5.31 Length Scale for Longitudinal Velocity Development

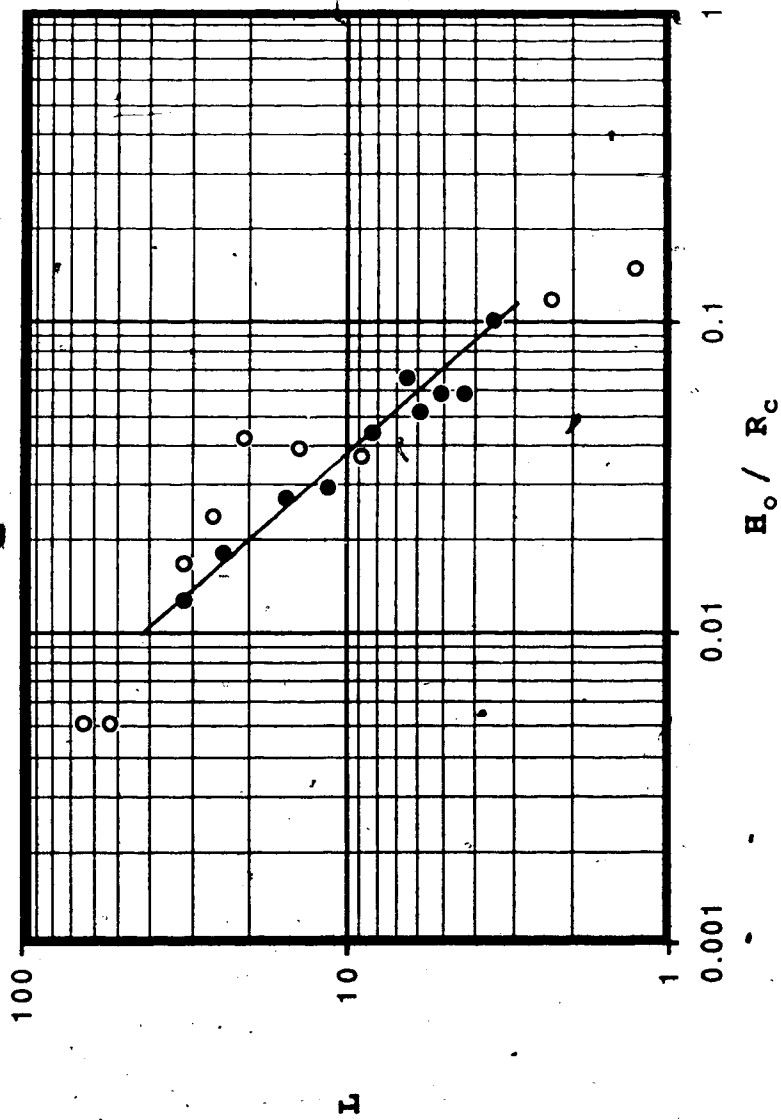


Figure 5.32 Length Scale for Longitudinal Velocity Development



## 6. An Example of the Application for a Curved Channel

The general procedure for estimating the flow in zone II is as follows.

### 6.1 DATA

It is assumed that the channel width ( $B$ ), the average flow depth ( $H_o$ ), the average velocity ( $U_m$ ) and the radius of channel curvature ( $R_c$ ) for a given reach are provided.

Then, for example :

$$B = 30 \text{ cm}$$

$$H_o = 4 \text{ cm}$$

$$U_m = 30.67 \text{ cm/s}$$

$$R_c = 90 \text{ cm}$$

Therefore

$$\frac{B}{H_o} = 7.5$$

$$\frac{R_c}{b} = 0.333$$

$$\frac{R_c}{H_o} = 22.5$$

### 6.2 Step 1

The known  $\frac{B}{R_c}$  and  $U_m$ , obtain the corresponding value of  $U_1$  from the plot of  $\frac{U_1}{U_m} = f\left(\frac{B}{R_c}\right)$  in Figure 5.6. Therefore in the example,  $\frac{U_1}{U_m} = 0.8335$

### 6.3 Step 2

Using  $\frac{B}{H_o}$  and  $U_m$  obtain  $U_u$  from Figure 5.29. Therefore  $\frac{U_u}{U_m} = 1.1$

### 6.4 Step 3

Using the values of  $\frac{R_c}{H_o}$  or  $\frac{H_o}{R_c}$ , the development length scale,  $L$ , can be obtained from Figure 5.30 or 5.31. Therefore,  $L = 9$ .

### 6.5 Step 4

Values of  $U$  are obtained from Figure 5.28. Table 6.1 gives the calculation worksheet for the example above. Sections (4) and (5) in Table 6.1 are used to plot a nondimensional velocity curve in the bend for the given channel (see Figure 6.1).

### 6.6 Step 5

Select the critical point,  $C'$ , from the region indicated on Figure 6.1 and obtain the value of

Table 6.1 Calculation Worksheet

$x_b/L$	$(U - U_i) / (U_u - U_i)$ (1)	$x_b/H_0$ (2)	$U/U_m$ (3)	$x/H_0$ (4)	$U/U_m$ (5)
0.0	0.00	0.0	0.8335	0.00	1.0000
0.5	0.28	4.5	0.9081	3.75	0.8335
1.0	0.45	9.0	0.9534	8.25	0.9081
1.5	0.65	13.5	1.0067	12.75	0.9534
2.0	0.80	18.0	1.0467	17.25	1.0067
2.5	0.92	22.5	1.0787	21.75	1.0467
3.0	1.00	27.0	1.1000	26.25	1.0787
				30.75	1.1000

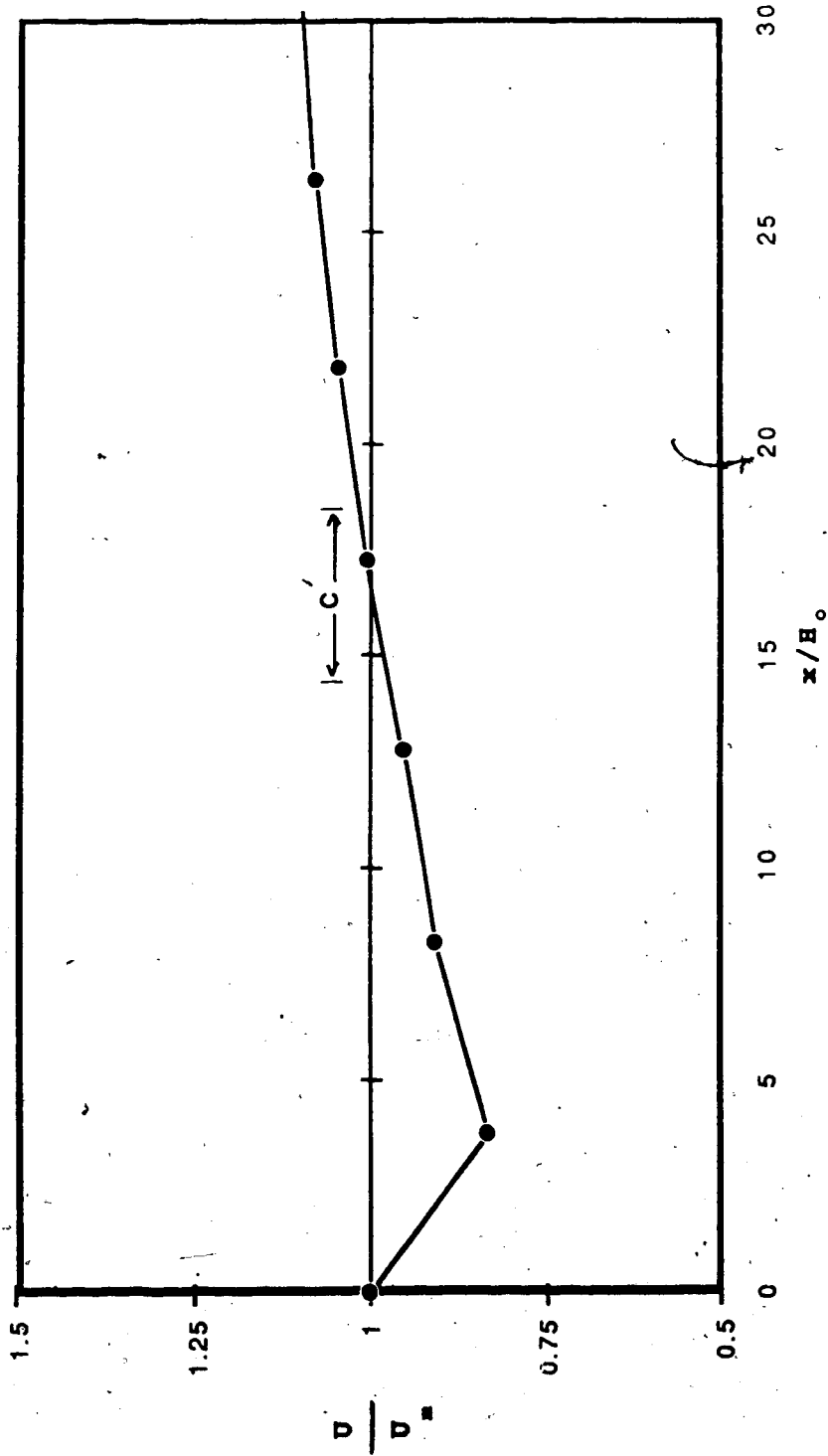


Figure 6.1 The Estimated Channel Velocity Distribution Near the Outer Bank

$x_1 = x'_1 + H_1 + 0.5B$ .  $x_1$  is the distance which measured from the entrance of the bend to the starting of the protection structure.

## 7. Conclusion

The purpose of this study was to attempt an empirical analysis to predict the longitudinal velocity and the potential for bank erosion near the outer bank of a curved channel. To this end the scales  $U_1$ ,  $U_u$  and  $L$  were introduced and correlated to the channel geometry and flow parameters.

It is found that the minimum velocity depends mainly on the channel width to radius of curvature ratio and the ultimate velocity depends primarily on the aspect ratio which was confirmed to some extent by the theoretical prediction. Theoretical prediction for the length scale  $L$  indicated that it only depended on  $C_c^2$ . The experimental results show that this is only true for very large values of  $\frac{R_c}{H_0}$ . For small and moderate values of  $\frac{R_c}{H_0}$ , the length scales are significantly reduced. Very little data in the transition region ( $\frac{R_c}{H_0}$  is between 50 and 200) is presently available. This should be a topic for further research. It was also found that for the limited ranges of Reynold's and Froude numbers represented no significant effects were observed.

The use of these scales ( $U_1$ ,  $U_u$  and  $L$ ) would help the design engineer to estimate the location and resistance of the protection works in a real bend. With the idealizations of constant width, constant radius and simple cross-sectional geometry significant judgement will be

required.

This study is based on flat bed flumes. Further research is needed to model natural channels. The research should be addressed to gain more data for natural channels, downstream of bends and rough banks. Some measurements in natural channels have been made (Bridge and Jarvis 1977, Odgaard 1981 and de Vriend and Geldof 1983) but there is not sufficient data for a separate empirical correlation. It would be useful, however, to analyse and compare these results to the present research.

In summary, a detailed literature review, and empirical analysis have been presented to introduce the three scales to predict the longitudinal velocity distribution in curved channels. It is felt that this approach to the determination of the location of bank protection in real bends has provided some valuable results and potential for further studies.

## Bibliography

1. Bridge, J.S., and J. Jarvis. 1977. Velocity profiles and bed shear stress over various bed configurations in a river bend. *Earth Surface Processes* :281-294.
2. Einstein, H.A., and J.A. Harder. 1954. Velocity distribution and the boundary layer at channel bends. *Transactions of the American Geophysical Union* 35(1): 114-120.
3. Engelund, F. 1974. Flow and bed topography in channel bends. *Journal of the Hydraulics Division, ASCE* 100(HY11) : 1631-1648.
4. Francis, J.R.D. and A.F. Asfari. 1971. Velocity distribution in wide curved open-channels flows. *Journal of Hydraulic Research, IAHR* 9(1): 73-90.
5. Hooke, R.L. 1974. Shear stress and sediment distribution in a meander bend. Department of Physical Geography, University of Uppsala Sweden. Report No. 30, 58 pp.
6. Ippen, A.T., and P.A. Drinker. 1962. Boundary shear stresses in curved trapezoidal channels. *Journal of the Hydraulics Division, ASCE* 88 (HY5): 143-179.
7. Kikkawa, H., S. Ikeda and A. Kitagawa. 1976. Flow and bed topography in curved open channels. *Journal of the Hydraulics Division, ASCE* 102(HY9): 1327-1342.
8. Nouh, M.A., and R.D. Townsend. 1979. Shear stress distribution in stable channel bends. *Journal of the Hydraulics Division, ASCE* 105(HY10) 1233-1245.
9. Odgaard, A. Jacob. 1986. Meander flow model. I: Development *Journal of Hydraulics Engineering*, Vol.112(12):1117-1136.
10. Rosovskii, I.L. 1961. Flow of water in bends of open channels. Jerusalem Isreal Program for Scientific Translation. 233 pp (Translated from Russian).
11. Schlichting, H. 1979. *Boundary-Layer Theory* (seventh ed.). New York: McGraw-Hill. 817 pp.
12. Steffler, P.M. 1984. *Turbulent Flow in a Curved Rectangular channel*. Ph.D. Thesis, University of Alberta. 262 pp.
13. Steffler, P.M., N. Rajaratnam and A.W. Peterson. 1985. Water Surface at Change of Channel Curvature *Journal of*



the Hydraulics Engineering, Vol. 111(5):866-870.

14. Varshney, D.V., and R.J. Grade. 1975. **Shear distribution in bends in rectangular channels.** Journal of the Hydraulics Division, ASCE 10(HY8) :1053-1066.
15. de Vriend, H.J. 1976. **A Mathematical Model of Steady Flow in Curved Open Shallow Channels.** Communication on Hydraulics. Department of Civil Engineering. Delft University of Technology. Report No. 76-1. 116 pp
16. de Vriend, H.J. 1981. **Velocity redistribution in curved rectangular channels.** Journal of Fluid Mechanics. 107: 423-439.
17. de Vriend, H.J. and H.J. Goldof. 1983. **Main flow Velocity in short river Bends.** Journal of the Hydraulic Engineering, ASCE 109(7): 991-1011.
18. Yen, B.C. 1965. **Characteristics of subcritical flow in a meandering channel.** Institute for Hydraulic Research, University of Iowa. 76 pp.
19. Yen, C.L. 1970. **Bed topography effect on flow in a meander.** Journal of the Hydraulics Division, ASCE 96(HY1): 57-73.
20. Yen, C.L., and B.C. Yen. 1971. **Water surface configuration in channel bends.** Journal of the Hydraulics Division, ASCE 97(HY2): 303-321.
21. Zimmermann, C., and J.F. Kennedy. 1978. **Transverse bed slopes in curved alluvial streams.** Journal of the Hydraulics Division, ASCE 104(HY1): 33-48.